Fall 2018

Three-Way Catalysts in Passive Selective Catalytic Reduction Systems

Calvin Thomas

Recommended Citation

Thomas, C.(2018). *Three-Way Catalysts in Passive Selective Catalytic Reduction Systems.* (Doctoral dissertation). Retrieved from https://scholarcommons.sc.edu/etd/5067

THREE-WAY CATALYSTS IN PASSIVE SELECTIVE CATALYTIC REDUCTION
SYSTEMS

by

Calvin Thomas

Bachelor of Chemical Engineering
Auburn University, 2013

_____

Submitted in Partial Fulfillment of the Requirements

For the Degree of Doctor of Philosophy in

Chemical Engineering

College of Engineering and Computing

University of South Carolina

2018

Accepted by:

Jochen Lauterbach, Major Professor

William Mustain, Committee Member

Erdem Sasmaz, Committee Member

Todd Toops, Committee Member

Cheryl L. Addy, Vice Provost and Dean of the Graduate School

DEDICATION

This work is dedicated to my brothers and sisters: Micah, Megan, Charles, Jessica, and Alexandra. They have been with me through my whole life and I wouldn't be where or who I am without them. It is also dedicated to my dog Fritz because he is a very good boy.

ACKNOWLEDGEMENTS

ABSTRACT

Conventional gasoline-powered engines operate with a stoichiometric air-fuel ratio (AFR), but greater fuel economy is achieved in lean burn engines by increasing the AFR. The primary drawback to these engines is the nitrogen oxide (NO_X) emissions, which cannot be reduced over a conventional three-way catalyst (TWC). Passive selective catalytic reduction (SCR) is a promising approach for the control of NOX emissions in lean burn systems. By periodically decreasing the AFR to fuel-rich levels, ammonia (NH_3) can be produced over a TWC and stored on a downstream SCR catalyst for the reduction of NOX during normal lean operation. While passive SCR has shown promise, work to date has not sufficiently examined the effects of physical or chemical degradation on the TWC in a passive SCR system or how these factors are affected by the transient nature of passive SCR. Furthermore, many questions about the formulation of the TWC have yet to be answered.

This work is focused on answering these questions to better understand NH_3 production over TWCs and the degradation mechanisms of passive SCR. Using commercially formulated TWCs, the effects of hydrothermal aging and sulfur dioxide (SO_2) are examined, while model catalysts are synthesized to investigate the roles of ceria on the catalyst. Hydrothermal aging at 920°C for 100 hours results in significant noble metal sintering as well as degradation of both oxygen storage and NOX storage components. Long term exposure to 2 ppm SO_2 results in significant deactivation of catalyst activity, which is attributed primarily to the deactivation of water gas shift and

steam reformation reactions. These sulfur effects can be partially mitigated by lowering the AFR during rich operation. Finally, in the investigation of ceria, it was found that low levels of ceria promote water gas shift, but elevated levels result in inhibition of catalyst reduction.

TABLE OF CONTENTS

LIST OF TABLES

LIST OF FIGURES

LIST OF ABBREVIATIONS

AFR .... Air-Fuel-Ratio

DOC .... Diesel Oxidation Catalyst

NSC .... NO_X Storage Capacity

NSR .... NO_X storage and reduction

OSC .... Oxygen Storage Capacity

SCR .... Selective Catalytic Reduction

TWC .... Three-Way Catalyst

CHAPTER 1

INTRODUCTION

1.1 Motivation

Despite the growing prevalence of alternative fuels and renewable energy, petroleum-based fuels still accounted for 92% of transportation energy use in 2017 [1]. The combustion of these fuels produces several gas phase environmental pollutants. Chief among these are carbon monoxide (CO), nitrogen oxides (NO_X), and unburned hydrocarbons (HC). The primary means by which automotive emissions from gasoline engines are controlled is a three-way catalyst (TWC). The TWC derives its name from its ability to eliminate the three primary environmental pollutants present in automobile exhaust through the simplified reaction set shown in equations 1.1–1.3.

$$CO \quad + \quad (O_2, NO_X) \quad \rightarrow \quad CO_2 \quad (1.1)$$

$$C_xH_y \quad + \quad (O_2, NO_X) \quad \rightarrow \quad CO_2 + H_2O \quad (1.2)$$

$$NO_X \quad + \quad (H_2, CO, HC) \quad \rightarrow \quad N_2 \quad (1.3)$$
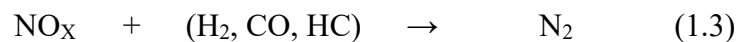
TWCs contain platinum group metals (PGM), usually Pd, Pt, and/or Rh, as their primary active sites and are usually supported on a metal oxide like alumina (Al_2O_3) or ceria (CeO_2). In order for all of the pollutants to be reduced through this process, the engine must be run with a stoichiometric air-fuel ratio (AFR). This allows for the oxidation reactions to fully convert CO and HC emissions, while also allowing for the reduction of NO_X to take place.

While a TWC is effective in decreasing the emissions of these harmful pollutants, it can do nothing to decrease CO_2 emissions. The only methods for decreasing CO_2 emissions are through carbon capture, which is not very feasible for mobile sources, or a decrease in the consumption of hydrocarbon-based fuels. Of the petroleum used in the United States, 42 was used to power gasoline engines in cars and light trucks, as shown in Figure 1.1 [1]. This is a significant portion of the total United States energy consumption and represents a viable target sector for combatting the rising demand for petroleum in the United States. Even a modest increase in the fuel economy of these small gasoline engines can have a significant impact on the rising petroleum consumption of the United States and, by extension, its production of environmental pollutants.
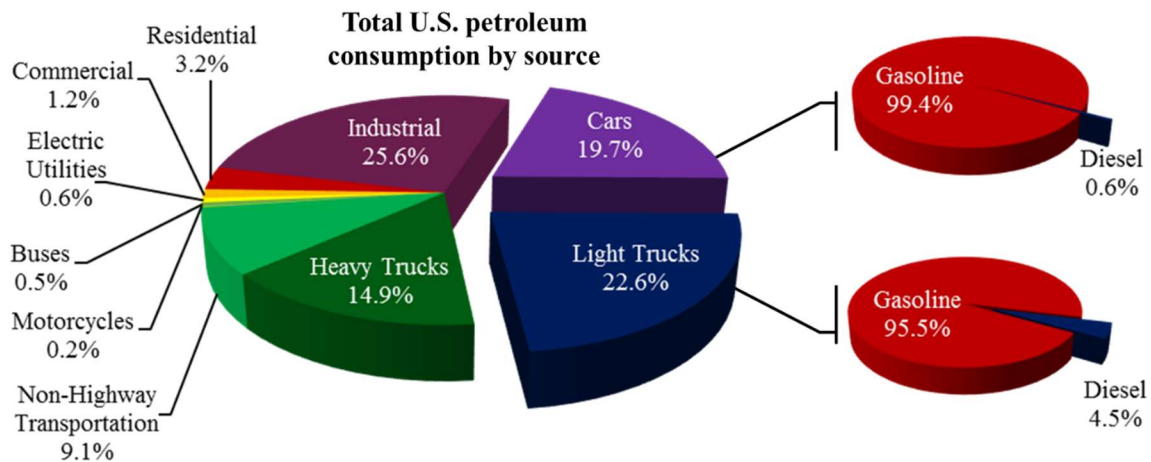
Figure 1.1: United states petroleum use by source.

Lean-burn gasoline engines are a promising technology to improve fuel economy. By combusting gasoline with a high AFR, lean burn engines provide increased fuel efficiency and, by extension, decreased carbon dioxide (CO_2) emissions. Research conducted by Parks *et al.* has shown that operating in a fuel lean environment can

increase an engine's efficiency by up to 15% over stoichiometrically operated engines [2]. However, because the TWC needs a stoichiometric AFR, operating a system with excess air prevents the TWC from fully converting NO_X due to a lack of reductants. In fact, even with a TWC, the system studied by Parks *et al.* produced NO_X emissions up to 0.35 g/mile, far exceeding the 0.03 g/mile combined NO_X and non-methane organic gas (NMOG) limit set by EPA Tier 3 regulations [3]. This limitation of TWCs represents a significant hurdle and currently the primary obstacle to the widespread commercial implementation of highly efficient lean-burn engines.

The challenges related to NO_X abatement in oxygen-rich exhausts have been a well-known obstacle for both lean burn gasoline engines and diesel engines for decades. The primary methods for the elimination of NO_X in these exhaust systems fall into two categories: NO_X storage and reduction (NSR), which has previously been used in lean-burn gasoline engine exhaust, and selective catalytic reduction (SCR), which has seen widespread implementation in diesel engine exhaust systems [4]. Much like standard TWCs, NSR catalysts use PGM for the oxidation and reduction reactions. In addition, these NSR catalysts incorporate a NO_X storage component (NSC), usually Ba, to trap the inlet NO_X as nitrate species for later reduction [5]. To reduce the NO_X stored on the catalyst and regenerate it, NSR systems require the engine to run with an excess of fuel for a brief period (< 5 s) before resuming lean operation for a much longer period (1-2 min). The first NSR systems were designed by Toyota in the mid 1990's [6]. Since then, NSR systems have seen some commercial success, being implemented by various automobile manufacturers over the last 20 years [7]. However, these systems, in their current form, are unable to meet United States emissions standards. This is because

during the rich phase regeneration of the NSR catalyst, a significant portion of the stored NO_X is not fully reduced to N_2. This results in a large amount of N_2O and NO_X emissions [8,9].

The alternative to an NSR system is the SCR of NO_X in the exhaust using an added reductant. Urea is the most commercially successful SCR reductant, being implemented into both stationary pollution sources and diesel engines [10,11]. In a urea-SCR system, the oxidation of CO and HC emissions take place upstream on a diesel oxidation catalyst (DOC). The DOC has similar composition to a typical TWC, though specialized for oxidation reactions [12]. Downstream from the DOC, a urea solution is injected into the hot exhaust where it is rapidly hydrolyzed into NH_3. This NH_3 is utilized over a specialized SCR catalyst to reduce excess NO_X emissions. There are three main types of catalyst used for SCR in diesel exhausts: vanadia, Cu-exchanged zeolite, and Fe-exchanged zeolite catalysts. Vanadia SCR catalysts have a long history of research and they have been implemented in various diesel exhaust treatment systems [13,14]. However, these vanadia catalysts have several deficiencies. These include high activity for the formation of N_2O and SO_3, rapid hydrothermal degradation at temperatures above 550°C, and vanadia's toxicity combined with its volatilization above 650°C [15–17]. Ion-exchanged zeolite catalysts were first developed in the 90's and have received a significant amount of attention more recently because they address many of these issues [15,16]. Though early ion-exchanged zeolite catalysts had issues with hydrothermal stability, more recent work has produced small-pore Cu-zeolite catalysts with excellent hydrothermal resistance that are able to maintain their activity over a wider temperature window such as SSZ-13 and SAPO-34 [18,19]. The full mechanism, surface species

formed, and rate limiting step of urea-SCR on a Cu-zeolite catalyst were studied by Janssens *et al.* They concluded that the "standard" SCR and "fast" SCR reactions (equations 1.4 and 1.5) form a complementary reaction cycle, where the rate-limiting step is the oxidation of NO into a nitrate on the Cu site [20].

$$4NH_3 \quad + \quad 4NO \quad + \quad O_2 \quad \rightarrow \quad 4N_2 \quad + \quad 6H_2O \quad (1.4)$$

$$2NH_3 \quad + \quad NO \quad + \quad NO_2 \quad \rightarrow \quad 2N_2 \quad + \quad 3H_2O \quad (1.5)$$

While they have proven effective in reducing NO_X emissions in exhaust systems for diesel engines, there are some concerns with implementing one of these urea-SCR emission control systems in a lean burn gasoline engine. They require several additional design considerations over traditional, stoichiometrically operated gasoline systems. First, they require an additional tank to store the urea solution. This can be costly for a small vehicle where space is at a premium, and it can be off-putting to consumers to have an additional tank to fill. Second, they require a urea injection and control system. This can be expensive to produce for the automobile manufacturer since it requires several additional sensors and plumbing to transport and inject the urea [21].

An alternative to traditional urea SCR systems is a system called passive SCR, which was first proposed in 2010 by Li *et al.* at GM [22]. This system requires the engine to periodically operate in a fuel rich phase, much like an NSR system. However, rather than the reduction of stored NO_X, the goal of this rich phase is to produce NH_3 over a TWC. This NH_3 can then be stored on a downstream Cu-exchanged zeolite catalyst, allowing for reduction of NO_X during lean operation. A significant amount of work has shown that NH_3 yield can approach 100% under appropriate conditions [23]. While this

system has shown some promise, there remain many factors that have not been thoroughly examined thus far. There are distinct challenges in evaluating the TWC in this system that have not been addressed previously in literature.

1.2 Three-way catalyst activity

Because this work is concerned with the evaluation of TWCs in passive SCR systems, it is important to first discuss TWCs themselves. It is important to be aware that these reactions are occurring in parallel on the catalyst surface, with many surface species potentially interacting. Furthermore, many of these individual reactions have a multitude of potential reaction pathways suggested in the literature, and there is still significant debate on dominant pathways. For discussion purposes, the reactions will be divided into three categories: the elimination of CO, the elimination of HCs, and the elimination of NO_X.

The elimination of CO occurs through the reactions shown in equations 1.6-1.8. CO can be oxidized directly by O_2, producing CO_2. Because, fundamentally, the oxidation of CO by O_2 only requires the introduction of a single oxygen atom, the reaction is easily studied, and a significant amount of work has been conducted on its activity [24–29]. This body of work shows that, while it is a simple reaction, it is possible that CO oxidation can occur through several different mechanisms on an automotive TWC. The first and most common is the Langmuir-Hinshelwood mechanism [30,31]. In this case, the reaction occurs between an adsorbed CO and an adsorbed O atom on the PGM surface. This adsorbed O atom is primarily generated from the dissociative adsorption of O_2. Another suggested mechanism is the Eley-Rideal mechanism whereby a

gaseous CO reacts with an adsorbed O atom [32]. Finally, research has shown that CO oxidation can occur through a Mars-van Krevelen mechanism [31]. In this case, CO reacts with a lattice O in a metal oxide (usually ceria), creating an oxygen vacancy. This vacancy can then be refilled by O_2 in the exhaust.

$$CO \quad + \quad O_2 \quad \rightarrow \quad CO_2 \qquad\qquad (1.6)$$

$$CO \quad + \quad H_2O \quad \leftrightarrow \quad CO_2 \quad + \quad H_2 \quad (1.7)$$

$$CO \quad + \quad NO_X \quad \rightarrow \quad CO_2 \quad + \quad N_2 \quad (1.8)$$

CO can also be oxidized by NO_X, as shown in equation 1.8. This process is generally considered to exclusively occur through a Langmuir-Hinshelwood mechanism whereby an adsorbed CO species and an adsorbed NO (or NO_2) species react over the PGM to form CO_2 and an adsorbed N atom [33]. Finally, CO can be eliminated through reaction with H_2O via the water gas shift reaction, producing both H_2 and CO_2. There are two primary mechanisms that have been suggested for this reaction: the associative mechanism and the redox mechanism [34]. For the associative mechanism, it has been suggested that the H_2O can dissociatively adsorb on the metal oxide support, creating both an adsorbed OH species and an adsorbed H atom. The CO then reacts with the adsorbed OH species at the interface between the metal oxide and noble metal, producing a formate intermediate. This intermediate can then dissociate into CO_2 and an adsorbed H atom, which can then recombine to form molecular H_2. The redox mechanism relies on the interface between the metal oxide support and the PGM surface. In this mechanism, the metal oxide at the interface goes through a redox cycle. First, it is reduced by a CO on the PGM surface, leaving an oxygen vacancy. This vacancy is subsequently filled by an

adsorbed H_2O, producing molecular H_2. Numerous studies, both computational [35], and experimental [36,37], have illustrated the importance of this interface in the activity for the water gas shift reaction. While there is still a debate on the dominant reactive pathway, a large amount of evidence seems to suggest that the redox mechanism is dominant [38].

The elimination of hydrocarbons is shown in equations 1.9-1.11. Each reaction listed is the elimination of the HC with different oxidants. In general, for the oxidation reaction, the hydrocarbon adsorbs on the catalyst surface, and is then oxidized piecemeal by adsorbed NO_X or O_2 on the surface. It was suggested by Burch *et al.* that the most important fundamental step is the activation of the first C-H bond [39]. They claimed that, after this initial activation, the sequential oxidation of the hydrocarbon is "relatively facile." Still, a multitude of potential reactive intermediates have been suggested during the oxidation of hydrocarbons [40]. The elimination of hydrocarbons is distinct from the elimination of CO due to the presence of numerous fundamental steps. This can result in several intermediates that are sufficiently stable for desorption, such as CO and lower chain hydrocarbons.

$$C_XH_Y \quad + \quad O_2 \quad \rightarrow \quad CO_2 \quad + \quad H_2O \qquad\qquad (1.9)$$

$$C_XH_Y \quad + \quad NO_X \quad \rightarrow \quad CO_2 \quad + \quad H_2O \quad + \quad N_2 \quad (1.10)$$

$$C_XH_Y \quad + \quad H_2O \quad \leftrightarrow \quad CO_2 \quad + \quad H_2 \qquad\qquad (1.11)$$
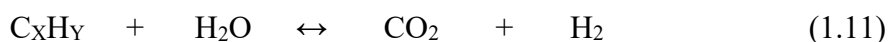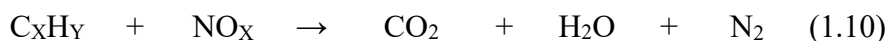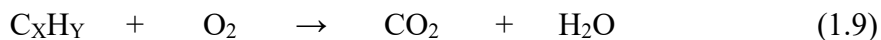
The reactions that participate in the elimination of NO_X are shown in equations 1.12-1.14. The reduction of NO_X is generally considered to occur through the adsorption and reduction of NO or NO_2 on the PGM surface. The reduction of adsorbed NO is

caused by the interaction with H, CO, or hydrocarbon adsorbates on the PGM surface, leaving an N atom adsorbed on the surface. An alternative to the reduction of NO adsorbed on the surface is the dissociative mechanism discussed at length by François Garin [41]. In this mechanism, the adsorbed NO can simply dissociate into N and O on the surface, followed by the scavenging of the adsorbed O species by reductant species. Regardless of the mechanism of generation, the adsorbed N species can recombine with each other to form N_2. However, the adsorbed N atoms can also react with other species on the surface. If an adsorbed N atom reacts with an adsorbed NO species, they can desorb as N_2O [42,43]. Alternatively, if the N atom reacts with H atoms on the surface, it can be hydrogenated to form NH_3. In a real exhaust system, when the engine operates at a low AFR, more NH_3 will be produced, while a higher AFR will result in NO_X breakthrough.

$$NO_X \quad + \quad CO \quad \rightarrow \quad N_2 \, (N_2O, NH_3) \quad + \quad CO_2 \qquad (12)$$

$$NO_X \quad + \quad H_2 \quad \rightarrow \quad N_2 \, (N_2O, NH_3) \quad + \quad H_2O \qquad (13)$$

$$NO_X \quad + \quad C_XH_y \quad \leftrightarrow \quad N_2 \, (N_2O, NH_3) \quad + \quad H_2 \qquad (14)$$

The literature presented here shows a complex and interconnected network of reactions. Even when considering isolated reactions on individual components, much of the literature is still in disagreement as to the fundamental reaction steps taking place. When all of the reactions are taking place at the same time, with multiple potential reductants and oxidants, the complexity is increased dramatically. Understanding the reactions taking place on a TWC is further complicated by the fact that the operating conditions, both temperature and chemical composition, can change dramatically during

operation. Even in a stoichiometrically operated engine, there will always be fluctuations in the operational AFR [44]. AFR value changes the concentration of both oxidants (NO_X and O_2) and the reductants (CO, H_2, and HCs) in engine exhaust. This can alter the conversion of various pollutants, as well as the products that result from their conversion. When operating even slightly rich, CO and HC emissions increase drastically, and NO_X emissions are converted to NH_3. Likewise, when operating under a lean AFR, NO_X becomes very difficult to reduce.

1.3 Three-way catalyst composition

The active metals used in the TWC formulation can have a strong effect on the activity for these various reactions. The most common components are Pd, Pt, Rh, Ce, and Ba. The primary active metal on TWCs is generally Pd and/or Pt. These noble metals have very good activities for the primary reactions, particularly the oxidation of HCs and CO [25]. Pt was the standard TWC material for a long time. This is due to Pt's high activity for the three primary reactions as well as its high resistance to chemical deactivation from sulfur and other contaminants in engine exhaust. This activity was often supplemented with a small loading of Rh, to provide the catalyst with additional activity for NO reduction [45]. Pd catalysts saw widespread implementation more recently to lower costs of TWCs. While much of the initial interest in Pd catalysts was economic, they have proven to have several advantages over the more traditional Pt/Rh TWC. Pd catalysts have shown improved hydrothermal stability and increased activity for the conversion of hydrocarbons. However, these catalysts have also shown increased susceptibility to chemical poisoning by contaminants in the exhaust, such as SO_2. Thus,

as gasoline composition regulations become stricter, the drawbacks of Pd catalysts continue to be diminished. However, in recent years, Pd prices have increased to match those of Pt, so the economic benefits have diminished. Currently, many commercial TWC formulations will include some loading of all three components.

In addition to the PGM loading, modern automotive catalysts will often include Ce and/or Ba for oxygen storage or NO_X storage, respectively. Ce was first suggested as a promoter for TWCs in 1982 by Gwan Kim [46]. Since then, Ce has seen widespread implementation as both an oxygen storage material and a catalytic promoter [47,48]. It acts as an oxygen storage component due to the Ce^{3+}/Ce^{4+} redox cycle. The storage of oxygen is very important for the treatment of gasoline engine exhausts. Because a stoichiometrically operated engine has small fluctuations between slightly rich and slightly lean, the presence of an oxygen storage component allows for the catalyst to use stored oxygen when the engine exhaust is slightly rich, and for it to regenerate the stored oxygen while the exhaust is slightly lean [49]. Beyond its use as an oxygen storage component, Ce acts as a promoter in several areas. First, it improves the stability of the catalyst through increased hydrothermal resistance to PGM particle sintering and support decomposition [50]. Second, it is essential in the TWC's activity for the water gas shift reaction. It has been shown that the interface between the PGM and ceria is far more active than the interface between the PGM and alumina. These interface sites have also been shown to have lower activation energy for CO oxidation. Furthermore, Ce has been shown to decrease CO light off temperature due to electronic interactions with the PGM particles. In many catalyst formulations, the activity of Ce is promoted by incorporating Zr. When Zr is incorporated into Ce, its stabilization effects and oxygen storage behavior

are both significantly improved [48,51]. The mobility of oxygen through bulk Ce-Zr is also more active than that of Ce alone [52].

NSR catalysts for lean-burn gasoline engines require a large amount of NO_X to be stored on them during lean operation [7]. Ba performs well as a NO_X storage component due to the fact that it readily forms barium nitrates ($BaNO_3$) on its surface [53,54]. Then, during the rich catalyst regeneration, the $BaNO_3$ species decompose into NO_X which is reduced after its release. By this consistent, reversible process, the catalyst can eliminate the majority of NO_X emissions throughout its useful life. While storage materials, such as Ce, Ce-Zr, and Ba provide essential functionality in the control of emissions, they also present additional challenges. These storage materials strongly bind sulfur species present in the exhaust, resulting in steady deactivation of the catalyst throughout its operation [55–57].

1.4 Evaluating three-way catalysts for passive selective catalytic reduction

In literature, most applied TWC evaluations are conducted under stoichiometric or fuel lean conditions. Stoichiometric conditions are used to simulate the operation of a standard gasoline engine, while lean conditions are used to simulate the operation of diesel or lean-burn gasoline engines. Evaluating catalysts for Passive SCR presents unique challenges when compared to these stoichiometric or lean evaluations. The operation of a passive SCR system requires long-term rich operation, during which the direct oxidation of all reductants will not be possible. Therefore, the activity of water gas shift and steam reforming reactions are significantly more important to control CO and HC emissions in comparison to stoichiometric or lean operation. Furthermore, relatively

little of the extensive TWC research has been conducted on the production of NH_3 which is essential in the operation of a passive SCR system.

The production of NH_3 through the reduction of NO_X has long been seen as a reaction route to be minimized in order to prevent excess NH_3 production. However, since the passive SCR system has been proposed, research has been conducted on the promotion of NH_3 production on TWCs, optimizing reaction conditions and catalyst formulations to maximize NH_3 yield and further understand the underlying effects [58]. The reaction mechanism for NH_3 production from NO_X and H_2 over Pd was investigated by Rahkamaa-Tolonen *et al.* [59]. They suggested that NH_3 was produced primarily through the sequential hydrogenation of surface N species by surface H species. As discussed above, the N species are produced through the reduction of NO on the surface, while H species are produced primarily through the dissociative adsorption of H_2. Work by Oh and Triplett showed that the presence of CO in the exhaust stream can have beneficial effects on the reduction of NO_X to NH_3 on Pd-based TWCs [60]. They found that the presence of CO can lead to the production of additional H_2 via the water gas shift reaction. Also, CO can aid in the reduction of NO, meaning that less H_2 is required to fully reduce the NO to NH_3. It is possible that the addition of CO is also leading to the creation of isocyanate species on the surface. The hydrolysis of these species has been suggested as another NH_3 production mechanism, and was researched extensively my Mark Unland in the 1970's [61–63]. In this mechanism, surface N species react with adsorbed CO to form an isocyanate. This isocyanate can then be hydrolyzed by adsorbed H_2O, forming NH_3. The comparative contribution of sequential hydrogenation and isocyanate hydrolysis is still contested in the literature, though it is likely that their

contribution is heavily influenced by the temperature and the reductants present in the exhaust [58,60,64].

A study by Adams et $al.$ focused on NH_3 production on supported Pt and Pd catalysts [65]. They found that both Pt and Pd on Al_2O_3 were very effective for the production of NH_3. However, it was determined that Pd catalysts were more effective due to their increased activity for WGS and the potential for reactive intermediates, such as isocyanates, to form on the surface. Furthermore, previous studies within this research project have used simulated exhaust studies to show that TWCs can produce the required NH_3 during fuel rich operation to reduce NO_X emissions, and still have up to 10% increased fuel economy [66]. These results were validated through testing on a real engine [67]. This work has shown that NH_3 production over TWCs is a viable route for the delivery of NH3 to an SCR catalyst. However, for passive SCR to become commercially viable, the system must be able to continue to perform even after physical and chemical deactivation. Physical deactivation is caused by the harsh hydrothermal conditions in the exhaust stream where temperatures can reach an excess of 900°C, leading to extensive catalyst sintering and loss of activity. Chemical deactivation is caused by the presence of chemical species, particularly lead, phosphorus, and sulfur, which bind strongly to the catalyst, leading to blocked sites, formation of stable inactive species, and structural degradation.

When evaluating TWCs in this work, there are several key gas phase species that are relevant in a passive SCR system. These fall into two categories: nitrogen species and reductants. The nitrogen species monitored are NH_3, NO_X, and N_2O, while the reductants measured are H_2, CO, and C_3H_8. Monitoring the nitrogen species illustrates the extent of

NO_X reduction over the TWC. The inhibition of NO_X reduction can prevent the formation of NH_3 and increase the formation of N_2O. Meanwhile, monitoring the reductants, and their relative concentrations, can help elucidate changes in the activity of secondary reactions, such as the water gas shift and steam reforming reactions.

NH_3 production is necessary for the passive SCR system to function, therefore maximizing its production during the rich phase is a primary objective. Monitoring NO_X is also necessary for TWC evaluation. NO_X in the lean phase is not expected to be reduced over the TWC, it can be reduced over the downstream SCR catalyst. However, NO_X slip in the rich phase is a much greater concern. The SCR of NO_X, as discussed above, functions through a redox cycle, which requires oxygen to be present. Therefore, if any NO_X is not converted over the TWC in the rich phase, it will likely not be reduced over the SCR catalyst. The final nitrogen species being monitored is N_2O, which is a very strong greenhouse gas. While N_2O is rarely found in engine-out exhaust, it can be produced over the TWC through partial reduction of NO_X. Previous literature on NSR systems has found that the formation of N_2O can be a significant concern during the transition from lean operation to rich operation [9,68].

On the reductants side, the key gas phase species are CO, C_3H_8, and H_2. CO, while it can be beneficial to the reduction of NO_X to NH_3, should be minimized in the rich phase. Since the rich phase will have insufficient oxidants for the conversion of CO, this is accomplished through the water gas shift reaction to convert CO and H_2O to H_2 and CO_2. It is aksiC$_3$H$_8$ is used to simulate unburned hydrocarbons in these experiments due to its prevalence in automotive exhaust and its difficulty in being oxidized during lean phase operation compared to similarly prevalent hydrocarbons. Much like rich phase

CO control through the water gas shift reaction, C_3H_8 control in the rich phase is primarily through the steam reforming reaction. The production of H_2 through both the steam reforming and water gas shift reactions is very beneficial for the production of NH_3, as shown in previous literature [69,70]. Thus, while the CO and C_3H_8 emissions should be minimized during rich operation, H_2 should be maximized.

.

CHAPTER 2

EXPERIMENTAL

2.1 Experimental Techniques

2.1.1 Scanning Transmission Electron Microscopy (STEM)

Electron microscopy is a powerful tool for the characterization of catalytic materials. In this work, STEM is used for imaging and elemental mapping of the catalyst surface on a nm scale. Specifically, images are collected using High Angle Annular Dark Field (HAADF) imaging and energy dispersive X-ray (EDX) spectroscopy. STEM works by taking a concentrated beam of electrons and scanning that beam over the catalyst surface in a raster pattern. A detector is positioned on the opposite side of the sample. This detector is used to create an image of the catalyst based on the intensity of the electrons.

HAADF images are obtained by contacting the catalyst sample with the electron beam at a high angle. The electrons are scattered incoherently through the Rutherford scattering mechanism. This leads to an image with a strong Z-contrast. Images obtained from HAADF can help differentiate between elements with very different Z values, issues arise when elements have similar molecular weights or heavier elements are used in the support. This creates a situation where the intensity from the support can saturate the image and prevent the identification of lower molecular weight particles on the surface. EDX can be used to accurately determine the presence of individual elements across the catalyst surface, even when many elements are present. When an element is

contacted with the high energy electron beam, it releases a characteristic x-ray emission. These x-rays are detected at each location for the STEM and can be used in conjunction with the z-contrast images obtained from HAADF to increase the confidence in the identification of specific elements on the catalyst surface.

The STEM images used in this work were obtained from the FEI Talos F200X S/TEM system at the Oak Ridge National Laboratory Low Activation Materials Development and Analysis (LAMDA) facility [71]. It is a 200 keV S/TEM, equipped with an XFEG high-brightness Schottky-type field emission gun electron source. The system has four STEM detectors: three detectors used for high-angle, medium-angle, and low angle annular dark field imaging and one detector used for bright-field imaging. In addition to the STEM detectors, the system includes four silicon drift detector units arranged symmetrically around the sample used for EDX.

2.1.2 X-Ray Diffraction

XRD is a technique that allows for the characterization of crystalline materials. When a monochromatic x-ray beam of a known wavelength (λ) is fired at a crystalline surface, the angle (θ) at which constructive interference occurs can be used to determine the spacing between individual atoms (d) in a crystal plane. This relation is called Bragg's Law and is shown in equation 2.1. Each XRD spectra will contain several peaks corresponding to the d-spacing in different crystal planes. This d-spacing is characteristic of individual elements and can be used to identify not only what elements are present, but also the presence of any alloys.

$$n\lambda = 2dsin(\theta) \qquad\qquad (2.1)$$

The intensity and width of these XRD peaks are also useful in catalyst characterization. The width of a peak on a 2θ scale at half its maximum intensity (also called the full-width at half maximum or FWHM) is inversely proportional to the degree of crystallinity in the sample. This is because, when the number of crystal planes is limited, the range of angles that can be diffracted is increased. When the x-ray wavelength (λ), angle of diffraction (θ), and the FWHM in radians (β) are known, the crystallite size (τ) can be determined using Scherrer's equation shown in equation 2.2. This equation also includes a shape factor (K), that is determined by the shape of the crystallites in the sample.

$$\tau = \frac{K\lambda}{\beta \cos(\theta)} \qquad (2.2)$$

2.1.3 Fourier Transform Infrared (FTIR) Spectroscopy

FTIR is a useful technique for the identification of chemical species and their concentration in catalyst evaluation. Infrared spectroscopy works by measuring the wavenumbers of infrared radiation that are absorbed by a sample due to its vibrational states. Specifically, infrared spectroscopy selects for vibrational modes that correspond to a change in the dipole moment of the analyte. What differentiates FTIR is the use of an interferometer, which allows for the entire IR spectra to be measured simultaneously in the form of an interferogram. This interferogram undergoes a Fourier Transform which results in the final spectra.

In this work, gas phase FTIR is conducted with an MKS MultiGas 2030 FTIR Continuous Gas Analyzer. The infrared source is Silicon Carbide @ 1200°C. The

reference laser is a Helium Neon laser with a wavenumber of 15798.2cm^{-1}. The IR detector is a mercury cadmium telluride (MCT) detector cooled by a liquid N_2 reservoir. The system contains a 200 mL volume and 5.11 m pathlength multi-pass gas cell. The cell is constructed from nickel-plated aluminum, while the mirrors are coated in gold. The windows for the gas cell are zinc selenide to prevent degradation. The system is capable of a 5hz scanning rate, with a detection limit of ~1ppm for most species of interest.

2.1.4 Mass Spectrometry

Mass spectrometry is a technique for the identification of chemical species based on their molecular mass. By ionizing molecules and accelerating them through a tuned electric field, individual mass/charge ratios can be isolated. These are then detected using a secondary electron multiplier (SEM). This theoretically allows for the detection of any gas in the 1-200 amu range. However, due to the extensive overlap of molecular weights and the tendency for molecules to fragment in mass spectrometry, there is a significant amount of cross sensitivity when multiple gases are present.

In this work, a Pfeiffer Vacuum PrismaPlus mass spectrometer is used in conjunction with gas phase FTIR for residual gas analysis during catalyst evaluation in a cycling reactor system. Mass spectrometry is useful in this regard because it can detect chemical species, such as O_2 and H_2, that cannot be detected through FTIR, while FTIR can be used to accurately detect many different chemical species present. Both measurement techniques also provide good time resolution to capture transient activity during cycling

2.1.5 Wet Impregnation

Wet impregnation is a catalyst synthesis method used in this work to synthesize a range of model $Pd/CeO_X/Al_2O_3$ catalysts. Wet impregnation involves adding a known mass of catalyst support into a solution with a known concentration of metal precursor. This mixture is then dried to remove moisture which results in the deposition of metal precursor onto the dried support. After deposition, the catalyst is calcined at high temperature to stabilize the metal deposited on the surface and remove contaminants. Finally, the catalyst is often reduced to remove metal oxides and other contaminants that were not removed under calcination conditions.

2.2 Catalysts and Reactors

2.2.1 Commercial Catalyst Formulations

Commercial catalysts were used to evaluate the effects of hydrothermal aging and sulfur exposure on TWCs in passive SCR. Catalyst samples were cut from fully formulated commercial catalyst monoliths in 2 cm diameter, 5 cm length cylindrical cores. Table 2.1 gives an overview of the two catalysts evaluated. The Pd-TWC sample was taken from the front end of a dual zone TWC inside a 2009 PZEV (Partial Zero Emissions Vehicle) Chevrolet Malibu. It contains Pd as the primary active metal on the surface, but also contains low loadings of other metals, including Ce and Ba, as promoters. The NS-TWC sample was provided by Umicore. While the NS-TWC still has a significant loading of Pd, the catalyst also contains Pt and Rh, as well as significant amounts of Ce for oxygen storage capacity (OSC) and Ba for NO_X storage capacity (NSC).

Table 2.1: Commercial catalyst formulations

Description	Pt (g/L)	Pd (g/L)	Rh (g/L)	OSC	NSC
Pd-TWC	0	7.33	0	Low	Low
NS-TWC	2.47	4.17	0.05	High	High

These two catalysts are used extensively throughout this work and were chosen based their high performance in previous reactor studies at Oak Ridge National Laboratory [72]. In these reactor studies, the Pd-TWC showed better high temperature activity than any other formulation evaluated, maintaining high NH_3 production up to 650°C. Under the same conditions, the NS-TWC showed better low temperature activity than the other catalyst formulation tested. This is attributed to the NSC, which allows the catalyst to store NO_X in the lean phase, extending the amount of time running lean. However, the NS-TWC's performance suffered at higher temperatures (>550°C), where the Ba is not as active for NO_X storage, and the Ce is still active for oxygen storage. This leads to longer reduction times during the transition from lean to rich phase, causing longer rich times.

These two catalysts also illustrate two distinct approaches to the TWC component of a passive SCR system. The Pd-TWC has very low loadings of storage materials. Because of this, during lean/rich cycling, the Pd-TWC will rapidly transition to a steady state activity after the operating condition changes. In contrast, the NS-TWC has substantial amounts of both OSC and NSC. This could be very beneficial because a passive SCR system undergoes constant lean/rich cycling, much like an NSR system. This can allow for the storage of NO_X in the lean phase, and the usage of stored NO_X to form NH_3 in the rich phase, further improving fuel efficiency. However, many of the

same problems that generally effect NSR systems could also hamper the performance of the NS-TWC such as N_2O and NO_X emissions during transition from lean to rich operation.

2.2.2 Steady state reactor

A flow reactor was used for the steady state evaluation of commercial catalyst samples in this work. The system is equipped with MKS 1179A Mass-Flo controllers to control the flow of reactor gases including O_2, CO, H_2, NO, SO_2, C_3H_8, CO_2, and N_2. Water is introduced to the system through an Eldex Optos HPLC pump. The catalyst is loaded into a 25 mm diameter quartz tube reactor, which is heated by a Thermo Scientific Lindberg/Blue M TF55035C tube furnace. The catalyst itself lies outside of the heated zone, in a heavily insulated area as shown in figure 2.1. In this case, the furnace acts much like a gas preheater, rather than heating the catalyst directly. This more closely simulates the realistic operation of a TWC, where the catalyst itself is unheated, which leads to more realistic temperature profiles during operation. An omega k-type thermocouple is used to monitor the temperature of the gas entering the catalyst, and three more are used to monitor the catalyst temperature at the inlet, the middle, and the outlet.
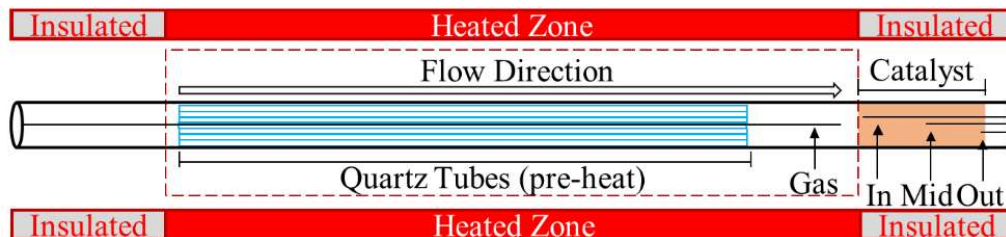
Figure 2.1: Standard reactor configuration

2.2.3 Cycling Reactor

Cycling activity of catalyst monolith samples is measured in a flow reactor controlled through a LabVIEW program. The apparatus is equipped with 13 MKS 1479A Mass-Flo controllers to control inlet gases. Water delivery is handled through an Eldex Optos HPLC pump. The water is introduced through a capillary tube heated to 250-350°C to vaporize it before introduction into the carrier gas. The carrier gas temperature is maintained at ~200°C to prevent water condensation. After water introduction, the reactive gases are added to the gas mixture before the introduction to the catalyst. The catalyst is housed in a 25mm quartz tube heated by a Thermo Scientific Lindberg/Blue M TF55035C tube furnace under the same configuration shown in Figure 2.1. While the bulk of the reactor effluent is flowed into the gas phase FTIR for analysis of most gas phase species, a small sample is pulled through a capillary tube to determine the concentration of H_2 and O_2 by mass spectrometry. The FTIR used is the MKS Multigas 2030HS, outlined in section 2.1.3. The mass spectrometer is a Pfeifer Vacuum PrismaPlus, outlined in section 2.1.4. The backgrounds for both of these instruments is taken in pure N_2 flow.

Because this system is designed to measure the cycling activity of a catalyst sample, it is necessary to be able to consistently and quickly switch between lean and rich phases. A LabVIEW program controls the switching in automated cycles. The switching itself is conducted through pneumatically actuated 1/8-inch Valco medium temperature switching valves. These allow for switching times of < 0.5 seconds with ideally zero dead volume. The LabVIEW program is capable of automated cycling based on a variety of

conditions. The conditions used in this work are timed cycles and integrated cycles. During timed cycles, rich phase time and lean phase time are designated, and the program switches between the lean and the rich phase based on that timing. During integrated cycling, the cycles are controlled through the integration of FTIR or mass spectrometer signals. During passive SCR tests, the lean phase is controlled through the integration of the combined NO and NO_2 signal (NO_X), while the rich phase timing is controlled through the integration of NH_3 as shown in figure 2.2. This is beneficial for the evaluation of a passive SCR system because it assures that the requisite NH_3 to reduce the NO_X will always be produced. The program integrates the outlet NO_X during the lean phase, switching to the rich conditions when the total NO_X reaches 0.027 mol/L catalyst. Then, the program monitors the outlet NH_3, and switches back to the lean conditions when the total NH3 reaches the same 0.027 mol/L catalyst limit. This threshold was chosen because it corresponds to 25% of the NH_3 storage capacity on a Cu-zeolite catalyst of an equivalent volume.
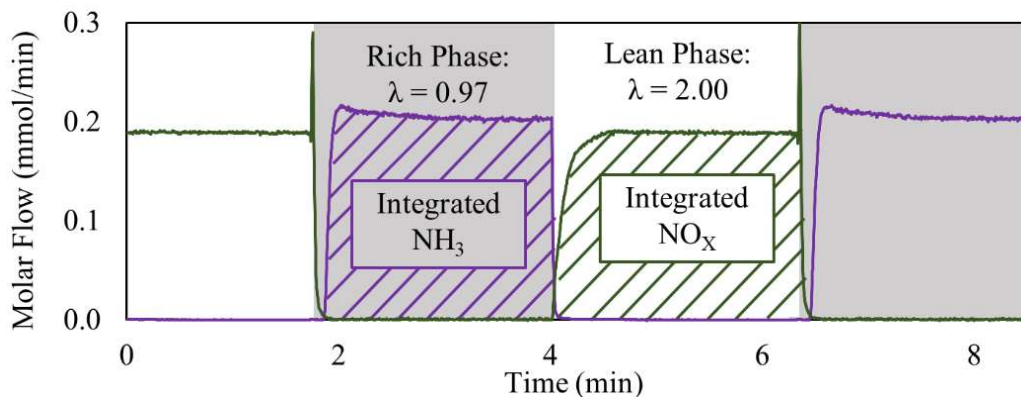
Figure 2.2: Time series data for NO_X and NH_3 showing automated integration and switching method used for feedback-controlled cycling

During operation, the consistency of the cycling as well as the calibration of the chemical measurement is essential for the evaluation of these catalysts. To this end,

before each evaluation, a bypass run is conducted to ensure consistency of cycling measurements as well as provide calibration points for the interpretation of FTIR and mass spectrometry data. Figure 2.3 shows the signal for CO from FTIR and H_2 from mass spectrometry. The signal for CO shows very consistent readings, matching very close to the 0.2% and 1.6% targets for lean and rich operation, respectively. The H_2 signal must be normalized to the desired concentrations of 0% and 0.8% in the lean and rich phase. The mass spectrometer signal can also show variations, and the signal can be altered based on other chemicals present in the gas mixture. This is corrected by the operation of a bypass run using simulated exhaust before each reactor evaluation. This gives a two-point calibration for the lean and rich H_2 concentrations being used. The H_2 signal during operation can then be normalized to the bypass.
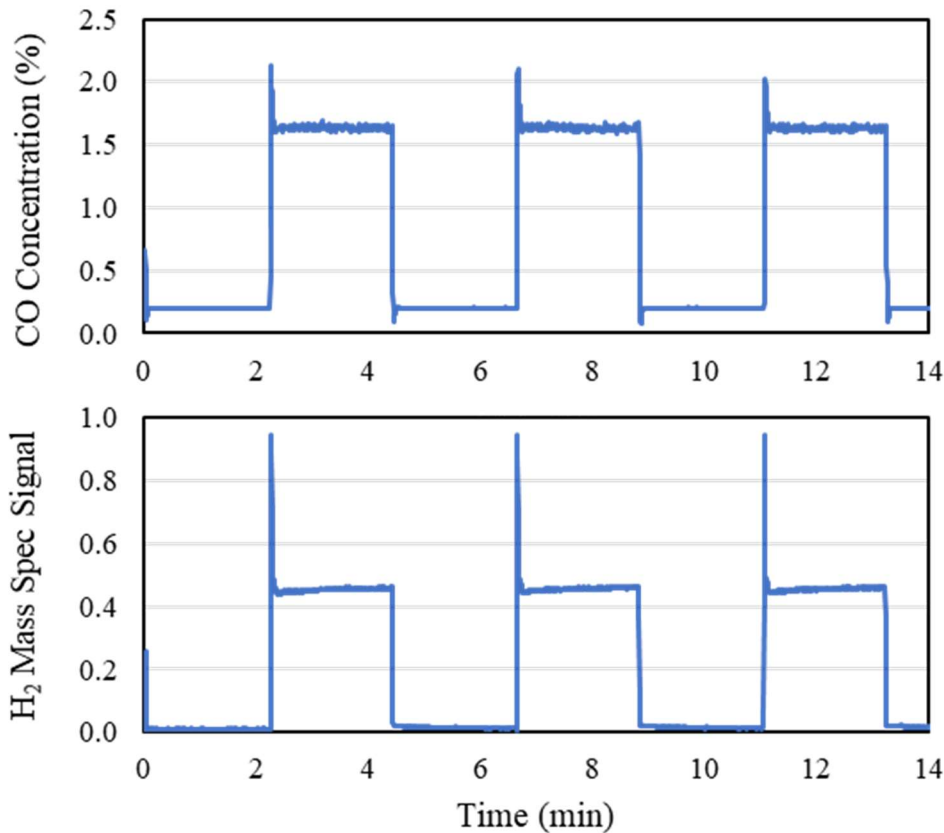
Figure 2.3: Bypass signal for CO from FTIR and H_2 from mass spectrometry.

CHAPTER 3

THE EFFECTS OF HYDROTHERMAL AGING ON THREE-WAY CATALYST PERFORMANCE IN PASSIVE SELECTIVE CATALYTIC REDUCTION SYSTEMS

3.1 Introduction

Hydrothermal aging of TWCs has been a major concern since their inception. Research throughout the years has shown that metal sintering is one of the primary sources of catalyst deactivation during operation [73,74]. Researchers have looked at several methods to reduce metal sintering in TWCs, from promoters to the effects of different supports [75,76]. However, to date, there has not been an adequate method for maintaining small particles in realistic exhaust conditions due to the harsh hydrothermal conditions present. As such, an increase in metal particle size on the TWC will always occur during regular operation and continue throughout the useful life of a TWC [77]. Another consideration is the loss of interaction between the active metal and the oxygen storage component (OSC) present on the catalyst. The interaction between these species is beneficial for low temperature CO oxidation as well as the water gas shift and steam reforming reactions [78]. Beyond the sintering of the metal on these catalysts, the species responsible for oxygen storage (Ce) and NO_X storage (Ba) can also deteriorate. Under aging conditions, ceria loses a large amount of surface sites from phase segregation and agglomeration on the surface [52,78]. NO_X storage capacity (NSC) suffers from degradation through a different mechanism. While the barium does lose surface sites

27

from sintering, the majority of its deactivation comes from the formation of barium aluminate and barium cerate at elevated temperatures [79,80]. The formation of these stable mixed metal oxides prevents the formation of barium nitrate, thus reducing the potential NO_X storage on the catalyst.

The effects of hydrothermal aging on the SCR catalyst is also a concern. Previous work has shown that some Cu-zeolite SCR catalysts can degrade under hydrothermal conditions, particularly Cu-ZSM-5 [81,82]. However, as illustrated by Fickel *et al.* some small-pore Cu-zeolite formulations can show high hydrothermal resistance [19]. While the effects of SCR catalyst aging will be a concern for the real-world implementation of a passive-SCR system, the evaluation of these effects is outside of the scope of the current work.

Here, we examine the effects of 100 hours of four-mode hydrothermal aging on two commercially formulated TWCs for the purposes of implementation into a passive SCR system. This aging procedure exposes the catalyst to stoichiometric CO oxidation conditions in addition to periodic oxidizing and reducing conditions. These periodic oxidizing and reducing conditions are essential to model the aging of a catalyst in a passive-SCR system, where lean/rich cycling is a continuous process during operation. The metal particle size and CO light-off temperature are monitored throughout the aging process. Furthermore, the activity of the fully aged catalyst samples is compared to the activity of degreened samples under both steady state and lean/rich cycling evaluations. The primary activities of concern in these evaluations are the conversion of CO, NO_X, and hydrocarbons, as well as the production of NH_3. Furthermore, in the lean/rich cycling experiments, changes in NO_X storage and oxygen storage are also monitored.

3.2. Experimental

3.2.1 Catalyst Formulations

The catalysts used in this work are those discussed in Chapter 2.2.1. The catalyst formulations are shown in Table 3.1.

Table 3.1: Commercial catalyst formulations

Description	Pt (g/L)	Pd (g/L)	Rh (g/L)	OSC	NSC
Pd-TWC	0	7.33	0	Low	Low
NS-TWC	2.47	4.17	0.05	High	High

3.2.2 Four-mode Hydrothermal Aging Procedure and Apparatus

The apparatus used to conduct catalyst aging utilizes four MKS Mass-Flo 1179A mass flow controllers to control the flow of UHP N_2, CO_2, CO, and O_2. The water is introduced through a temperature-controlled bubbler with N_2 flowing through it. The gases then flow through a Thermo Scientific Lindberg/Blue M TF55035C tube furnace with a 25 mm quartz tube reactor. Two O_2 sensors (LCAN N6) are installed at the inlet and outlet of the reactor. These allow for monitoring of the oxygen content and ensure proper cycling. Inside of the reactor tube, quartz rods are used to help preheat the gas, and the catalyst is insulated just outside of the heated zone of the furnace, as shown in Figure 3.1. This allows for the catalyst to be heated through the exothermic CO oxidation, and more closely resembles a real system, where the catalyst itself is not heated. Omega K-type thermocouples are used to measure the temperature of the inlet gas, catalyst inlet, catalyst mid bed, and catalyst outlet (Gas, In, Mid, Out, respectively). The mass flow rates, bubbler temperature, and furnace are all controlled through LabView on a connected PC. The O_2 concentration at the reactor inlet and outlet as well

as the temperatures measured by the thermocouples in the reactor tube are recorded through the same LabView program.
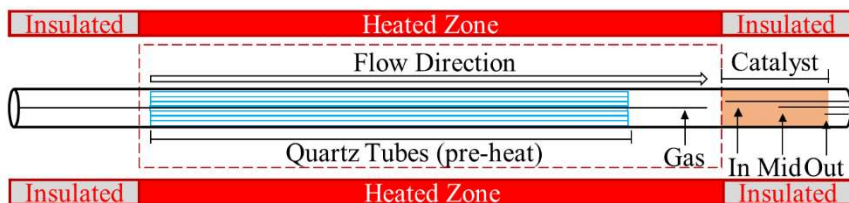
Figure 3.1: Hydrothermal aging reactor setup

Catalyst aging begins with a ramp up to aging temperature under stoichiometric operating conditions. Once it reaches the desired temperature, it is exposed to cycling conditions using the four-mode hydrothermal aging procedure shown in Table 3.2. The transition between the phases was controlled through the variation of O_2 and N_2 flow to maintain a constant space velocity. The first portion is a stoichiometric phase lasting for 330 seconds during which the catalyst is used for CO oxidation at 920°C in the presence of water. The second phase is a short fuel rich phase where the oxygen flow is turned off, leading to reduction of the catalyst. Next, the catalyst is again operated under stoichiometric conditions for 10 seconds before transitioning to the fourth phase: a short fuel lean phase, where the O_2 flow is increased, while the N_2 and, by extension, the H_2O are decreased to compensate. Catalyst samples were aged for 25, 50, and 100 hours using this procedure.

Table 3.2: Four-mode hydrothermal aging procedure

	Time	Temperature	H_2O	CO_2	CO	O_2	N_2	SV (hr^{-1})
Phase 1: Stoich	330s	920°C	10%	10%	2%	1%	Bal.	50,000
Phase 2: Rich	10s	890°C	10%	10%	2%	0%	Bal.	50,000
Phase 3: Stoich	10s	910°C	10%	10%	2%	1%	Bal.	50,000
Phase 4: Lean	10s	900°C	9%	10%	2%	10%	Bal.	50,000

Each sample was aged in five segments, with the temperature being ramped down and back up between each segment. This means that the 25 hr aged sample was ramped up to 920°C under stoichiometric conditions, aged for 5 hours using the aging procedure, and then ramped back down under stoichiometric conditions. Similarly, the 50hr aged sample was aged in 10 hr aging segments, and the 100 hr aged sample was aged in 20 hr segments. During the ramp up on each of these segments, the temperature in the catalyst mid bed (T_{Mid}) increases sharply as the exothermic CO oxidation reaction lights off, as shown in Figure 3.2. By monitoring the point that T_{Mid} intersects with T_{Gas} it is possible to determine changes in the light-off temperature. While this number is not equivalent to the standard measurements of T_{90} or T_{50}, it does give an idea of the qualitive changes in CO oxidation light off during the hydrothermal aging process.
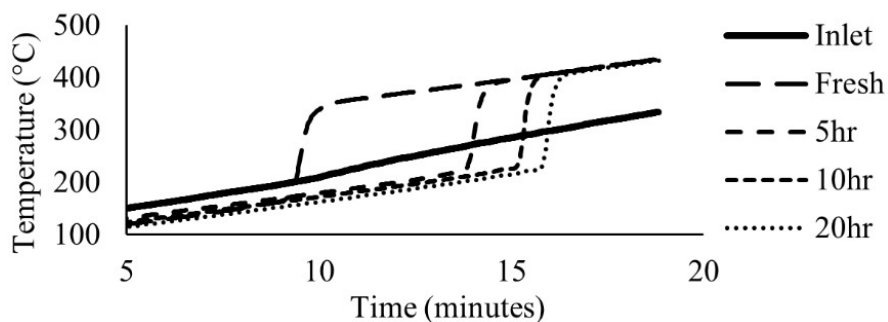
Figure 3,2: Light-off on the Pd-TWC during first 20 hours of aging

After 25, 50 and 100 hours of aging, palladium particle sizes were determined using both STEM and H_2 chemisorption measurements. Samples for this evaluation were obtained by grinding the catalyst monolith. STEM images were taken on the TALOS system at the Oak Ridge National Laboratory's Low Activation Materials Development and Analysis (LAMDA) facility [71]. The particle sizes were determined by sampling at

least 100 metal particles using a combination of high angle annular dark field (HAADF) images and energy dispersive x-ray spectroscopy (EDX) images. The chemisorption measurements were taken using H_2 titration on a Micromeretics AutoChem II Chemisorption Analyzer system with UHP H_2. The dispersion of Pd on the surface was determined, and particle size measurements were estimated assuming hemispherical metal particles.

3.2.3 Steady State Activity

Fresh and aged catalyst samples are evaluated in the steady state reactor outlined in Section 2.2.2. The catalysts are tested at 400°C under conditions simulating various λ values as shown in Table 3.3.

Table 3.3: Gas compositions simulating various λ values

λ	0.95	0.96	0.97	0.98	0.99	1.00
O_2 (%)	0.96	1.02	1.07	1.12	1.17	1.22
CO (%)	2.0	1.8	1.6	1.4	1.2	1.0
H_2 (%)	1.0	0.9	0.8	0.7	0.6	0.5
NO (%)			0.06			
C_3H_8 (%)			0.1			
H_2O (%)			11			
CO_2 (%)			11			
SV (hr^{-1})			27,000			

The reactor gas for these evaluations is composed of O_2, CO, H_2, NO, C_3H_8, H_2O, CO_2, and balanced with N_2 at a space velocity of 27,000 hr^{-1}. Values of λ are varied

through the flow of O_2, CO, and H_2. C_3H_8 is chosen as the model hydrocarbon due to its difficulty in being oxidized under lean conditions, which allows us to evaluate this approach under a worst-case scenario basis [66]. During evaluations, the outlet steady state concentrations of four components were analyzed: NH_3, CO, C_3H_8, and NO_X. From these concentrations, the conversion of NO, CO, and C_3H_8 were calculated, as well as the production of NH_3.

3.2.4 Cycling Activity

The activity of the catalysts after 100 hours of hydrothermal aging was evaluated under lean/rich cycling conditions in the cycling reactor outlined in Chapter 2.2.3. These catalysts were compared to catalysts degreened at 700°C for 16 hours in 10% O_2, 10% H_2O, balance N_2. The catalysts were tested under two separate cycling conditions, fixed load and load step. The fixed load condition simulates regular operation of the engine, where the same engine load is required for both the lean and rich phases. This means that the fuel being fed into the engine is constant, but during the lean phase, additional air is introduced to increase the λ value, leading to increased space velocity in the lean phase. Load step simulates the opportunistic production of NH_3 during periods of high load on the engine. During these periods, the fuel introduced into the engine is increased, resulting in higher space velocity and increased temperatures in the engine. This period of increased load leads to high levels of NO_X being present in the engine exhaust, allowing for a large amount of NH_3 to be produced and stored on the downstream SCR catalyst. These conditions are outlined in Table 3.4. Both conditions simulate cycling between a lean phase λ of 2.0 rich phase λ of 0.97, found to be the optimum in previous reactor and

engine experiments. Due to the lean/rich cycling, the temperature of the catalyst is changing constantly throughout the evaluation. Because of this, the results are reported as a function of the gas inlet temperature for all cycling experiments.

Table 3.4: Simulated exhaust cycling conditions

Fixed Load		Load Step		
Rich	Lean	Rich	Lean	
0.97	2.0	0.97	2.0	λ
1.07	10	1.07	10	O_2 (%)
1.6	0.2	1.6	0.2	CO (%)
0.8	0	0.8	0	H_2 (%)
0.06	0.036	0.12	0.036	NO (%)
0.1	0.06	0.1	0.06	C_3H_8 (%)
11	6.6	4.95	6.6	H_2O (%)
11	6.6	4.95	6.6	CO_2 (%)
27,000	45,000	60,000	45,000	SV (hr^{-1})

For the cycling experiments, several quantities were calculated. The NO_X storage was calculated by integrating the NO_X breakthrough during the transition from rich to lean. The oxygen storage was calculated by integrating the reductant breakthrough during the transition from rich to lean. The rich phase NH_3 yield was calculated by measuring the average NH_3 produced during the rich phase and comparing it to the inlet NO_X. Rich phase CO conversion was calculated by measuring CO slip during the rich phase and comparing it to the inlet CO. The average C_3H_8 conversion was calculated over both the lean and rich phase. To determine projected fuel consumption, in-engine fuel consumption for both fixed load and load step operation was measured directly on a lean-

burn gasoline engine under lean and rich conditions [83]. These numbers were then used to calculate the projected fuel consumption based on the amount of time running rich vs. lean using feedback-controlled cycling. These numbers assume that the downstream SCR catalyst is capable of storing and reducing the requisite NO_X during operation.

3.3 Results and Discussion

3.3.1 Hydrothermal Aging Progression

The four-mode hydrothermal aging procedure led to significant sintering of the active metal on Pd-TWC samples. The particle sizes were measured by both STEM and chemisorption at four stages during the aging procedure: a fresh catalyst sample, which has not been aged, as well as samples aged for 25 hours, 50 hours, and 100 hours. The sample that has been aged for 100 hours represents a catalyst at the end of its projected useful life. An example of the contrast between HAADF and EDX maps are shown in figure 3.3. This comparison illustrates the limitations of using exclusively HAADF to determine particle sizes as the z-contrast is not high enough. However, when EDX maps are implemented, the boundaries between different elements becomes clear, and individual particles can be measured.
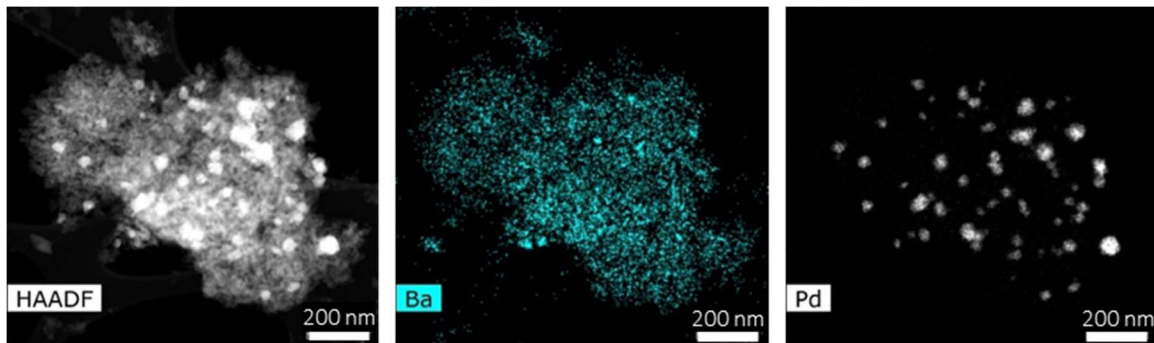
Figure 3.3: HAADF, Ba EDX map, and Pd EDX map on 50hr aged Pd-TWC sample

The particle size distributions for the Pd-TWC samples at each stage of aging, as well as the number of particles analyzed, and their average size are summarized in figure 3.4. As the catalyst is aged, the average particle size increases from 3.9 nm for the fresh catalyst, to 36 nm for the catalyst aged for 100 hours. In addition to the increase in average particle size, the particle size distribution also increases. As the catalyst is aged, the standard deviation of the Pd particle size increases from 0.8 nm to 13 nm.

Catalyst Aging Time	Number of Particles Sized	Average Particle Size	Standard Deviation
Fresh	110	3.9nm	0.8nm
25hr	126	22nm	7nm
50hr	199	30nm	11nm
100hr	170	36nm	13nm
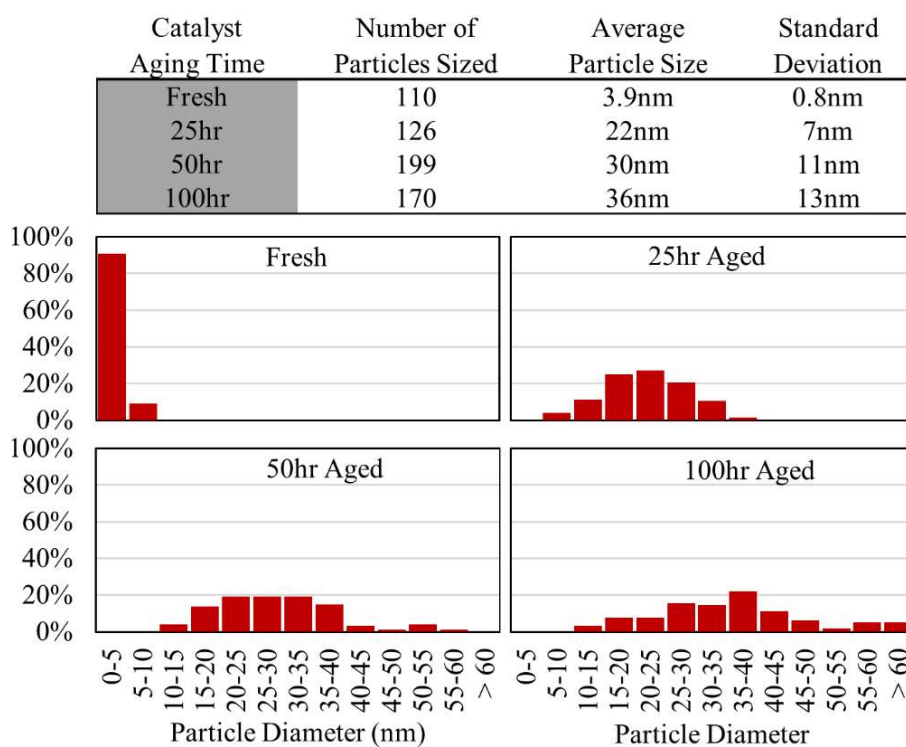
Figure 3.4: Particle size distribution from STEM for Pd-TWC samples

STEM results were supported by hydrogen chemisorption measurements on the catalyst samples. Particle sizes determined for Pd-TWC samples from both STEM and chemisorption tests are summarized in Figure 3.5. In contrast to STEM measurements, which are two dimensional pictures of catalyst particles, chemisorption measures the

metal dispersion and calculates the particle size assuming hemispherical particles. Despite the differences the measurement techniques, the calculated particle sizes show close agreement. While the average diameter of the metal particles is initially less than 5 nm, after 25 hours of aging, the particle size exceeds 20nm according to both chemisorption and STEM measurements. Continued aging leads to further increased particle sizes and after the full 100 hours of aging, the average particle size exceeds 30 nm regardless of method used.
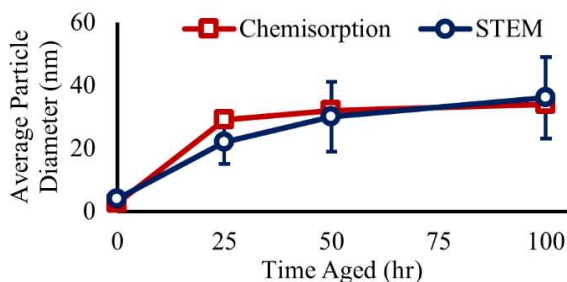
Figure 3.5: Particle sizing for the Pd-TWC
catalyst throughout aging

Aging also led to increases in CO light off temperature for both catalysts, which is a concern due to the potential increase in cold-start emissions [84–86]. Figure 3.6 shows the change in light-off temperature for both the Pd-TWC and the NS-TWC catalysts as monitored in the aging reactor. The light-off temperature rapidly increases during the first 5-10 hours of aging and remains constant for the remainder of the aging time. This is consistent with previous research, where smaller metal particles have been shown to be more active for low temperature CO oxidation because they can more closely interact with OSC on the catalyst [87,88]. Once the particles begin to sinter, this interaction becomes less effective, which leads to a sharp increase in light off temperature during the

initial 10-20 hours of aging. After this initial increase in light off temperature, the light

off temperature stays constant throughout the remaining aging time.
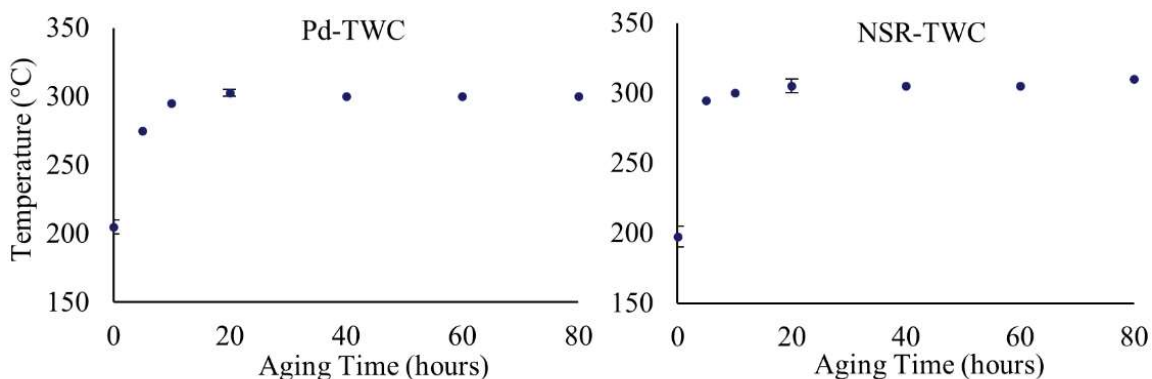
Figure 3.6: Light off temperature measurements taken during first 80 hours of aging for the Pd-TWC and the NS-TWC samples

3.3.2 Steady State Activity

The effect of hydrothermal aging on steady state activity was determined through experiments testing fresh catalysts and samples aged for 100 hours. These samples were tested under a range of λ values, as described in section 2.2. The results shown in Figure 3.7. illustrate the difference between fresh catalysts and aged catalysts. CO and C_3H_8 slip are increased strongly through hydrothermal aging on the Pd-TWC sample. This deactivation can be attributed to a combination of oxidation activities for the various reductants present in the simulated exhaust, as well as the water gas shift and steam reforming reactions. Small PGM particles improve the activity of these reactions through interactions with the OSC and by increasing the prevalence of interface sites between the PGM and oxide. Interactions between the OSC and the PGM are beneficial for the oxidation reactions, while the interface sites have been shown to be active for the water gas shift reaction [37,87]. When the catalyst is aged and both the PGM and OSC sinter,

these interactions are no longer effective, and the prevalence of interface sites is drastically decreased, leading to deactivation in each of these reactions.
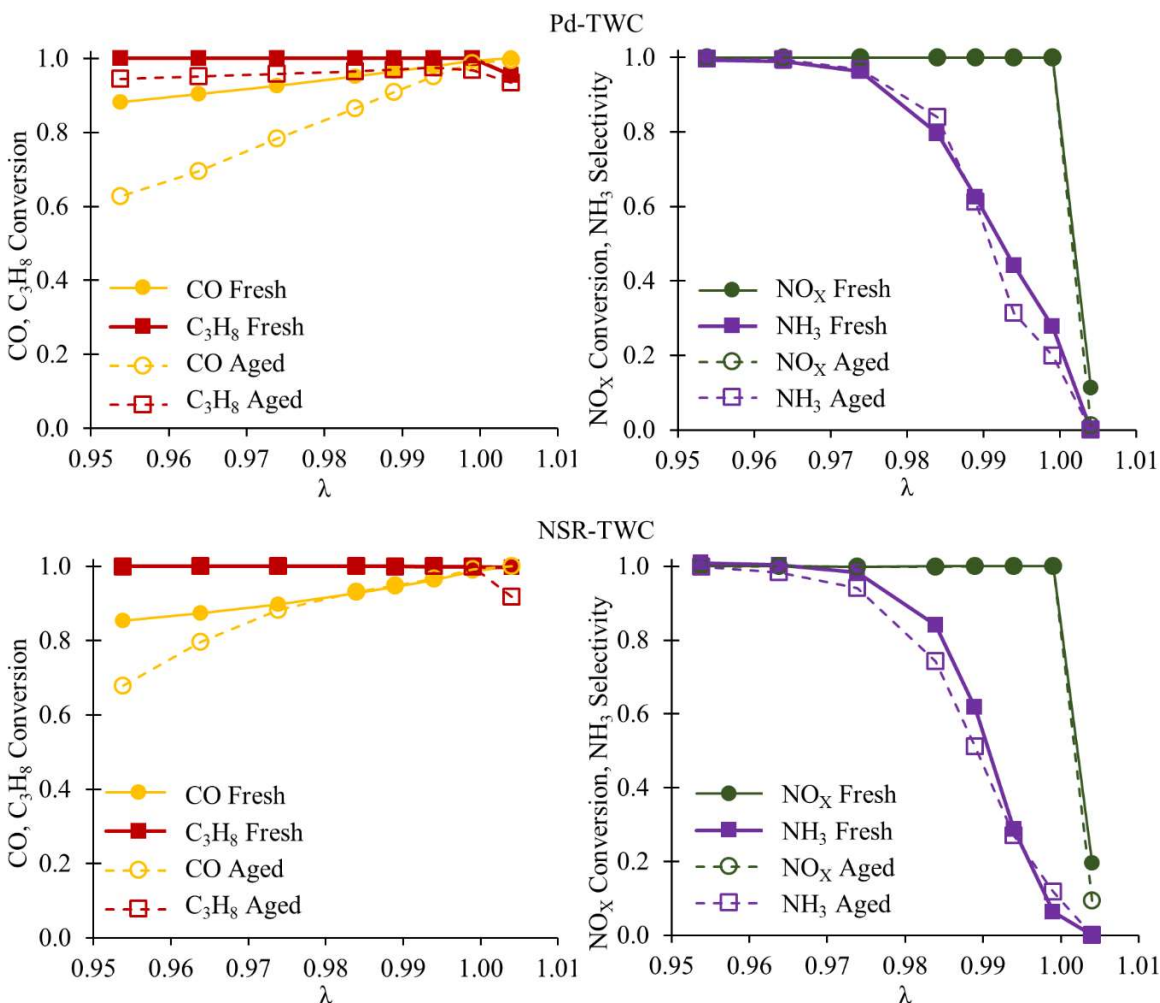
Figure 3.7: Steady state activity for the Pd-TWC (top) and the NS-TWC (bottom) at 400°C for λ values ranging from 0.95-1.01

Decreases in both CO and C_3H_8 conversion are also observed for the NS-TWC. However, the NS-TWC maintains near complete hydrocarbon conversion in the rich phase, even after the full 100 hours of aging. This is likely due to the increased activity for the steam reformation reaction originating from the increased ceria loading.

Furthermore, while the conversion of CO on the fresh NS-TWC sample was lower than the conversion on the fresh Pd-TWC sample, the effect of hydrothermal aging on the CO conversion over the NS-TWC is less than that observed on the Pd-TWC. This is particularly evident at λ values above 0.98, where the NS-TWC maintains the same conversion even after aging. Retention of catalyst activity is likely caused by the presence of substantially higher amounts of OSC on the NS-TWC, which leads to a higher amount of PGM-OSC interface sites, even after aging. This allows the NS-TWC to maintain its activity for oxidation, water gas shift, and steam reforming reactions.

In contrast to CO and C_3H_8 conversion, NO_X conversion is not strongly affected by hydrothermal aging, maintaining near 100% conversion at both stoichiometric and all rich λ values. Furthermore, the NH_3 selectivity is maintained at nearly 100% when operating at a λ lower than 0.98. While interface sites and OSC interaction will be more important for the removal of CO and C_3H_8, the same is not true for NO_X conversion and NH_3 production, both of which are active on the bulk PGM surface. Therefore, even though the catalyst undergoes extensive particle sintering, the available PGM surface is still sufficient for NO_X conversion and NH_3 production.

3.3.3 Cycling Activity

The activity of the catalysts under lean-rich cycling conditions was measured in a bench flow reactor capable of feedback-controlled cycling. The catalysts were cycled between λ values of 0.97 and 2.00, as outlined in Table 3.4. The measurements taken from the aged catalysts are compared to evaluations conducted on catalysts that were degreened at 700°C for 16 hours in a gas mixture of 10% O_2, 10%

H$_2$O, balance N$_2$. Time series data for the aged sample of the Pd-TWC under fixed load and load step conditions at 350°C are shown in Figure 3.8.
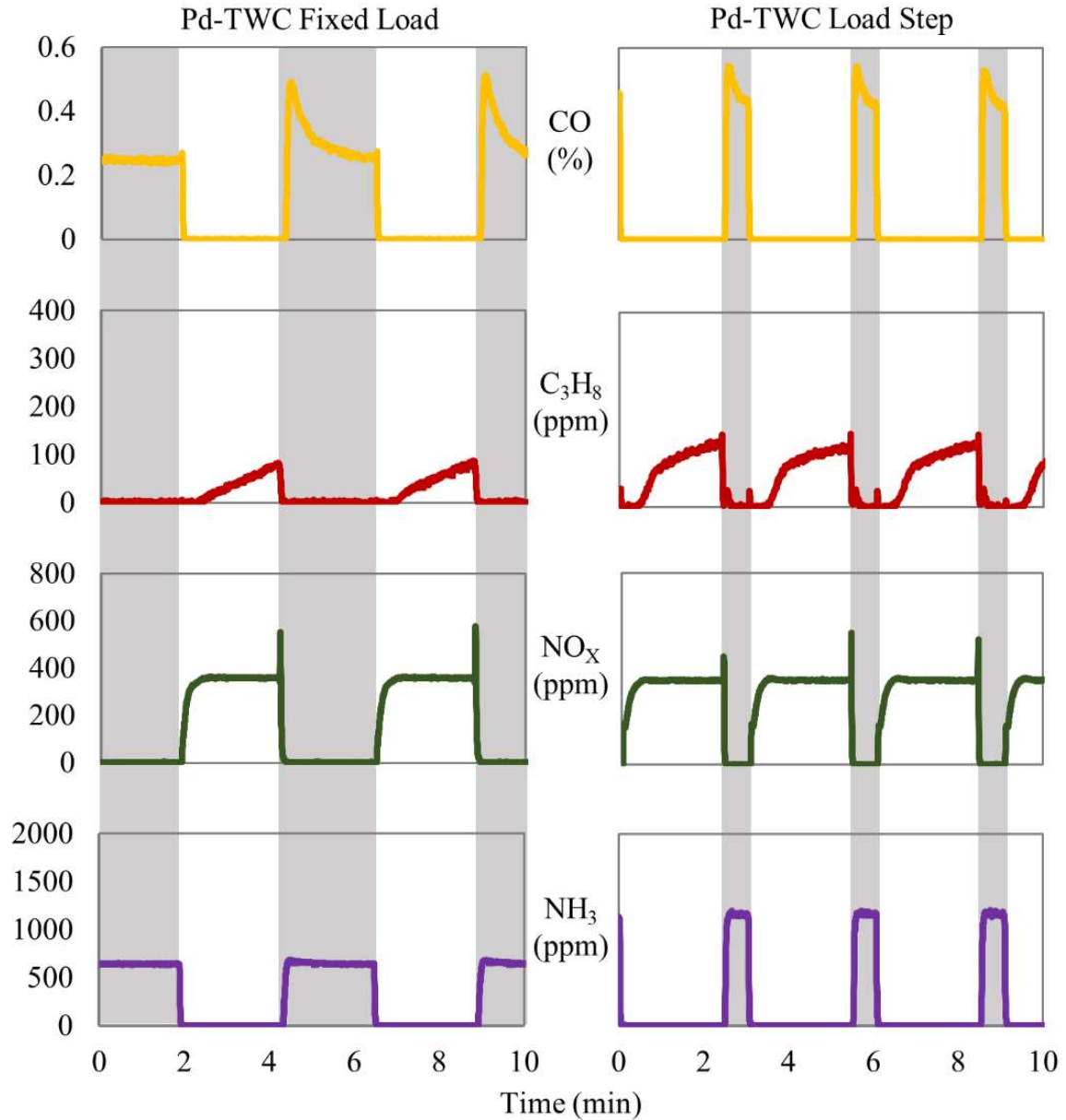
Figure 3.8: Time series data for fixed load and load step conditions on a hydrothermally aged Pd-TWC sample evaluated at 350°C.

Under fixed load conditions, where a constant load on the engine is simulated, the time spent in the lean phase and the time spent in the rich phase are relatively similar

because the NO_X flux in the system is constant. However, using load step, where the opportunistic generation of NH_3 during periods of high load is simulated, the rich phase is shorter because increasing the load on the engine results in greatly elevated NO_X flux, allowing for more NH_3 to be generated. These cycling experiments allow us to simulate catalyst performance under realistic operating conditions. They also allow us to capture the effects of hydrothermal aging on oxygen and NO_X storage capacity by studying the lean-rich transitions. This is particularly important for the NS-TWC, which includes significant levels of OSC and NSC, both of which showed significant deactivation during aging.

Figure 3.9 shows the strong deactivation of NSC from hydrothermal aging on both the Pd-TWC and NS-TWC. While the Pd-TWC does have a low loading of Ba that allows for the storage of NO_X, the NS-TWC stores significantly more NO_X under all conditions compared to the Pd-TWC samples. The NSC is heavily deactivated by the hydrothermal aging procedure shown here. At 350°C, the amount of NO_X stored on the aged NS-TWC sample is roughly 25% of that on the degreened sample. This is significant because it inhibits the primary advantage of using an NSR-type catalyst for passive SCR: using NSC to prolong the lean phase. The deactivation mechanisms of the NSC have been studied by previous researchers [79,80]. It has been shown that the primary mechanism for the loss of NSC is the formation of barium aluminate and cerate on the surface. This formation occurs above 800°C for the cerate and above 850°C for the aluminate. Therefore, the sample degreened at 700°C does not lose NSC through this mechanism, but the sample aged at 920°C loses a significant amount of NSC by forming these highly stable species. In a standard NSR system, the catalyst is only exposed to

such high temperatures during excursions to high temperature for the purposes of desulfation [57,89]. However, the hydrothermal aging presented here simulates a close-coupled catalyst, resulting in significantly higher temperatures. Because the NS-TWC loses a majority of its NO_X storage, the amount of time the system can operate lean is decreased, which will cause a net increase in projected fuel consumption; therefore, for this application and this catalyst it would be preferred to not exceed 850°C. This could be accomplished by moving the NS-TWC further downstream in the exhaust treatment system.
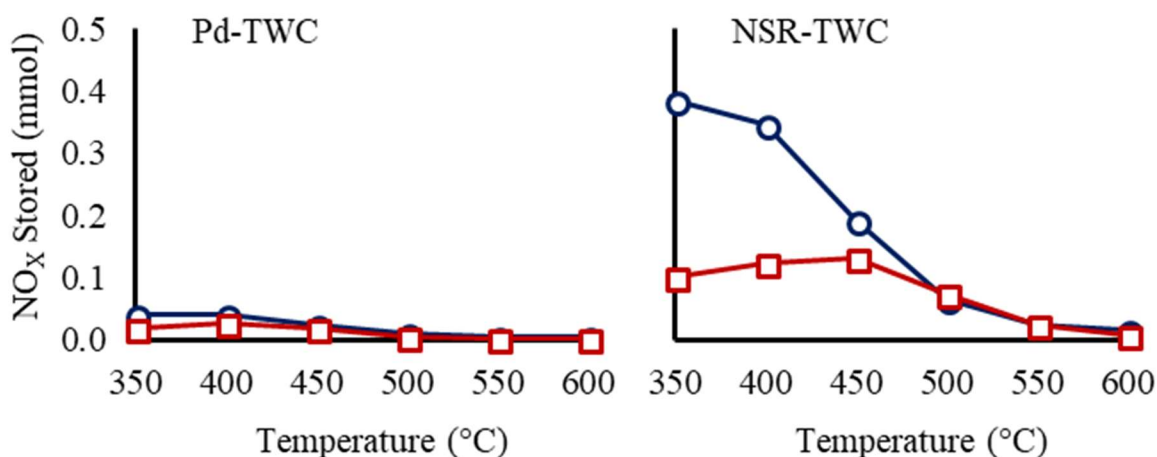
Figure 3.9: Average NO_X stored per cycle on the Pd-TWC and NS-TWC for degreened (circles) and aged (square) samples

Figure 3.10 shows the changes in OSC from hydrothermal aging for both Pd-TWC and NS-TWC. On the Pd-TWC, the low temperature OSC is decreased, but it is similar to the degreened sample above 450°C. Similarly, the NS-TWC also shows strongly deactivated low temperature OSC. However, above 450°C, the aged catalyst shows increased OSC during cycling. As previously mentioned, hydrothermal aging of catalysts containing ceria results in phase segregation between ceria and alumina, as well

as agglomeration of ceria on the catalyst surface [51,90]. This leads to significantly decreased surface ceria sites but can increase the total ceria available for oxygen storage. At low temperatures, only the surface ceria is active for OSC, but, as the temperature is increased the ceria becomes active for bulk oxygen diffusion. This results in significantly decreased low temperature OSC, but the high temperature OSC is increased.
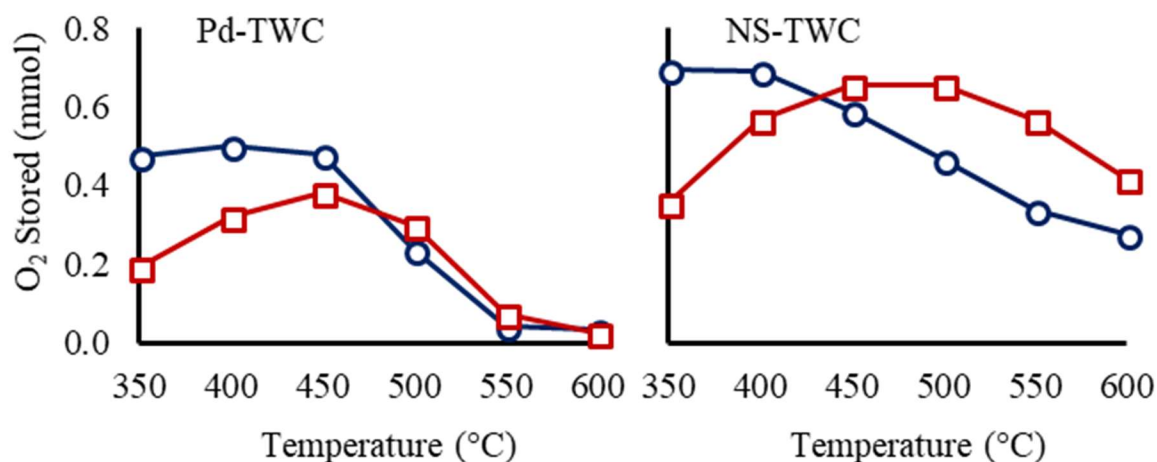
Figure 3.10: Average O_2 stored per cycle on the Pd-TWC and NS-TWC for degreened (circles) and aged (squares) samples.

Figure 3.11 shows the NH_3 yield for each catalyst sample and operating condition as a function of catalyst inlet temperature. On the Pd-TWC, the low temperature activity for NH_3 production remains unchanged, which is consistent with results from steady state experiments. However, at higher temperatures, the aged catalyst shows decreased activity. In contrast to the Pd-TWC, the NH_3 yield on the aged NS-TWC sample is increased at temperatures below 450°C and similar to the degreened activity above 450°C. The primary cause for this is the deactivation of the OSC on the NS-TWC. This loss of OSC could be due to phase segregation and/or degradation of the cerium oxide structure, leading to a loss of surface area, as suggested in previous literature [91]. During

the transition from lean to rich, the catalyst must be reduced before the production of NH_3 can begin. Because the hydrothermal aging procedure leads to significant loss of OSC on the NS-TWC, it allows for production of NH_3 in the rich phase to begin more quickly and allows for a shorter overall rich phase.

Figure 3.11: Rich phase NH_3 yield for Pd-TWC (top) and NS-TWC (bottom) for both fixed load (left) and load step (right) conditions comparing degreened (circles) and aged (squares) samples

The production of N_2O for each catalyst sample and operating condition is shown in Figure 3.12. N_2O production can be a concern for the operation of a lean/rich cycling system. In an NSR system, N_2O emissions frequently occur when the stored NO_X is being reduced due to only partial reduction of the surface nitrates. These catalysts show a

similar trend. Over the Pd-TWC, there is less than 1ppm average N_2O produced during the rich phase, regardless of whether the catalyst has been aged or degreened. In contrast, the degreened NS-TWC shows an average of 6-7ppm N_2O during the rich phase at 350°C. The aged NS-TWC sample shows decreased N_2O production. This is likely due to the decrease in NO_X storage as shown in Figure 3.9.
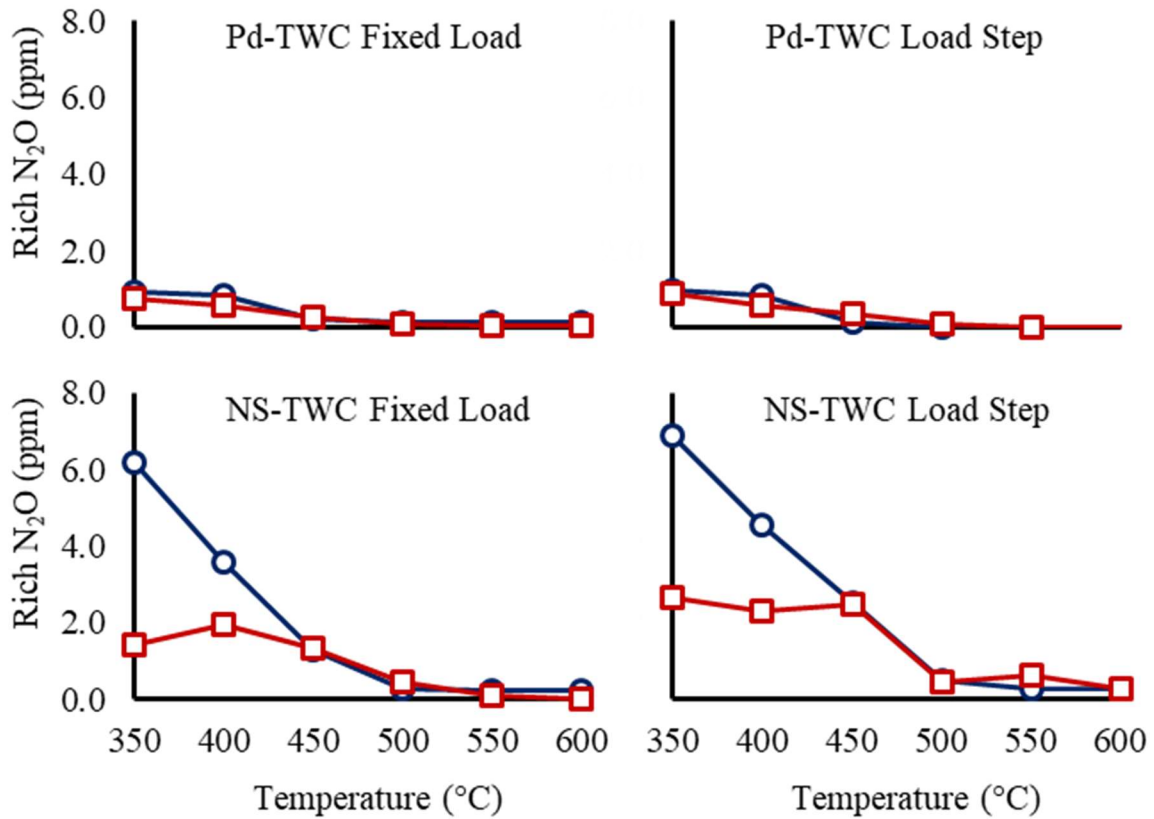
Figure 3.12: Average rich phase N_2O production for the Pd-TWC (top) and the NS-TWC (bottom) for both fixed load (left) and load step (right) conditions comparing degreened (circles) and aged (squares) samples

Figure 3.13 shows the effects of hydrothermal aging on CO conversion. The primary effect on both catalysts is a decrease in CO conversion at low temperatures, while at higher temperatures, the degreened and aged activities are closer. This is

consistent with steady state results and light off curves, which showed a strong decrease in CO oxidation activity at low temperature. As discussed previously, these low temperature changes are likely attributed to the loss of active surface area as well as PGM-OSC interface sites.
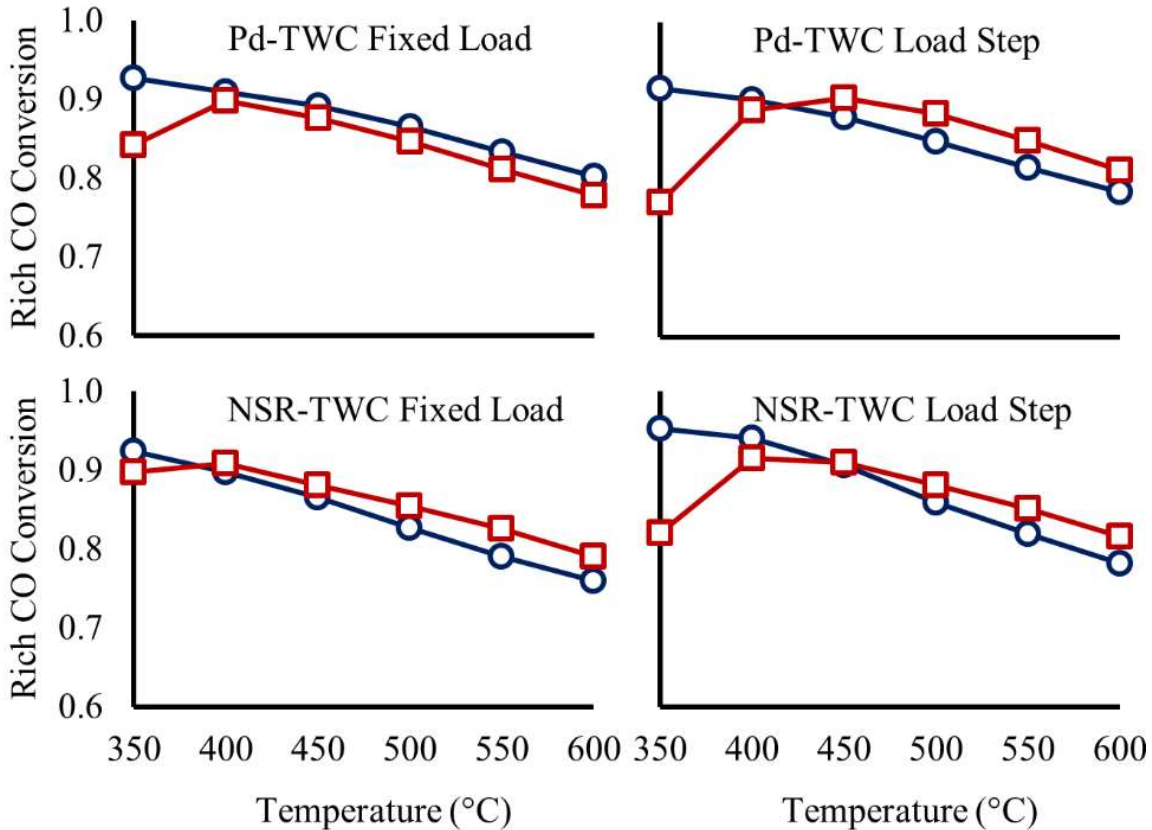
Figure 3.13: Rich phase CO conversion for Pd-TWC (top) and NS-TWC (bottom) for both fixed load (left) and load step (right) conditions comparing degreened (circles) and aged (squares) samples

On the NS-TWC, the low temperature CO conversion was not as strongly deactivated as it was on the Pd-TWC, which is consistent with results from the steady state experiments. Again, this is likely attributed to the higher loading of OSC, which allows for it to maintain a larger portion of the highly active PGM-OSC interface sites.

The effect of hydrothermal aging on overall C_3H_8 conversion is shown in figure 3.14. The Pd-TWC shows slight C_3H_8 breakthrough at 350°C. Under both fixed load and load step conditions, there is no significant change in the C_3H_8 conversion and both the aged and the degreened Pd-TWC samples show similar concentrations of C_3H_8 in the outlet. However, on the NS-TWC, the C_3H_8 conversion is significantly lower compared to the Pd-TWC. Furthermore, the aged sample shows better cycle-averaged conversion than the degreened sample.
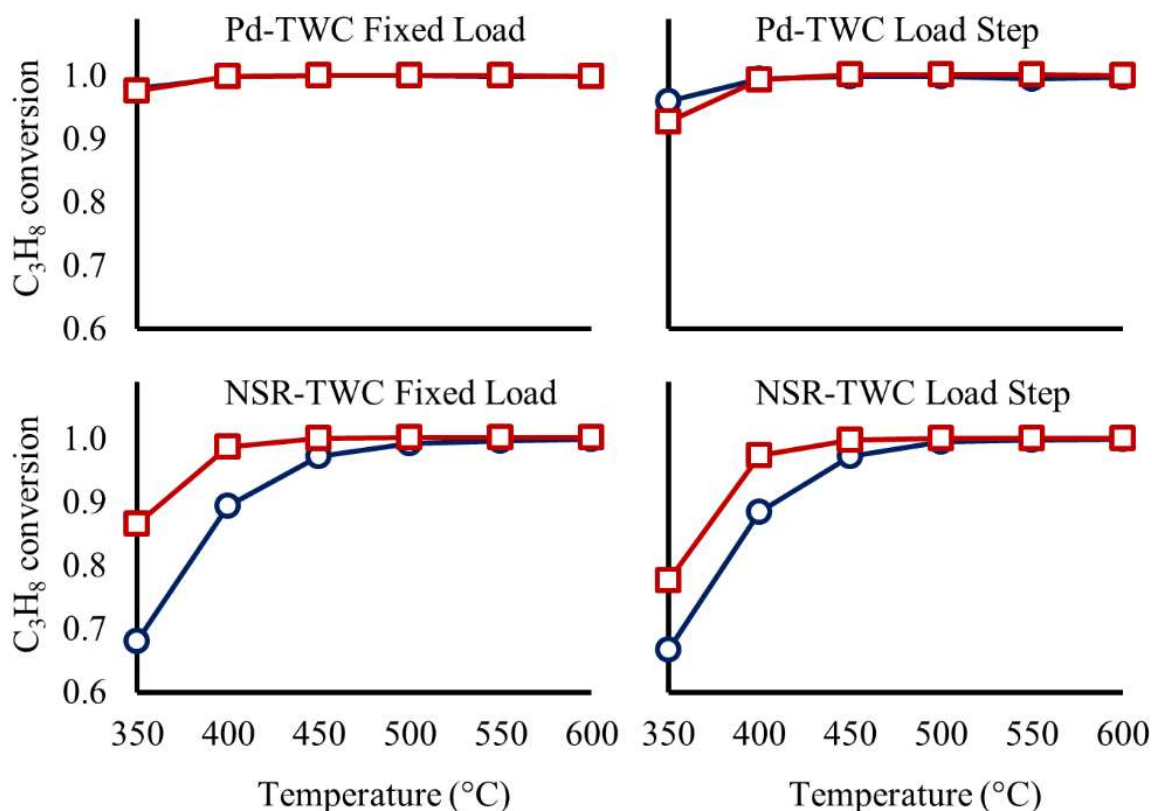
Figure 3.14: Average C_3H_8 conversion for Pd-TWC (top) and NS-TWC (bottom) for both fixed load (left) and load step (right) conditions comparing degreened (circles) and aged (squares) samples

These changes are primarily attributed to the deactivation of the NSC on the NS-TWC during hydrothermal aging. Because the degreened sample retains a large amount

of NSC, as shown in Figure 3.9, the lean phase lasts longer than it does when the aged sample is used. This leads to a longer time that the catalyst is under oxidizing conditions, leading to higher C_3H_8 slip. This is a significant concern for meeting the emissions regulations of 0.03 g/mile of combined NMOG + NO_X emissions. Because of this, it may be necessary to introduce an additional cleanup catalyst downstream from the SCR catalyst to deal with C_3H_8 and CO slip in the final emissions control system.
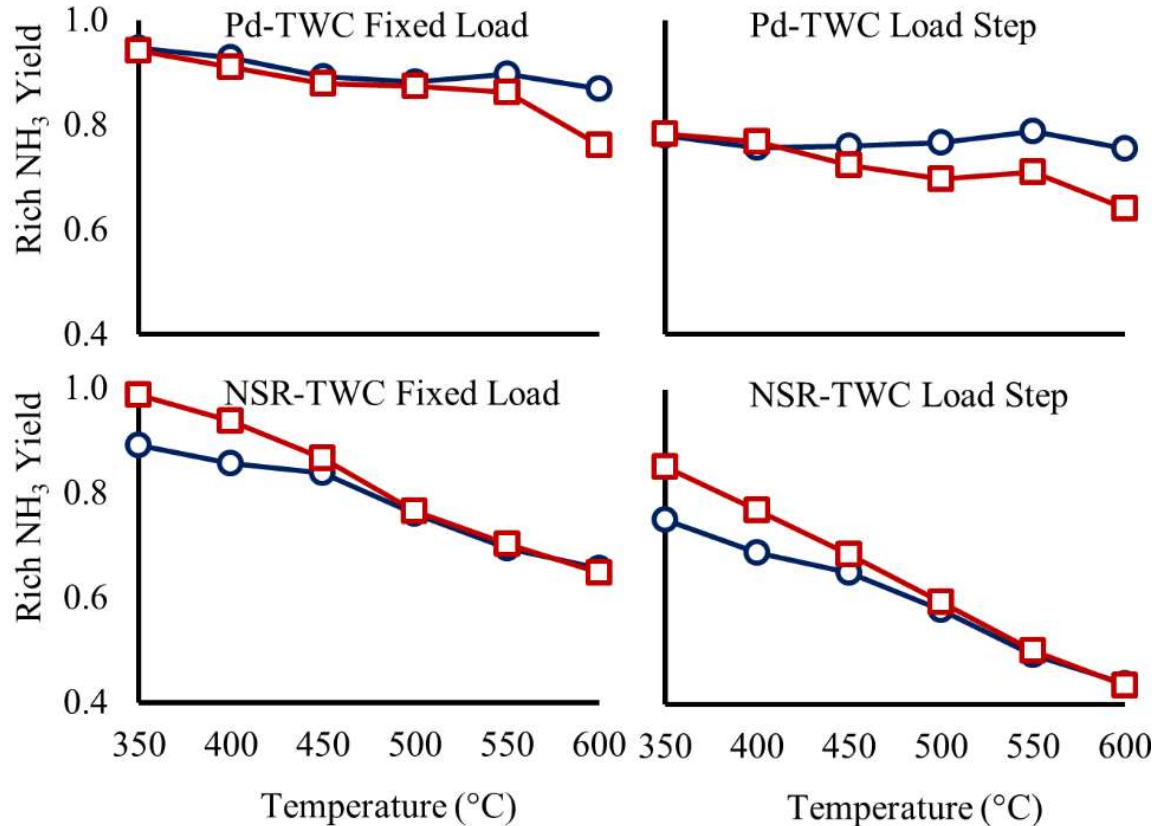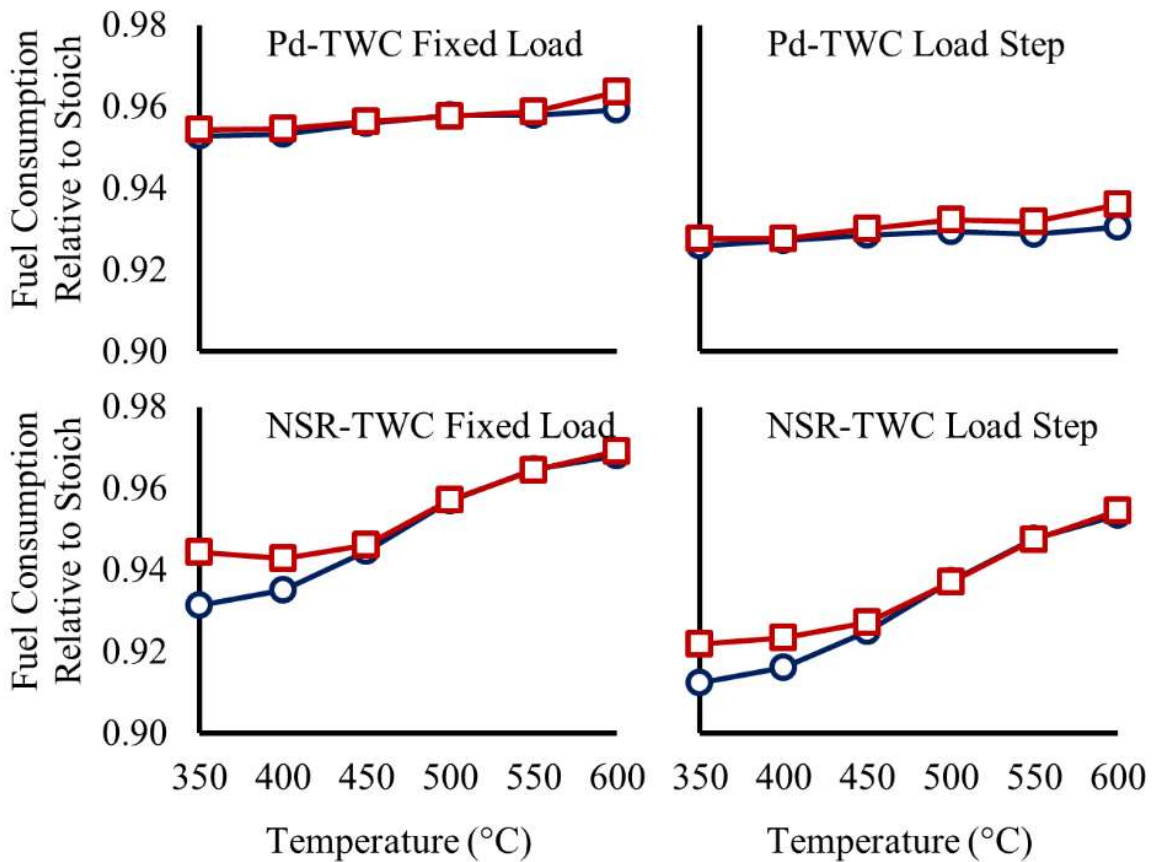

Figure 3.15: Projected fuel consumption for Pd-TWC (top) and NS-TWC (bottom) for both fixed load (left) and load step (right) conditions comparing degreened (circles) and aged (squares) samples

The projected fuel consumption relative to stoichiometric operation is shown in figure 3.15. While CO and C_3H_8 emissions are a concern, they do not affect the projected

fuel consumption because they do not influence the feedback-controlled cycling. The only factors that will have an effect are NH_3 production, NO_X conversion, and NO_X storage. On Pd-TWC, the projected fuel consumption benefits at high temperatures are slightly decreased due to the decrease in the NH_3 production on the aged catalyst. This increases the length of time the system must operate under fuel rich conditions, during which the fuel consumption is increased. However, the low temperature projected fuel consumption remains unchanged. On the NS-TWC, the projected fuel consumption benefit is decreased at lower temperatures due to the loss of NSC. This causes shorter lean phases at low temperatures and, by extension, higher projected fuel consumption. The loss of OSC proved beneficial on the NS-TWC because it allowed for a more rapid breakthrough of NH_3 during the rich phase. Despite the effects of aging, both catalysts maintained sufficient activity to operate a passive SCR system, with projected fuel consumption ranging from 91-98% of stoichiometric fuel consumption in the temperature range observed.

3.4. Conclusions

Hydrothermal aging using a four-mode aging protocol led to significant deactivation in two fully formulated commercial automotive catalysts. The primary means of deactivation is the sintering of the active metal, with the average diameter of palladium particles on a Pd-TWC increasing from < 5 nm to > 30 nm over the course of 100 hours of aging. The CO light off temperature also increased due to aging, particularly during the first 25 hours due to metal sintering and OSC degradation. After aging, the steady state activity of the two catalysts was measured using simulated exhaust gas

mixtures approximating a wide range of λ values at 400°C. In these experiments, the Pd-TWC showed significantly decreased activity for CO and C_3H_8 conversion. However, the NS-TWC was not as strongly affected and maintained higher steady state activity for the conversion of CO and C_3H_8. Despite the extensive hydrothermal aging, catalyst deactivation did not extend to the reduction of NO_X to NH_3. Both catalysts maintained close to 100% conversion of NO in all rich phase operation as well as a steady state selectivity to NH_3 near 100% for all λ values lower than 0.98.

Transient studies allowed for further probes into the effects of hydrothermal aging. Many of the results from the steady state tests were corroborated. For the most part, the catalysts maintained their NH_3 production, while the conversion of NO_X, CO, and C_3H_8 were heavily deactivated. However, under cycling conditions, the effects of OSC and NSC were far more pronounced. This led to significant differences between the Pd-TWC and the NS-TWC. There were significant levels of OSC and NSC degradation on the NS-TWC through aging, significantly affecting the cycling activity compared to a degreened sample. The loss of NSC led to shorter lean phases on the aged catalyst, causing higher projected fuel consumption. Degradation of the OSC led to decreased oxygen storage at low temperature. This proved beneficial for the system, as it caused the catalyst to be reduced more quickly in the rich phase, allowing for more rapid breakthrough of NH_3, leading to a shorter rich phase and reducing the overall fuel penalty accrued while running rich. However, the aged NS-TWC sample actually stored more oxygen than the degreened sample at temperatures over 450°C. Overall, while the four-mode hydrothermal aging procedure led to significant particle sintering, as well as loss of OSC and NSC, the aged catalysts still proved effective in producing the necessary NH_3

for the operation of a passive SCR system with projected fuel consumption ranging from

91-98% compared to stoichiometric operation.

.

CHAPTER 4

THE EFFECTS OF SULFATION ON THREE-WAY CATALYST
PERFORMANCE IN SIMULATED PASSIVE SELECTIVE CATALYTIC
REDUCTION EXHAUST

4.1 Introduction

Chemical deactivation of catalysts is a significant concern, particularly in the case of automotive catalysts, where several contaminants present in fuels and lubricants can lead to significant loss of catalyst activity. Lead, phosphorous, and sulfur are some of the most prevalent species that lead to significant chemical deactivation in automotive catalysts. Lead poisoning of automotive catalysts was one of the earliest concerns in their introduction. When Pt automotive catalysts were initially introduced for HC and CO control, lead-based additives to gasoline were prevalent. The effectiveness of these Pt-based catalysts was severely limited until regulations brought the lead content down. Still, the deactivation of catalysts by lead species was a major concern. Lead has been found to preferentially interact with noble metals, rather than the metal oxide support in several formulations [92]. Phosphorus poisoning of automotive catalysts is due primarily to the presence of the antiwear gasoline additive zinc dialkyldithiophosphate (ZDDP) [93]. In contrast to lead poisoning, phosphorus poisoning of catalysts occurs primarily through the formation of phosphates with the metal oxide support. Studies have shown evidence for both aluminum phosphates and cerium phosphates as well as other less prevalent species [94].

More recently, particularly as elements like Pd, Ce, and Ba have become more common, research into sulfur poisoning has become much more crucial. Sulfur poisoning under stoichiometric or oxidizing conditions leads to the formation of stable sulfate species on the catalyst, forming particularly stable compounds with Ce and Ba. Ce is used as a support, promoter, and oxygen storage component (OSC). When ceria is poisoned by sulfur, it forms highly stable ceria sulfates. This has been shown to increase CO light-off significantly in $Pd/CeO_2/Al_2O_3$ catalysts [56]. Ba is used primarily as a NO_X storage component (NSC). Barium sulfates have shown even greater stability than cerium sulfates, and the deactivation of barium due to sulfur is a large concern, particularly in NO_X storage and reduction (NSR) catalysts.

Regarding noble metals, Pd has shown a large degree of susceptibility to sulfur poisoning compared with Pt and Rh [95,96]. Furthermore, the susceptibility of noble metals to sulfation is increased under rich conditions, where research has found PtS species present on Pt-based NSR catalysts during regeneration [97]. One of the primary reasons that Pd catalysts have been implemented so widely in last 20 years is due to the improving gasoline contaminant regulations [98]. While the subject of sulfur poisoning on TWCs has received extensive attention in previous literature, its relevance to passive SCR has not been thoroughly investigated. This work is focused on evaluating the long-term effects of exposure to realistic concentrations of SO_2 on the TWC, with specific attention paid to considerations involved in the operation of a passive SCR system.

Here, we examine the effects of realistic levels of SO_2 in simulated exhaust on two hydrothermally aged, commercially formulated TWCs for the purposes of implementation into a passive SCR system. The catalysts are evaluated before sulfation,

after sulfation, and after desulfation. The sulfation procedure exposes the catalysts to 2ppm SO_2 at 350°C for 12.5 hours under simulated exhaust conditions. The catalysts are desulfated through cycling at 650°C for 3 hours.

4.2. Experimental:

4.2.1 Catalysts and Reactor:

The catalysts studied in this chapter are the catalysts that were hydrothermally aged for 100 hours from the previous chapter. These formulations are described in Chapter 2.2.1 and the specifications are shown in Table 4.1. The exhaust experiments presented in this chapter are conducted in the cycling reactor described in Chapter 2.2.3.

Table 4.1: Hydrothermally aged commercial catalyst formulations

Description	Pt (g/L)	Pd (g/L)	Rh (g/L)	OSC	NSC
Pd-TWC	0	7.33	0	Low	Low
NS-TWC	2.47	4.17	0.05	High	High

4.2.2 Simulated Exhaust and Sulfation Procedure

Exhaust is simulated under two different conditions, fixed load and load step. Fixed load simulates passive SCR operation when the engine is under a constant load. However, during automotive operation, the load requirements of the engine are changed frequently, and when the engine is under heavy load, the NO_X produced under rich conditions is increased. This increased NO_X can be used to opportunistically produce additional NH_3 by running rich when the load requirement of the engine is increased. This process is simulated by the load step condition, where the rich phase is under a

much higher simulated load. The conditions for lean and rich for both fixed load and load step conditions are shown in table 4.2. Throughout the simulated exhaust experiments, the catalysts undergo constant lean/rich cycling controlled through a LabVIEW program.

Table 4.2: Simulated exhaust conditions

	Fixed Load		Load Step	
	Rich	Lean	Rich	Lean
λ	0.97	2.0	0.97	2.0
O_2 (%)	1.07	10	1.07	10
CO (%)	1.6	0.2	1.6	0.2
H_2 (%)	0.8	0	0.8	0
NO (%)	0.06	0.036	0.12	0.036
C_3H_8 (%)	0.1	0.06	0.1	0.06
H_2O (%)	11	6.6	4.95	6.6
CO_2 (%)	11	6.6	4.95	6.6
SV (hr^{-1})	27,000	45,000	60,000	45,000

The procedure for the long term sulfation of the catalysts is shown in Figure 4.1. The catalyst is pretreated at a furnace temperature of 650°C and a λ of 0.95 for 30 minutes before being cooled to 350°C. Then, to determine the activity for the clean catalyst, it is heated in 50°C increments from 350°C – 650°C and evaluated under cycling conditions for 1 hr at each temperature. Once the catalyst reaches 650°C, it is again pretreated with a λ of 0.95 for 30 minutes and cooled to 350°C, where it is exposed to 2ppm SO_2 for 12.5 hr. This low SO_2 concentration and long exposure time is intended to more accurately represent realistic exhaust composition from gasoline engines, rather than using high concentration and a short exposure time, as has been done in many previous SO_2 poisoning studies [99]. This 2ppm SO_2 level is based on rich phase space

velocity. Therefore, the load step evaluation is being exposed to more total SO_2. After 12.5 hours, the flow of SO_2 is stopped and the catalyst is again evaluated in the temperature range 350°C – 650°C to determine the activity of the sulfated catalyst. At 650°C, the system is cycled between the lean and rich phase for three hours to desulfate the catalyst. After a final pretreatment, the catalyst temperature is dropped and its desulfated activity is measured between 350°C and 650°C. This procedure is repeated for both fixed load and load step operating conditions over the Pd-TWC and NS-TWC.
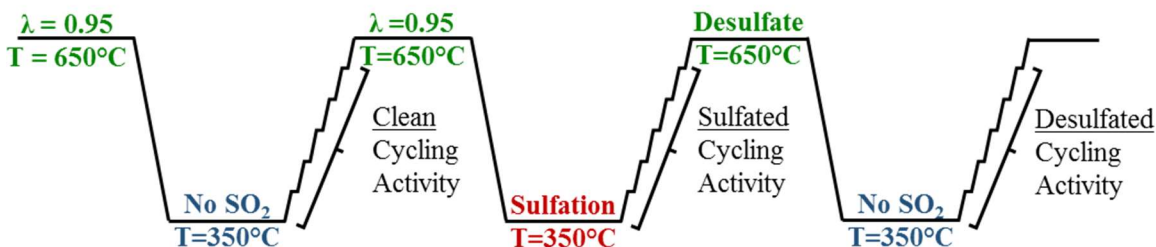
Figure 4.1: Procedure for long term sulfation experiments

4.3 Results and Discussion

4.3.1 Deactivation During Sulfation

To determine the effects of sulfation on the TWC formulations, hydrothermally aged samples were evaluated under cycling conditions before sulfation, after sulfation, and after desulfation. The catalysts were also monitored continuously throughout sulfation at 350°C. Figure 4.2 shows time series data during the first 30 minutes of sulfation under fixed load conditions for both the Pd-TWC and the NS-TWC. It can be seen from this data that, during the rich phase, there is significant CO breakthrough and NH_3 production, while NO_X and C_3H_8 show nearly complete conversion. Conversely, during the lean phase, there is no NH_3 production or CO breakthrough, while the NO_X

57

and C_3H_8 breakthrough is much higher. During the exposure to SO_2, the most immediate effect is the decrease in outlet NH_3 and increase in outlet CO. In contrast, during this time, there is not a significant change in the rich phase levels of either C_3H_8 or NO_X.
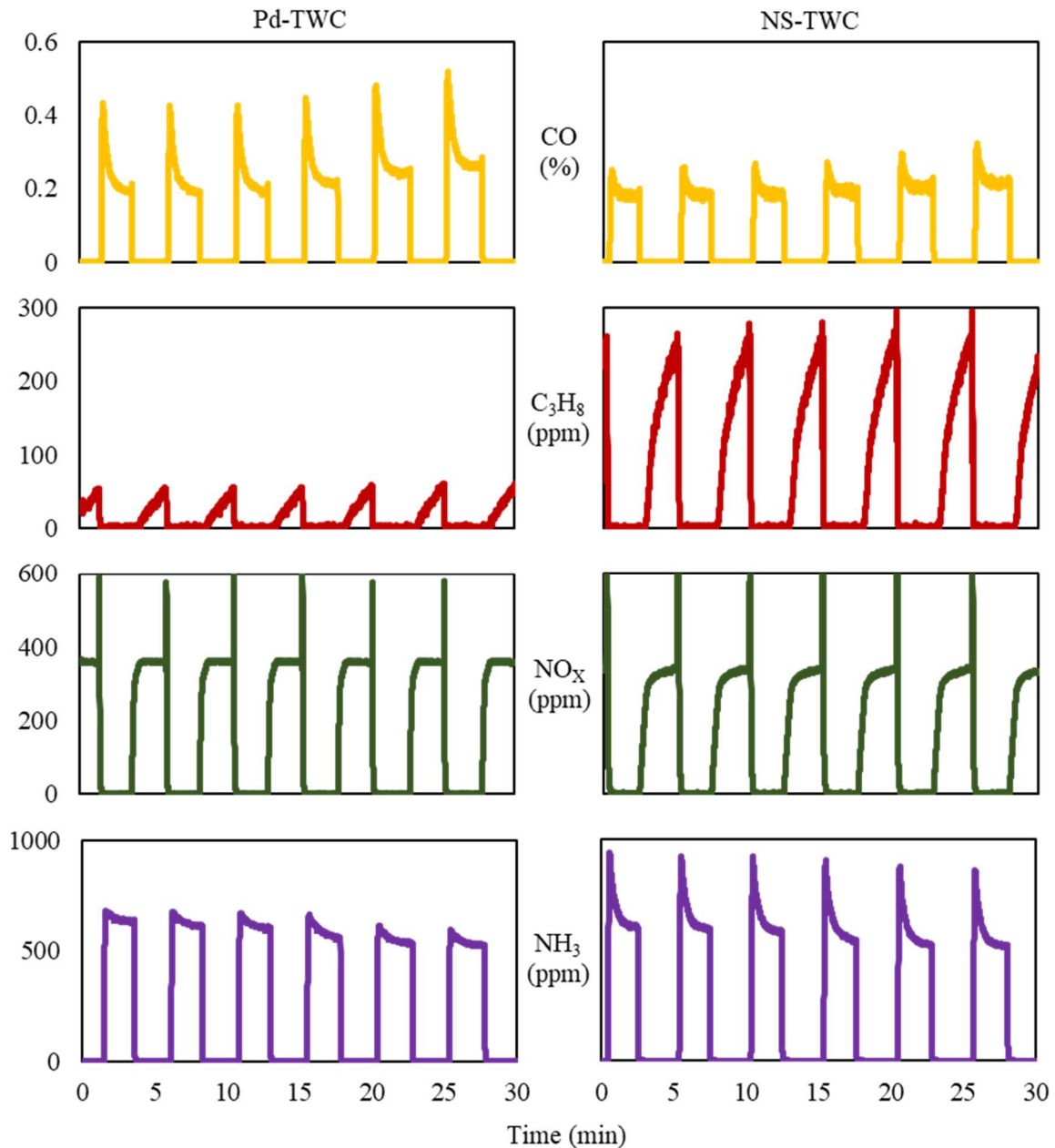
Figure 4.2: Time series data during first 30 minutes of sulfation on the Pd-TWC (left) and the NS-TWC (right) under fixed load conditions.

Figure 4.3 illustrates the continuous deactivation of the catalysts throughout the 12.5 hours of sulfation. As seen in Figure 4.2, there is a rapid drop in both CO conversion and NH_3 production within the first 30 minutes. On the Pd-TWC, the activity then continues to drop at a much slower pace as the sulfation continues. However, the NS-TWC shows stronger continuous deactivation throughout the sulfation process. This is likely due to the high loading of barium and cerium, which allows for a larger concentration of stable sulfur species to be formed. This causes the catalyst to continue being deactivated as the barium and cerium continue to store sulfur in the form of sulfate species [55,100].
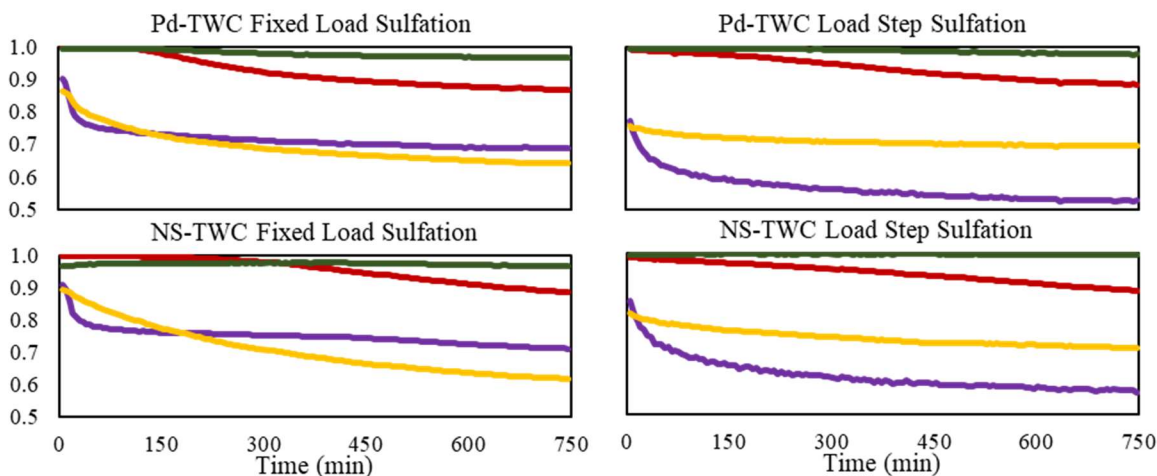
Figure 4.3: Changes in CO Conversion (yellow), C_3H_8 conversion (red), NO_X conversion (green), and NH_3 yield (purple) in the rich phase over the Pd-TWC (top) and the NS-TWC (bottom) under fixed load (left) and load step (right) conditions during 12.5 hours of sulfation at 350°C

The rich phase conversion of NO_X and C_3H_8 are not deactivated as early in the sulfation as NH_3 production and CO conversion. Rich phase NO_X conversion shows a small decrease, particularly on the Pd-TWC, during sulfation. However, the conversion remains above 95% throughout sulfation for each catalyst and operating condition. The

initially low conversion of rich phase NO_X on the NS-TWC under fixed load operation is due to the release of stored NO_X during the transition from lean to rich. As the catalyst is sulfated, the rich phase NO_X reduction is deactivated, but the NO_X storage is also decreased, leading to very little change in rich phase NO_X emissions. By the end of sulfation, the NO_X released during the transition is decreased, but there is significant breakthrough that is not present on the clean catalyst. While the rich phase conversion of C_3H_8 is close to 100% for both the clean Pd-TWC and the clean NS-TWC, it drops to roughly 90% for each catalyst and operating condition over the course of the sulfation. Deactivation of rich phase C_3H_8 conversion only occurs after 2 hours for fixed load conditions but is apparent in the first thirty minutes of the load step exposure for both catalyst samples. This is likely due to the higher space velocity in the load step rich phase, which exposes the catalyst to a higher level of SO_2.

The catalysts were also exposed to sulfur at 550°C to determine what effect the temperature of sulfation has on the extent of catalyst deactivation. This deactivation is shown in Figure 4.4. The relative deactivation depends on the chemical species of concern as well as the catalyst formulation. One of the key results is the much stronger deactivation of NH_3 production at 550°C. Each catalyst shows NH_3 yields decreasing to ~0.4 under fixed load operation and ~0.2 under load step operation. Also, this deactivation occurs over two distinct deactivation steps. The second stage of deactivation also corresponds to the strong deactivation in the conversion of CO, NO_X, and C_3H_8 conversion. This indicates that the second stage is likely the poisoning of the PGM surface. The deactivation in NO_X conversion is much stronger during sulfation at 550°C compared to 350°C.
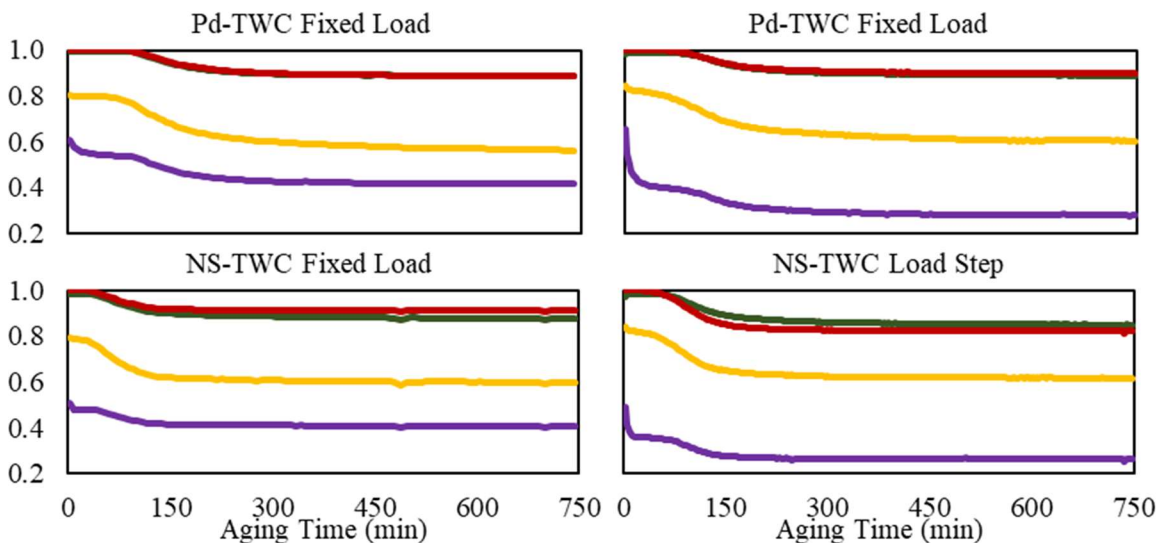
Figure 4.4: Changes in CO Conversion (yellow), C_3H_8 conversion (red), NO_X conversion (green), and NH_3 yield (purple) in the rich phase over the Pd-TWC (top) and the NS-TWC (bottom) under fixed load (left) and load step (right) conditions during 12.5 hours of sulfation at 550°C

4.3.2 Clean, Sulfated, and Desulfated Evaluation

As seen in the previous chapter, both the oxygen stored per cycle and the NO_X stored per cycle can have a large impact on the operation of a passive SCR system. Oxygen storage can lead to longer reduction times during the transition from lean to rich operation. This leads to a net decrease in the effectiveness of a passive SCR system because it increases the amount of time the system must operate under rich conditions. The oxygen storage of the catalyst before and after sulfation is shown in Figure 4.5. Overall, sulfation results in a decrease in low temperature oxygen storage on the NS-TWC, while having a negligible effect on the oxygen storage of the Pd-TWC. This difference is likely due to the high loading of ceria on the NS-TWC which is very susceptible to sulfur poisoning, forming highly stable sulfate species. However, at a sufficiently high temperature, the catalyst is able to recover its clean oxygen storage. Meanwhile the oxygen storage on the Pd-TWC is primarily from the Pd.
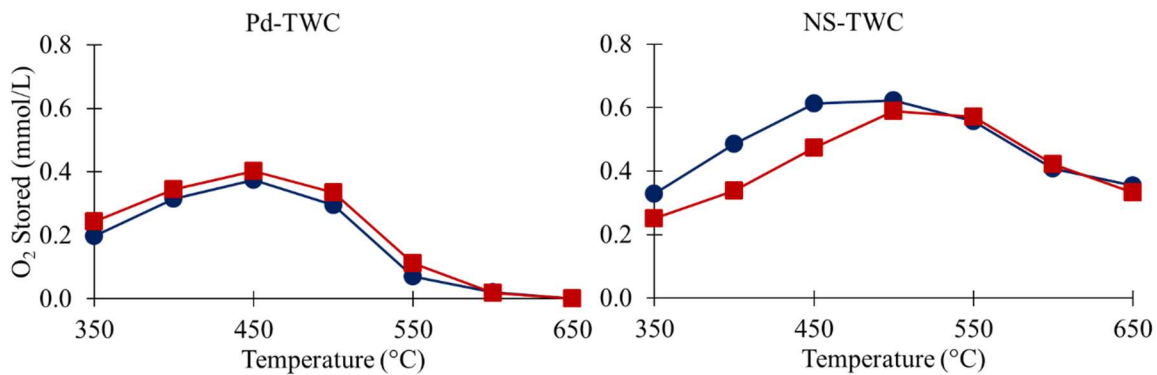
Figure 4.5: Clean (circles) and sulfated (squares) oxygen storage for the Pd-TWC (left) and the NS-TWC (right)

NO_X storage, in contrast to oxygen storage, has a beneficial effect on the operation of a passive SCR system. This is because a high level of NO_X stored means that the catalyst can operate under lean conditions for a longer period of time, because much of the NO_X present in the exhaust is stored in the form of nitrates. The NO_X storage for both catalysts before and after sulfation are shown in Figure 4.6.
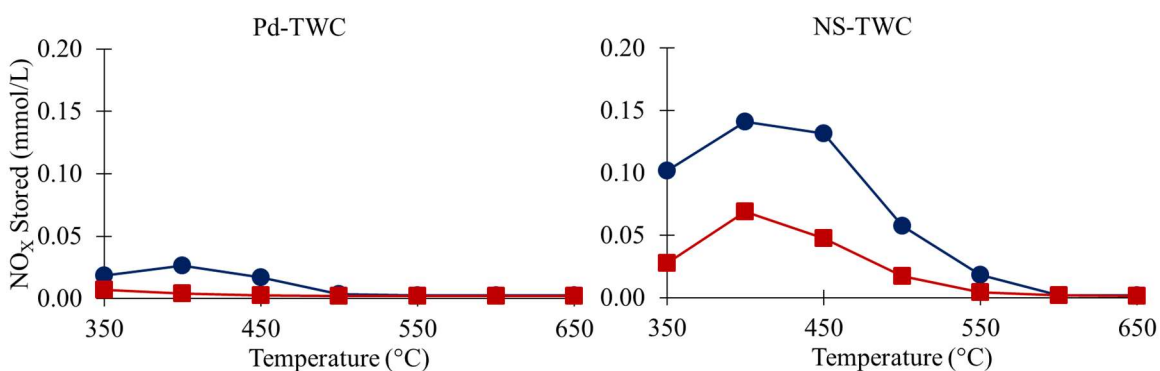
Figure 4.6: Clean (circles) and sulfated (squares) NO_X storage for the Pd-TWC (left) and the NS-TWC (right)

It can be seen from these results that the Pd-TWC has very little NO_X storage even before sulfation, while the NS-TWC still has a large amount, even after extensive

hydrothermal aging. However, the NO_X stored on both catalysts is heavily decreased by the effects of sulfation. This is because, much like ceria, barium will form highly stable sulfate species that prevent the storage of NO_X.

The NH_3 production for each catalyst and reactive condition are shown in Figure 4.7. Sulfation has a strong negative effect on the production of NH_3 under these conditions. This deactivation is strongest at higher temperatures, particularly around 550°C. Despite the strong deactivation, the clean catalyst activity was recovered through regeneration via lean/rich cycling at 650°C for three hours. This shows that, while sulfur poisoning is a concern, the deactivation is reversible through high temperature operation of a passive SCR system.

Figure 4.7: Clean (circles), sulfated (squares), and desulfated (triangles) NH_3 production for the Pd-TWC (top) and the NS-TWC (bottom) under Fixed Load (left) and Load Step (right) conditions

While the deactivation in NH$_3$ production is clear from figure 4.7, it is difficult to determine the source of this deactivation from this data alone. As previous studies have shown, the production of NH$_3$ in exhaust conditions is a complex process, with different reductants (H$_2$, CO, and various HCs) being active for the reduction of NO$_X$ to NH$_3$. Not only is this deactivation detrimental for the operation of passive SCR, it also extends the rich phase due to the feedback-controlled cycling being used in these experiments. Because of this rich-phase extension, the change in NH$_3$ production has a strong effect on the cycle-averaged levels of each other gas species of concern. This effect can be seen in Figure 4.8, which shows the production of NH$_3$ over a single rich phase in fixed load conditions for each catalyst and operating temperature for both clean and sulfated catalyst samples.

Figure 4.8: Isolated rich phases for NH$_3$ production during fixed load operation over the Pd-TWC (left) and the NS-TWC (right) under clean (top) and sulfated (bottom) conditions.

The NO$_X$ conversion under each condition is shown in Figure 4.9. Despite the strong deactivation of NH$_3$ production, the rich phase NO$_X$ conversion remains high for the Pd-TWC, only showing significant deactivation under load step operation above

450°C. This decreasing NO_X conversion is due primarily to the increased rich phase time, leading to a longer breakthrough of NO_X. This indicates that, while the specific reaction routes leading to the production of NH_3 are deactivated, the dissociation and reduction of NO_X remain relatively unaffected. In contrast to the Pd-TWC, the NS-TWC shows much lower rich phase NO_X conversion both before and after sulfation. Before sulfation, the NS-TWC does show a significant amount of NO_x slip in the rich phase, however, this slip is due exclusively to the release of stored NO_X when the system switches to rich operation. The activity for NO_X conversion was fully recovered through the desulfation procedure exposing the catalyst to lean/rich cycling at 650°C.

Figure 4.9: Clean (circles), sulfated (squares), and desulfated (triangles) rich phase NO_X conversion for the Pd-TWC (top) and the NS-TWC (bottom) under Fixed Load (left) and Load Step (right) conditions

Sulfation has two distinct effects on the rich phase breakthrough of NO_X on the NS-TWC. First, it deactivates the NO_X storage, leading to far less NO_X being released during the transition from lean to rich. Second, it deactivates the rich phase NO_X conversion on the catalyst, which leads to NO_X breakthrough towards the end of the rich phase. These effects are shown in figure 4.10, which compares the rich phase of both fixed load and load step before and after sulfation on the NS-TWC at 500°C, where the NO_X conversion is at its lowest.
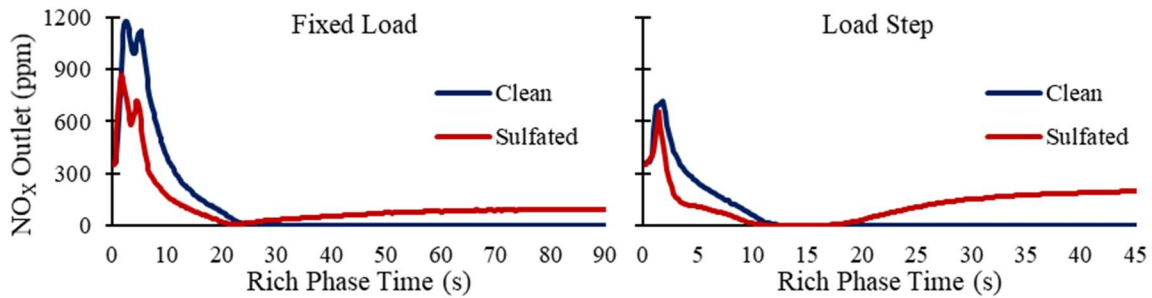
Figure 4.10: Rich phase breakthrough of NO_X on the NS-TWC catalyst before and after sulfation at 500°C.

The deactivation of the NO_X storage leads to far less NO_X released during the transition from lean to rich. This has a positive effect on the overall rich phase NO_X conversion. However, as the rich phase continues, a clear NO_X breakthrough is present on the sulfated catalyst while the clean catalyst shows no breakthrough. This long-term transition is seen in the analysis of various gasses. It is likely due to the propensity for sulfur to form a sulfide with the platinum group metal during rich operation, and to form sulfates on metal oxides during lean operation [101]. Thus, during the transition, these sulfates could be transitioning to the PGM surface in the form of sulfides. Because the NS-TWC likely stores a significant amount of sulfur from the NSC and OSC loading, there is more sulfur being trapped by the catalyst, which should result in stronger

deactivation during the rich phase when compared to the Pd-TWC which does not have high levels of storage materials.

The changes in rich phase N_2O production for both the Pd-TWC and NS-TWC are shown in Figure 4.11. For the clean catalysts, very little N_2O production is observed across all operating conditions. After sulfation, large increases in N_2O production are observed when operating under load step conditions for both catalysts and are especially high on the NS-TWC. Under fixed load conditions, the average N_2O production in the rich phase remains below 2ppm for the Pd-TWC and under 10 ppm for the NS-TWC. The increase during load step operation is likely due to the higher rich phase space velocity and inlet NO concentration.
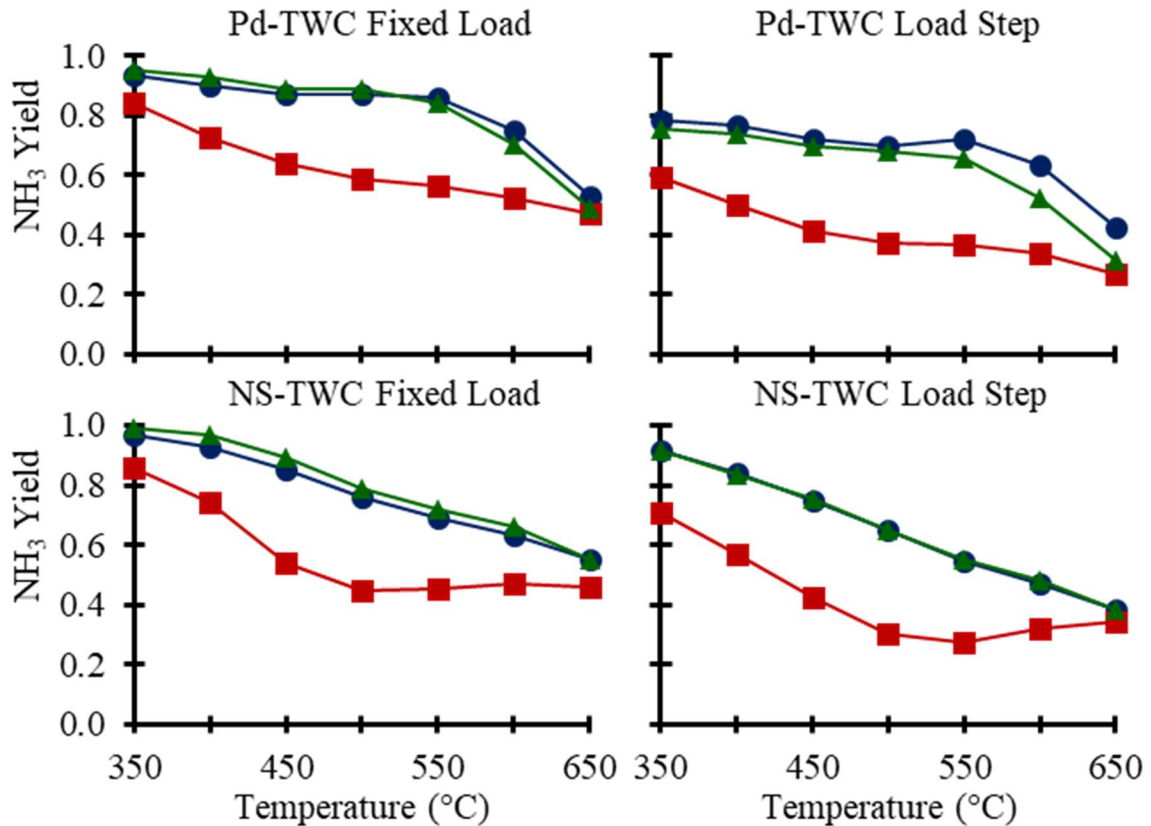

Figure 4.11: Clean (blue), Sulfated (red), and Desulfated (green) rich phase N_2O production for the Pd-TWC (top) and THE NS-TWC (bottom) under Fixed Load (left) and Load Step (right) conditions

The overall increase in N_2O production shown here is likely due to the presence of sulfur crowding the active metal and preventing full reduction of the inlet NO_X. Again, the desulfation procedure results in a return to the clean level of catalyst activity. Figure 4.12 shows the time series data for N_2O under load step conditions over the Pd-TWC and the NS-TWC during the rich phase.
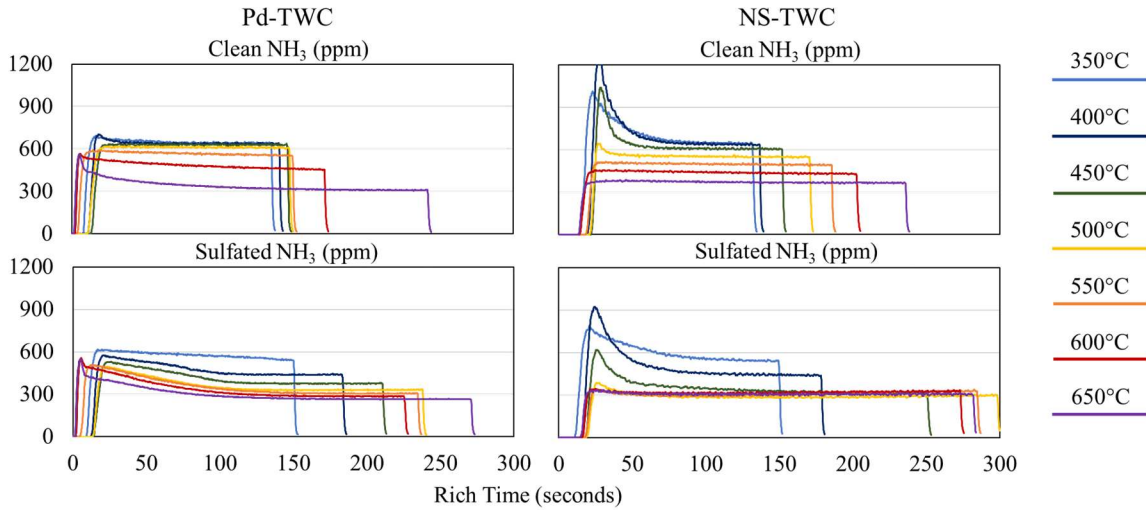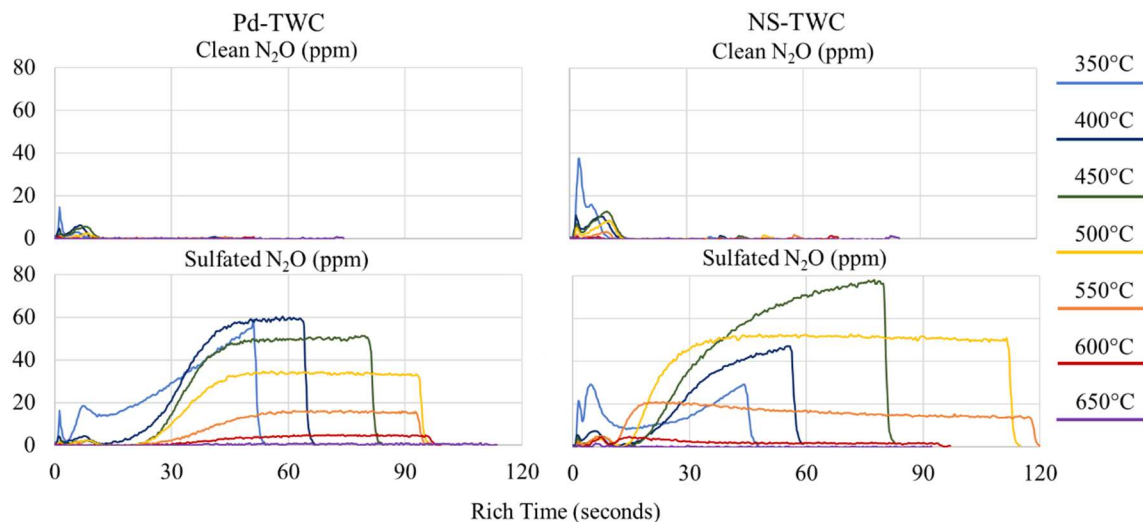

Figure 4.12: Isolated rich phases for N_2O production during fixed load operation over the Pd-TWC (left) and the NS-TWC (right) under clean (top) and sulfated (bottom) conditions.

This data further illustrates the multiple stages of transition within the rich phase, which is also seen in the NO_X conversion. There is an initial peak when the catalyst releases N_2O formed from partially reduced stored NO_X. After this, a small peak occurs while the catalyst is being reduced. Because much of the reductants are going towards reducing both the metal and the sulfur species, some of the incoming NO is only partially reduced to N_2O. Once the catalyst has been reduced, the production of N_2O begins to drop off. For the clean catalysts, the N_2O is only produced during the transition. However, on the sulfated catalysts, a long-term transition begins to occur which causes a

rapid increase in N_2O production until the rich phase ends. As the temperature is increased, the long-term transition is faster. However, once the temperature increases above 400-450°C, the maximum N_2O production begins to decrease. At the same time, the rich phase is extended due to the decrease in NH_3 production shown in Figure 4.7 and 4.8.
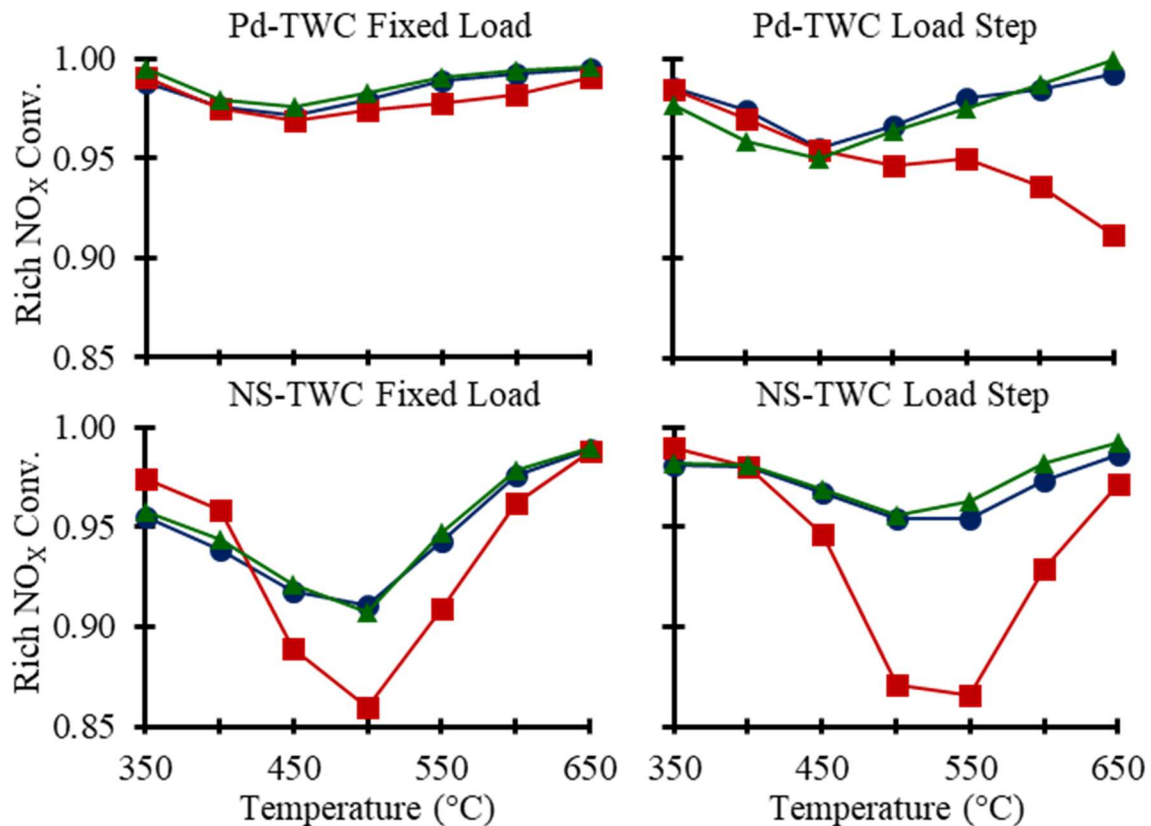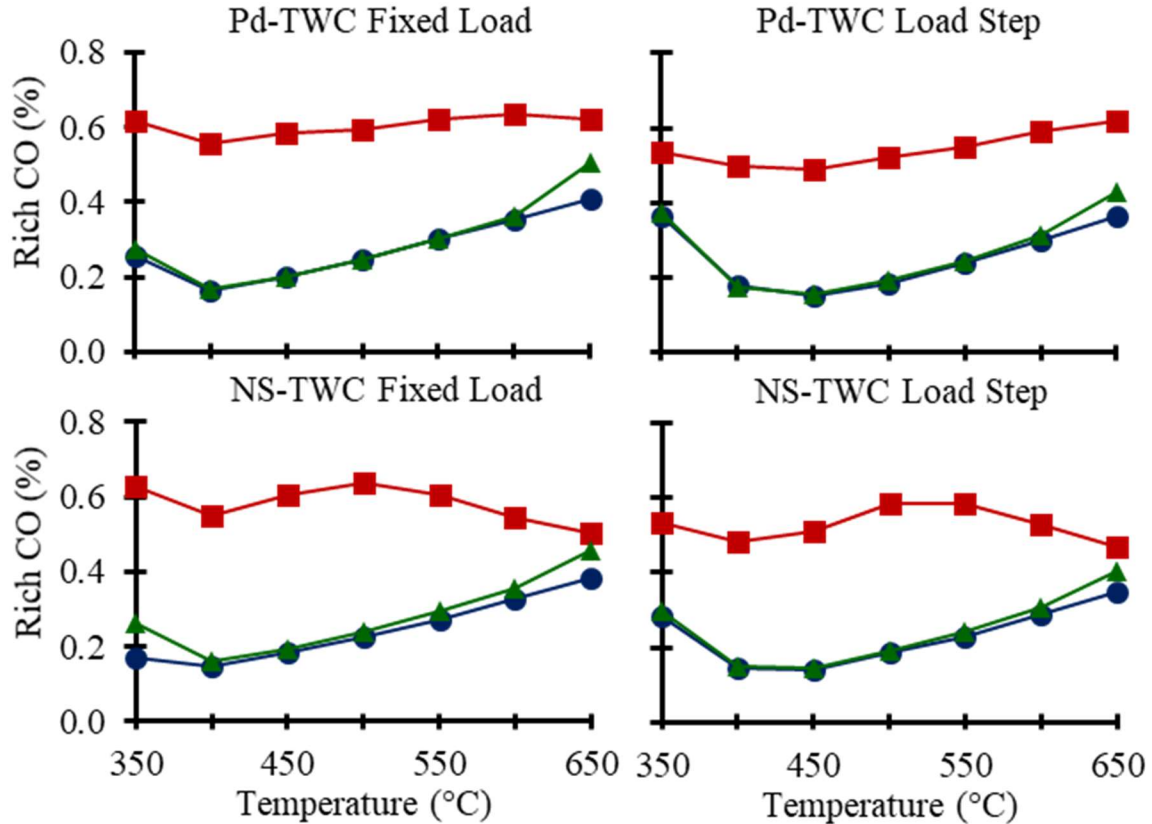

Figure 4.13: Clean (blue), Sulfated (red), and Desulfated (green) rich phase CO concentration for the Pd-TWC (top) and the NS-TWC (bottom) under Fixed Load (left) and Load Step (right) conditions

The concentration of CO is increased throughout the temperature range for each catalyst and operating condition as shown in Figure 4.13. The two routes for the deactivation leading to this increase are a change in the activity of the water gas shift reaction or a deactivation of the oxidation of CO. The water gas shift reaction has been

69

shown in previous literature to be strongly deactivated by the presence of sulfur on the catalyst [102]. There can also be a deactivation in CO oxidation at lower temperatures and under rich conditions [103–105].

Rich phase H_2 outlet shows a strong decrease across the temperature range tested as shown in figure 4.14. This decrease closely mirrors the increase observed for CO throughout the temperature range for each catalyst and reactive condition. This indicates that a deactivation in the water gas shift reaction is likely a large contributor to the concentration changes seen in these two species. The water gas shift reaction has been shown to have a strongly positive effect on the production of NH_3 from NO_X [60,69].
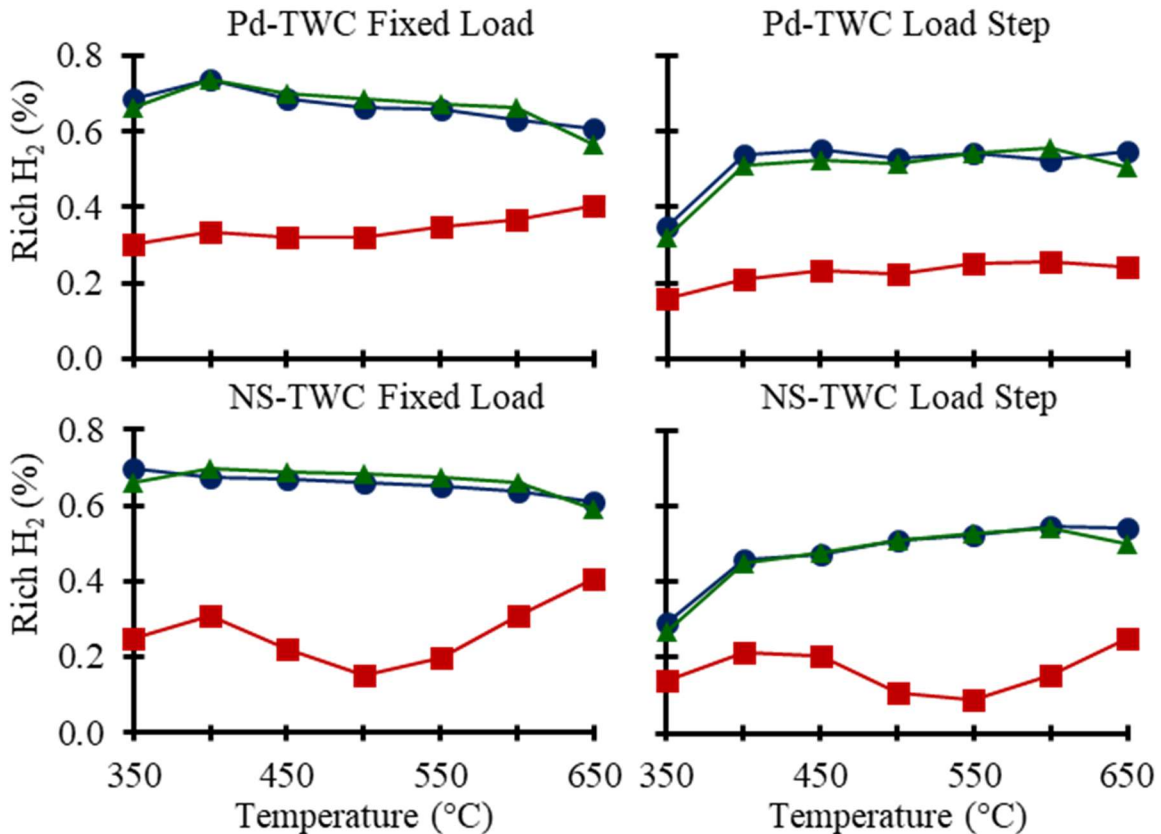
Figure 4.14: Clean (circle), Sulfated (square), and Desulfated (triangle) rich phase H_2 concentration for the Pd-TWC (top) and THE NS-TWC (bottom) under Fixed Load (left) and Load Step (right) conditions

Figure 4.15 shows the average outlet C_3H_8, measured in ppm, for each catalyst and reactive condition. Rich phase C_3H_8 in the effluent stream is increased for each catalyst and operating condition, though the deactivation is much more significant on the NS-TWC. Before sulfation, there was very little to no rich phase propane breakthrough, depending on catalyst and operating condition. This is due to the catalysts being highly active for the steam reformation reaction. Thus, it is likely that the increase in C_3H_8 breakthrough is due to reduced activity for the steam reformation reaction.
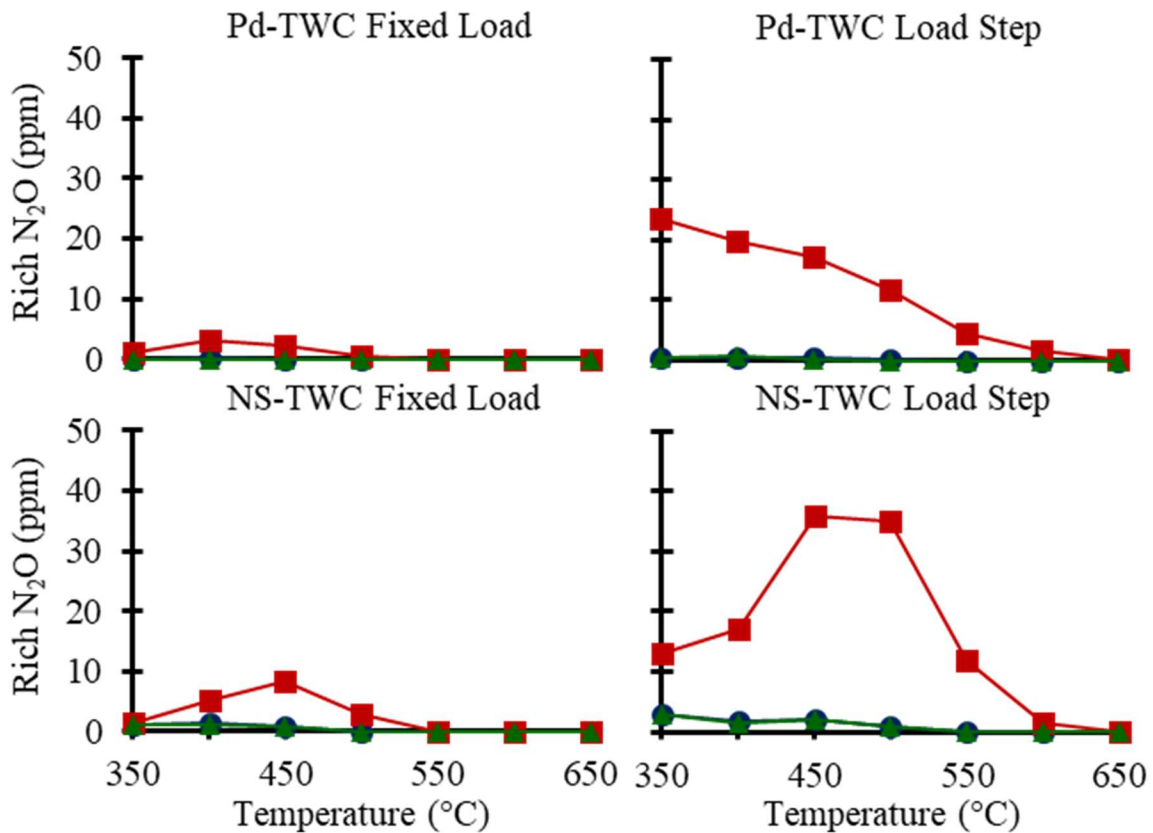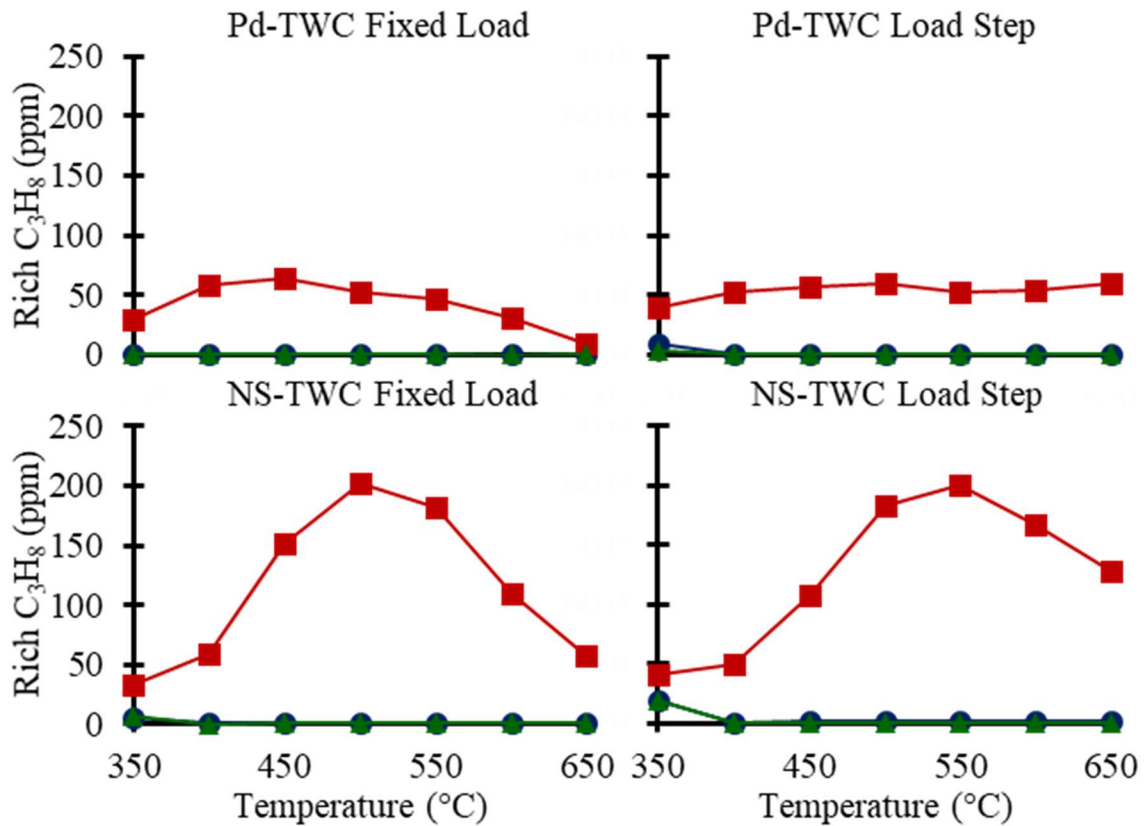

Figure 4.15: Clean (blue), Sulfated (red), and Desulfated (green) rich phase H_2 concentration for the Pd-TWC (top) and the NS-TWC (bottom) under Fixed Load (left) and Load Step (right) conditions

The argument for the deactivation of steam reforming is further evidenced by looking at the relative deactivation in the lean phase vs. the rich phase. Figure 4.16 shows

the breakthrough of C_3H_8 as a function of time for Malibu-1 under fixed load conditions at 350°C for both the clean and sulfated conditions. While the C_3H_8 breakthrough was strongly increased in the rich phase did not extend to the lean phase, where C_3H_8 is primarily converted through oxidation, rather than the steam reformation reaction.
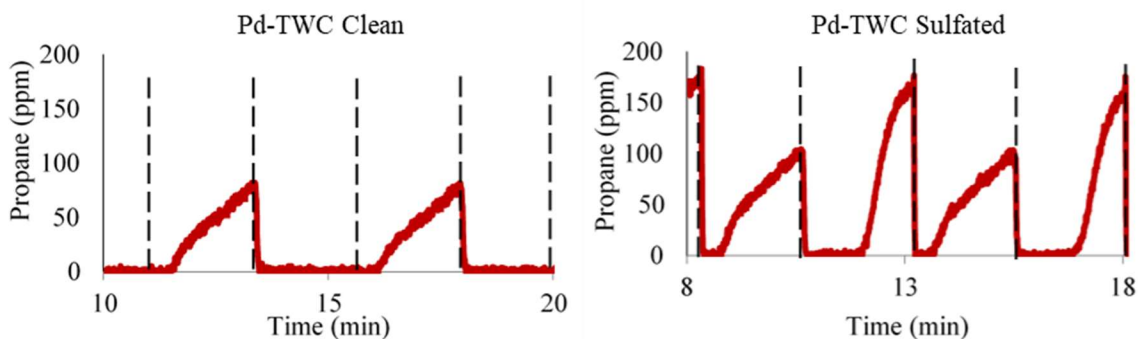
Figure 4.16: Fixed load propane breakthrough on the Pd-TWC at 350°C

4.4 Conclusions

Overall, sulfation has several effects on the TWC portion of a passive SCR system. It has a strong deactivating effect on NH_3 production, much stronger than the effect of hydrothermal aging, particularly at elevated temperatures. NO_X reduction activity was maintained on the Pd-TWC but was heavily deactivated on the NS-TWC. The NO_X breakthrough in the rich phase also illustrated the transient effects of sulfation, where the deactivation is increased as the rich phase proceeds. This transition is likely because sulfates on the metal oxide components are more stable in the lean phase, while sulfides on the PGM is more stable in the rich phase. This transient deactivation was seen in rich phase N_2O and C_3H_8 conversion as well. N_2O, while not a major concern at these temperatures over the clean catalyst, is dramatically increased, particularly for load step conditions and the NS-TWC after sulfation. This is consistent with previous literature showing increases in N_2O production after sulfation [106]. On the reductants side,

sulfation leads to higher rich phase CO and C_3H_8 slip, while lowering outlet H_2. This likely indicates that the water gas shift and steam reforming reactions are being deactivated. These reaction pathways for the production of H_2 have been suggested as important factors in the production of NH_3 [60,69]. This is further evidenced by sulfation having a negligible effect on the low temperature oxidation of C_3H_8 in the lean phase. In all cases, clean catalyst activity was recovered by cycling between lean and rich conditions at 650°C for 3 hours. This means that, while the effects of sulfur are detrimental to this system, catalyst activity can be recovered through a desulfation process that can take place in the exhaust.

.

CHAPTER 5

THE EFFECTS OF SULFATION ON THREE-WAY CATALYST PERFORMANCE IN ISOLATED REACTIONS FOR PASSIVE SELECTIVE CATALYTIC REDUCTION

5.1 Introduction

The work in the previous chapter was focused on the effects of sulfation on a fully simulated exhaust system. This is greatly beneficial to understanding what effects sulfur will have in a real system, and what challenges still remain for implementation of the system. However, it is not possible to understand how sulfation effects individual reactions from these experiments alone because of the many reactions happening in parallel. Additional work needs to be conducted to relate this simulated exhaust work to previous, fundamental work on the effects of sulfur on individual reactions. Many previous studies on the effects of sulfation have been conducted using very restricted reactive mixtures. CO elimination in the rich phase through both oxidation and the water gas shift reaction has been shown to be deactivated from sulfation [102]. The same is true for the elimination of hydrocarbons from oxidation and steam reforming [103]. Sulfation has also previously been shown to increase N_2O production and inhibit the production of NH_3 [107]. These findings are consistent with our simulated exhaust results. However, regarding the deactivation of NH_3 production, there has been very little work conducted to determine the cause of the deactivation or what reductant pathways are deactivated. Another consideration is that the simulated exhaust work in the previous chapter used

exclusively intermittent sulfation conditions, where the catalyst was sulfated between evaluations, but there was no SO_2 present during the evaluation itself. In a real exhaust, SO_2 will constantly be present during operation, therefore it is important to determine if there is a significant difference in catalyst activity when exposing the catalyst to intermittent sulfation or continuous sulfation.

Here, the desulfated catalyst samples from the simulated exhaust experiments presented in the previous chapter were exposed to isolated reaction conditions. These conditions were used to evaluate the production of NH_3 when H_2, CO, or C_3H_8 were used as reductants and the production of H_2 from the water gas shift and steam reformation reactions. The activity was evaluated in their desulfated state, under continuous SO_2 exposure, and after SO_2 exposure. The results from these experiments are then related back to previous simulated exhaust experiments to explain the overall deactivation seen in those evaluations. Furthermore, the results from intermittent sulfur exposure are compared to the results from continuous SO_2 exposure to determine distinctions between these two exposure methods.

5.2 Experimental

5.2.1 Catalysts and Reactor

The catalysts studied in this chapter are the catalysts that were sulfated and desulfated in the previous chapter. This is done to ensure that the results observed in this work are directly comparable to those of the previous chapter These formulations are described in Chapter 2.2.1 and the specifications are shown in Table 5.1. The exhaust experiments this chapter are conducted in the cycling reactor described in Chapter 2.2.3.

Table 5.1: Desulfated commercial catalyst formulations

Description	Pt (g/L)	Pd (g/L)	Rh (g/L)	OSC	NSC
Pd-TWC	0	7.33	0	Low	Low
NS-TWC	2.47	4.17	0.05	High	High

5.2.2 Isolated Reaction Evaluation

The catalysts are exposed to selected reactants in order to isolate individual reactions that are occurring on the TWC in passive SCR. The reactions evaluated are shown in Table 5.2. This set of reactions is designed to evaluate the production of NH_3 using H_2, CO, or C_3H_8. It is also designed to evaluate the production of H_2 from both CO and C_3H_8 through the water gas shift and steam reforming reactions. The experimental procedure allows for the reduction reactions to dominate in the rich phase, and for the oxidation reactions to dominate in the lean phase, while still allowing for the effects of transient cycling conditions to be present in the evaluation. The concentrations used here were chosen because they are close to the concentrations seen in real systems, while maintaining equivalent reduction capacities for each potential reductant, allowing for the direct comparison of results. These experiments are conducted with a constant space velocity of 27,000 hr^{-1} rather than changing the space velocity between the lean and rich phases as was done in the simulated exhaust experiments. The only difference between the lean and the rich phase in this evaluation is the presence of 10% O_2 in the lean phase, while there is no O_2 in the rich phase. The lean/rich cycling is controlled through a timer, so that the catalyst is exposed to 2 minutes rich followed by 2 minutes lean. This removes the changing lean and rich phase times present in the feedback controlled simulated exhaust evaluations.

Table 5.2: Reactive conditions for isolated reactions

	NH$_3$ from H$_2$ $NO + H_2 + H_2O$		NH$_3$ from CO $NO + CO + H_2O$		NH$_3$ from C$_3$H$_8$ $NO + C_3H_8 + H_2O$		WGS $CO + H_2O$		Reforming $C_3H_8 + H_2O$	
Cycled between 10% O_2 and N_2 balance with SV = 27,000 hr^{-1}	Rich	Lean	Rich	Lean	Rich	Lean	Rich	Lean	Rich	Lean
CO (%)	0	0	1.0	1.0	0	0	1.0	1.0	0	0
H$_2$ (%)	1.0	1.0	0	0	0	0	0	0	0	0
NO (%)	0.05	0.05	0.05	0.05	0.05	0.05	0	0	0	0
C$_3$H$_8$ (%)	0	0	0	0	0.1	0.1	0	0	0.1	0.1
H$_2$O (%)	5.0	5.0	5.0	5.0	5.0	5.0	5.0	5.0	5.0	5.0
O$_2$ (%)	0	10.0	0	10.0	0	10.0	0	10.0	0	10.0

The overall reaction evaluation and sulfation procedure is shown in Figure 5.1. The desulfated catalyst from previous work is pretreated using 1% H$_2$ and 5% H$_2$O in N$_2$ at 650°C to reduce the catalyst. Next, the catalyst temperature is dropped to 350°C and the catalyst is evaluated in 100°C increments from 350-650°C. At each of these temperatures, the catalyst is evaluated for each reaction in Table 5.2. After the initial desulfated activity, the catalyst is exposed to 2 ppm SO$_2$ under cycling conditions using the water gas shift reactant concentrations at 350°C. Once the changes from SO$_2$ exposure have stabilized, the catalyst is evaluated with continuous SO$_2$ flow from 350-650°C. Afterwards, the catalyst is again brought down to 350°C, stabilized under 2 ppm SO$_2$ and re-evaluated without SO$_2$ in the reactant feed. This allows for us to evaluate the effects of continuous SO$_2$ exposure and contrast it with intermittent SO$_2$ exposure, which was used in the simulated exhaust work.
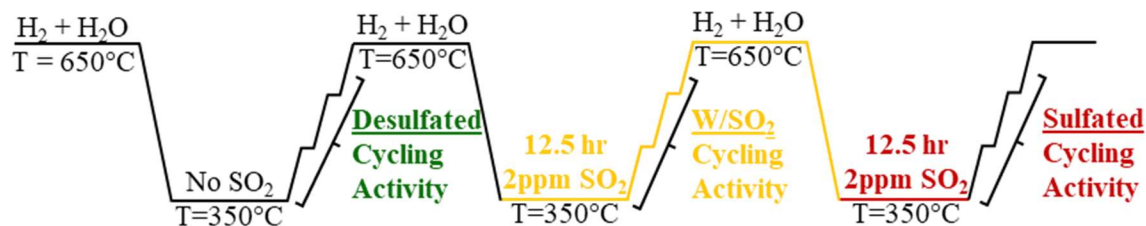
Figure 5.1: Procedure for testing isolated reaction activity

5.3 Results and Discussion

The production of NH_3 from NO, H_2, and H_2O for both catalysts is shown in Figure 5.2. Both catalysts show high activity for NH_3 production, maintaining rich phase NH_3 yields between 80% and 100% throughout the temperature range, with the NS-TWC showing slightly better performance at low temperature and the Pd-TWC showing slightly better performance at elevated temperatures, which matches with simulated exhaust results from the previous chapter. Furthermore, the production of NH_3 is not decreased significantly by intermittent sulfation at any point in the temperature range.
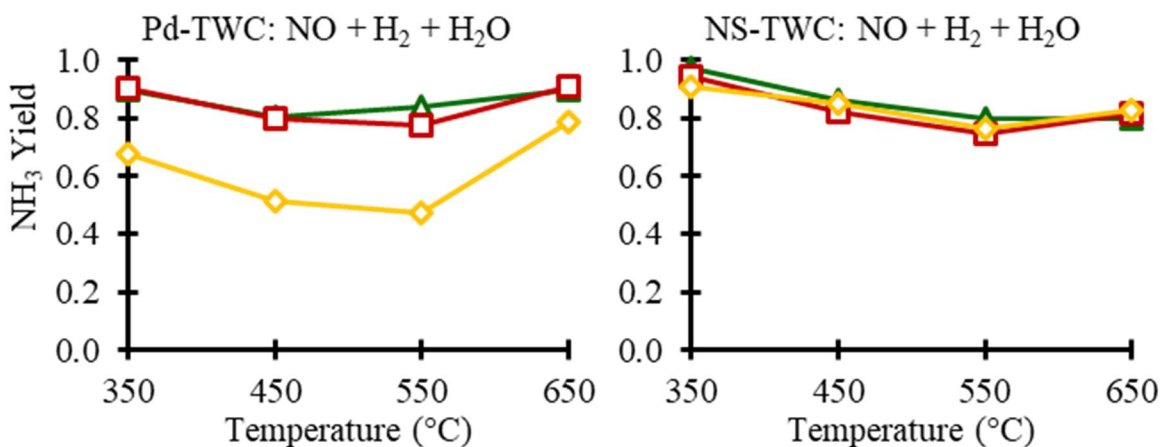
Figure 5.2: NH_3 production from H_2, NO, and H_2O on the Pd-TWC (left) and the NS-TWC (right) during SO_2 exposure (yellow), after SO_2 exposure (red), and after desulfation (green)

These results indicate that the production of NH_3 from NO and H_2 is likely not the primary mechanism of deactivation in the simulated exhaust studies. This lack of deactivation is likely because NO reduction by H_2 to form NH_3 takes place on the bulk PGM surface. Even when the catalyst is sulfated, if sufficient PGM sites remain for this reaction, it is unlikely that it will be heavily deactivated. However, when the catalyst is

exposed to continuous sulfation, the Pd-TWC shows significant deactivation, while the NS-TWC is still able to maintain its initial activity. This could be due to Pd's higher affinity for sulfur poisoning, which has been shown in previous literature [108,109].

Figure 5.3 shows NH_3 production from NO, CO, and H_2O for both the Pd-TWC and the NS-TWC. Much like NH_3 production from H_2, the reaction shows high activity before sulfation, with the NS-TWC showing better low temperature yield, and both catalysts showing very similar high temperature yields. However, in contrast to NH_3 production from H_2 is used as a reductant, when CO is used as a reductant, there is a significant change in activity before and after sulfation. This could be due to two different effects of sulfation. First, this could be due to the deactivation of the water gas shift reaction, which is shown in figure 5.4 and has been shown in previous literature to be strongly deactivated by sulfation [102]. Second, this could be from an inhibition of the hydrolysis of isocyanates on the surface, which has been proposed as an alternate means of production for NH_3 [58]. Similar to NH_3 production with H_2 as a reductant, when the catalysts are exposed to continuous sulfation, there is a strong deactivation in the production of NH_3 on the Pd-TWC, while the NS-TWC maintains its intermittently sulfated activity. This lends further evidence to the idea that the Pd-TWC is significantly different under continuous sulfation, rather than intermittent sulfation, while the NS-TWC does not see a significant difference. In addition to the stronger deactivation of the Pd, another contributing factor could be the presence of large amounts of OSC and NSC on the NS-TWC. These components are known to strongly bind sulfur in the form of sulfates. These sulfates are highly stable, which leads to the NS-TWC storing large amounts of sulfur, even when the catalyst is only exposed to intermittent sulfation. This

could lead to the catalyst being in a similar state from both intermittent sulfation and continuous sulfation.

Figure 5.3: NH_3 production from CO, NO, and H_2O on the Pd-TWC (left) and the NS-TWC (right) during SO_2 exposure (yellow), after SO_2 exposure (red), and after desulfation (green)

Figure 5.4 shows the production of H_2 from the water gas shift reaction on both the Pd-TWC and the NS-TWC with and without NO in the stream. At 350°C, neither catalyst is very active for H_2 production, showing 5-15% yield. As the temperature is increased, the activity for H_2 production increases rapidly for each catalyst. When NO is added to the reactive stream, there is a decrease in the high temperature H_2 production. This indicates that, at these elevated temperatures, the NH_3 is likely being produced from molecular H_2. However, at 350°C, there is not a significant change in H_2 production between the evaluation with NO and the one without. Despite this, the catalyst shows very high NH_3 selectivity at these temperatures, as seen in Figure 5.3, which could indicate that molecular H_2 is not a necessary intermediate in the production of NH_3 from NO + CO + H_2O. Furthermore, after sulfation, the H_2 production at 350°C remains

unaffected, even though NH_3 production decreases. This indicates that the deactivation route at this temperature is unlikely to be the production of H_2 and is likely due to a change in either the formation or the hydrolysis of isocyanate species on the surface. At elevated temperatures, the influence of sulfation becomes much more apparent. This helps explain simulated exhaust results in Chapter 4, where the outlet H_2 was strongly decreased, particularly at elevated temperatures around 500-550°C.

Figure 5.4: H_2 production from CO and H_2O with NO (top) and without NO (bottom) on the Pd-TWC (left) and the NS-TWC (right) during SO_2 exposure (yellow), after SO_2 exposure (red), and after desulfation (green)

When the catalyst is exposed to continuous sulfation, there is a stronger deactivation in water gas shift reaction for both the Pd-TWC and the NS-TWC, though,

again, the NS-TWC does maintain higher activity. The stronger deactivation on these catalysts under continuous sulfation is likely due to Pd's increased activity for the water gas shift reaction as well as its higher affinity for sulfur. Because Pd has better water gas shift activity than Pt, a large portion of these catalysts' activity is likely from Pd sites. However, because sulfur will poison these sites strongly, the Pd-TWC will have strongly decreased activity because Pd is the only noble metal present on the catalyst, while the NS-TWC maintains a larger portion of its activity because of its higher loading of Pt.

The production of NH_3 from C_3H_8, NO, and H_2O is shown in Figure 5.5. The trends in deactivation in this case are not as straightforward compared to the deactivation when CO is used as a reductant. On the Pd-TWC, the overall change in NH_3 production is not consistent throughout the temperature range, seeming to show slightly increased activity at low temperatures, slightly decreased activity at intermediate temperatures, but relatively similar activity at high temperatures. On the other hand, the deactivation over the NS-TWC is stronger. There is a consistent deactivation throughout the temperature range. Furthermore, under continuous sulfur exposure, the Pd-TWC sees strong deactivation at all temperatures, with NH_3 yields lower than 0.4 at temperatures below 650°C. In contrast, the NS-TWC only shows decreased NH_3 production at 550°C and 650°C. The reasons for this less straightforward deactivation are the complexities involved in using C_3H_8 as a reductant. Even though this reaction uses a single reductant, there are still several individual reactions that can occur. These include the steam reforming of C_3H_8 into lower chain hydrocarbons, CO, and H_2, as well as the production of NH_3 through reduction with C_3H_8 or any of the reductant byproducts. In order to further isolate the effects of sulfation, the conversion of C_3H_8, and the production of CO

82

and lower chain hydrocarbons were monitored in addition to the production of H_2 and NH_3 as is the case with previous results.
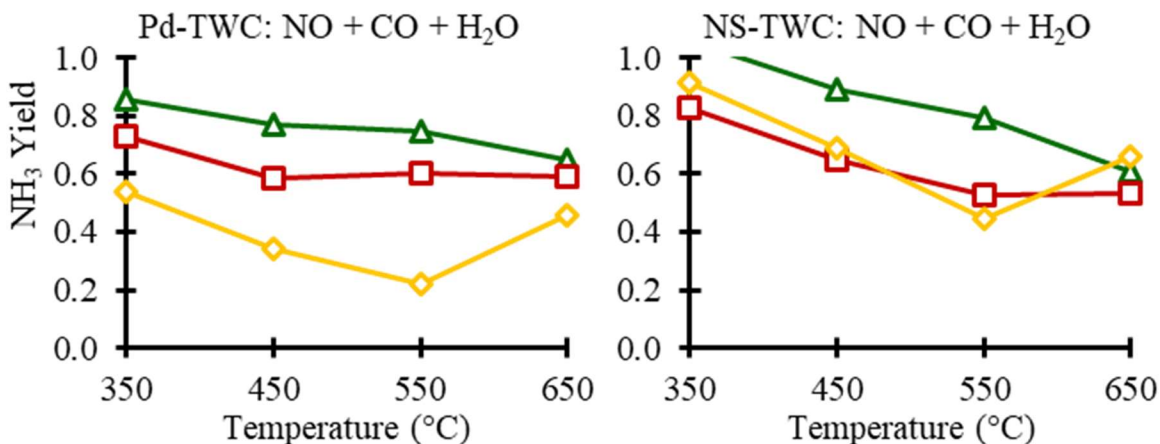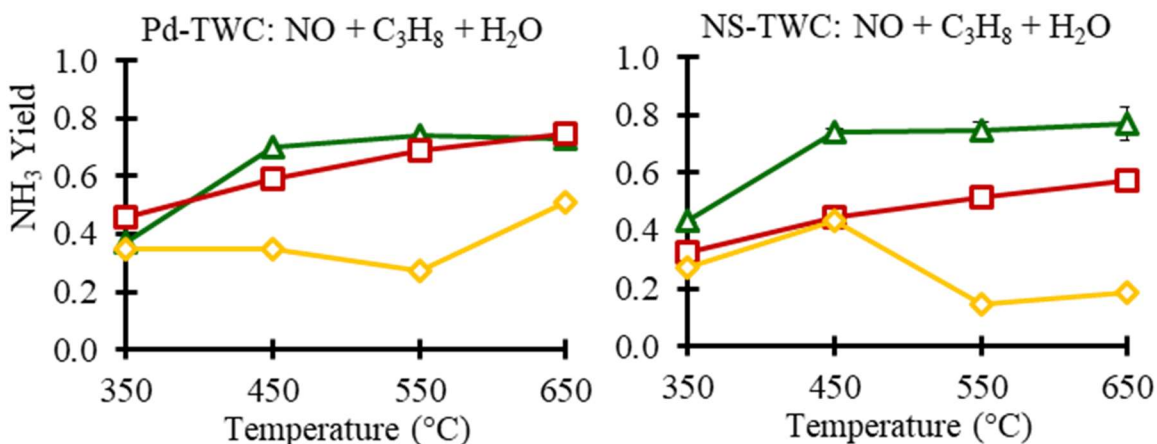

Figure 5.5: NH_3 production from C_3H_8, NO, and H_2O on the Pd-TWC (left) and the NS-TWC (right) during SO_2 exposure (yellow), after SO_2 exposure (red), and after desulfation (green)

The H_2 production from C_3H_8 and H_2O with and without NO is shown in figure 5.6. Unlike the NH_3 production, there is a very clear deactivation here. In the case of the Pd-TWC, the deactivation is consistent throughout the temperature range, showing stronger deactivation when NO is introduced. This is likely due to the consumption of reductant by the NO_X for the production of NH_3 during the multiple stages of steam reforming. In contrast, on the NS-TWC, the deactivation shows a much stronger reliance on temperature, with significant deactivation occurring at 550°C-650°C. Under continuous sulfur exposure, the Pd-TWC shows less than 30% H_2 yield across the temperature range, while the NS-TWC is still able to maintain significant H_2 production under intermediate temperatures. Again, because there are multiple individual reactions that can contribute to the production of H_2, the variation in other components must be observed to understand these changes.
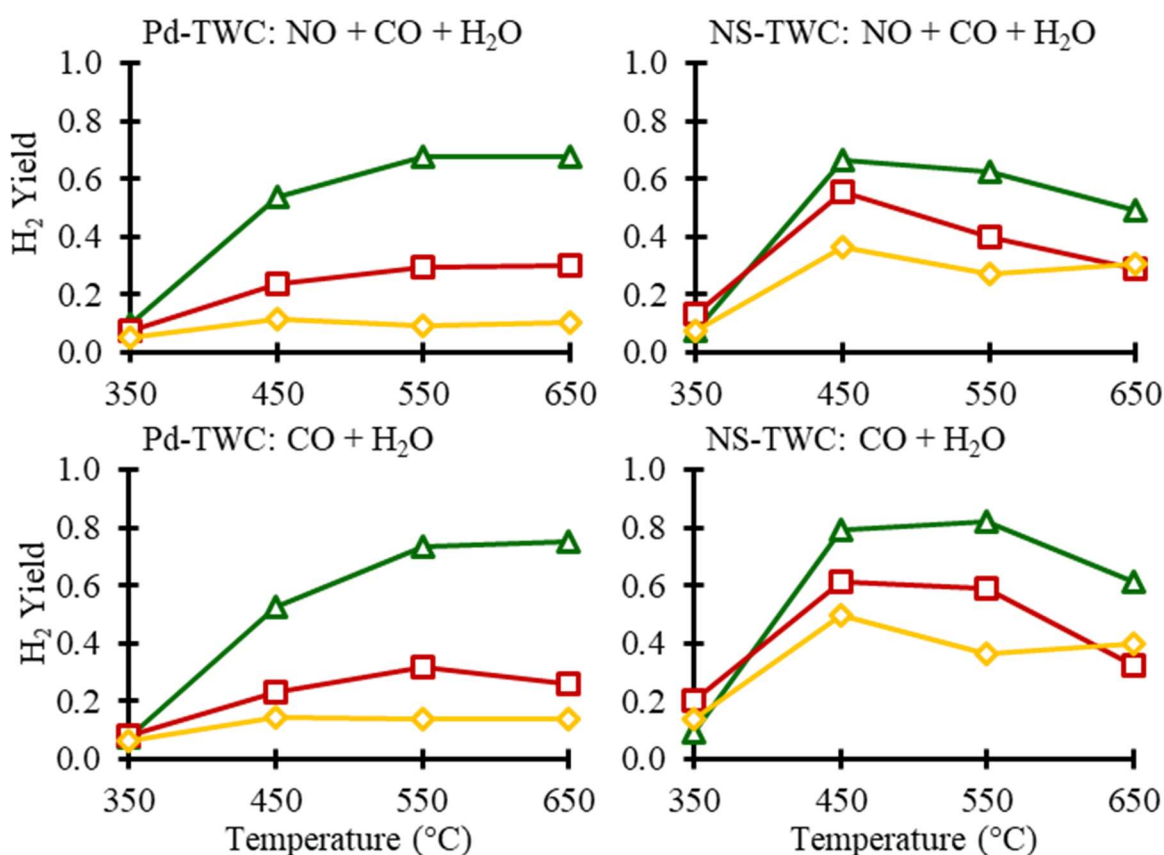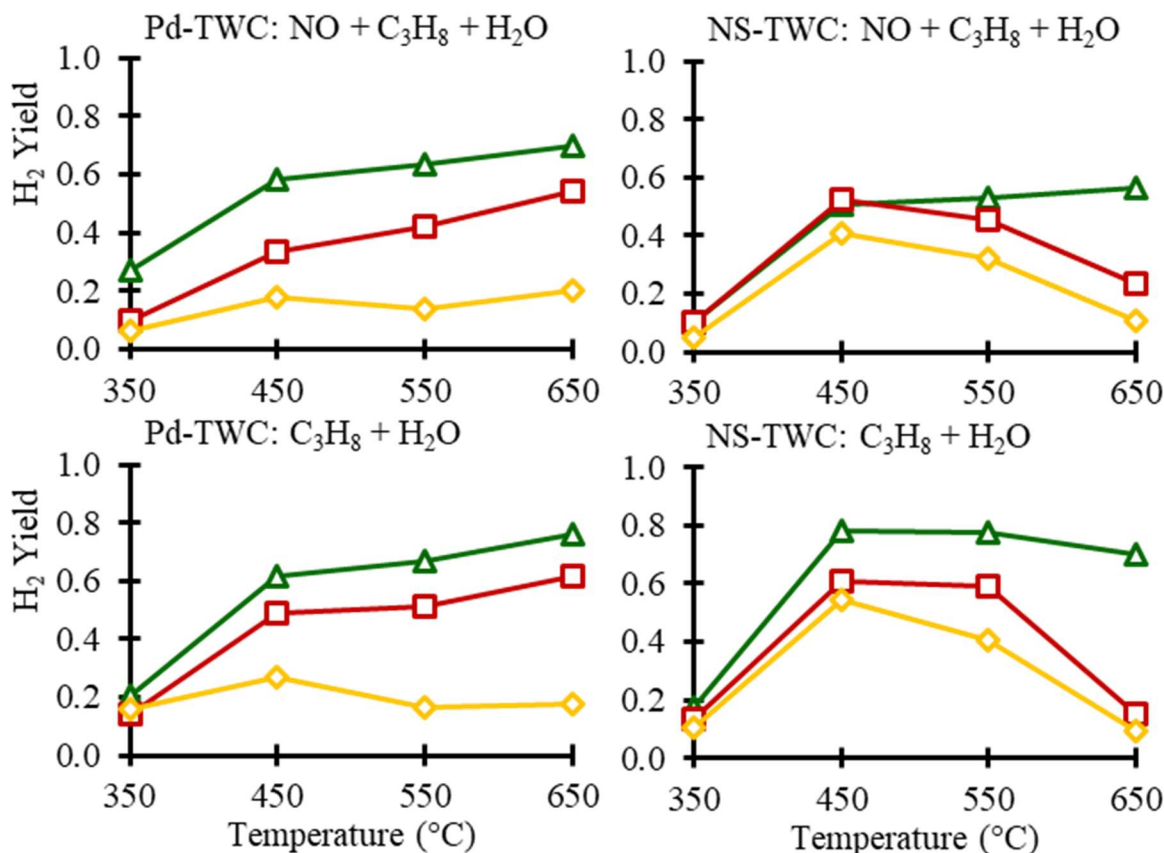
Figure 5.6: H_2 production from C_3H_8 and H_2O with NO (top) and without NO (bottom) on the Pd-TWC (left) and the NS-TWC (right) during SO_2 exposure (yellow), after SO_2 exposure (red), and after desulfation (green)

Figure 5.7 shows the propane slip for both the Pd-TWC and the NS-TWC when exposing the catalyst to C_3H_8 and H_2O. On the Pd-TWC, the effects of intermittent sulfation are negligible, and C_3H_8 only shows significant slip at 350°C. In contrast, the NS-TWC shows significant C_3H_8 breakthrough at 650°C. After sulfation. This explains the significant difference between H_2 production on the NS-TWC and the Pd-TWC from intermittent sulfation shown in figure 5.6. At these elevated temperatures, sulfation results in a strong deactivation of the NS-TWC's steam reforming reaction activity, while the Pd-TWC sees very little deactivation when exposed to intermittent sulfation. However, when the Pd-TWC is evaluated with SO_2 in the reactive stream, there is an

extreme level of deactivation. The conversion of C_3H_8 is strongly decreased and there is a significant amount of C_3H_8 that remains in the catalyst effluent. The deactivation from continuous sulfation on the NS-TWC is not as strong as that seen on the Pd-TWC but does result in more C_3H_8 breakthrough at intermediate temperatures.
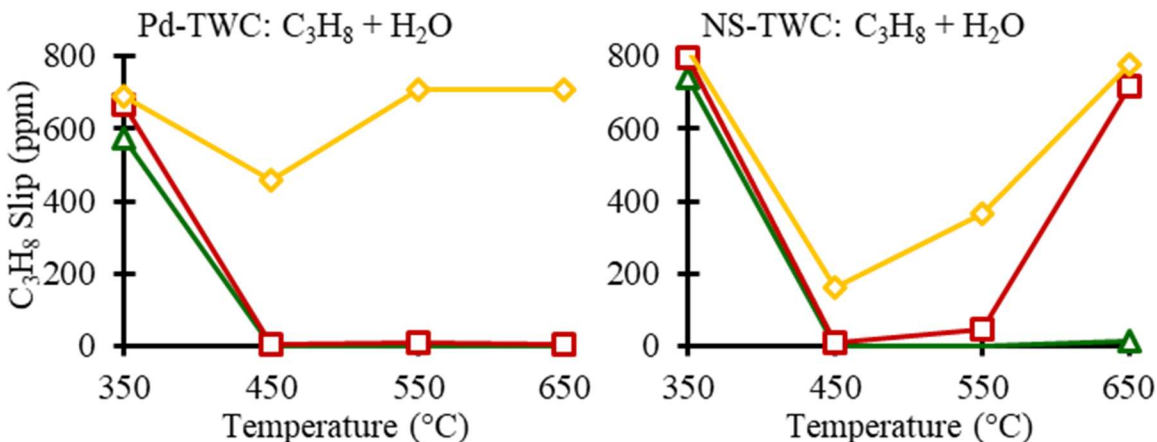
Figure 5.7: C_3H_8 slip from C_3H_8 and H_2O for the Pd-TWC (left) and the NS-TWC (right) during SO_2 exposure (yellow), after SO_2 exposure (red), and after desulfation (green)

Figure 5.8 shows the production of both CH_4 and C_2H_6 over both the Pd-TWC and the NS-TWC when exposing the catalyst to C_3H_8 and H_2O. Both catalysts show significant breakthrough of CH_4 at 450°C and very little C_2H_6 breakthrough regardless of temperature or sulfation. This CH_4 is believed to be due to the partial conversion of C_3H_8 from the steam reforming reaction, rather than the methanation of CO or CO_2. This is because there is no CH_4 produced during CO + H_2O exposure. Intermittent sulfation results in slightly increased CH_4 production over the Pd-TWC, and strongly increased CH_4 production over the NS-TWC. Again, this is likely due to the large loading of storage components on the NS-TWC, as discussed above. Under continuous sulfation, the NS-TWC shows very little change, while there is significantly lower CH_4 production

over the Pd-TWC. This is likely due to the very low conversion of C_3H_8 under these conditions.
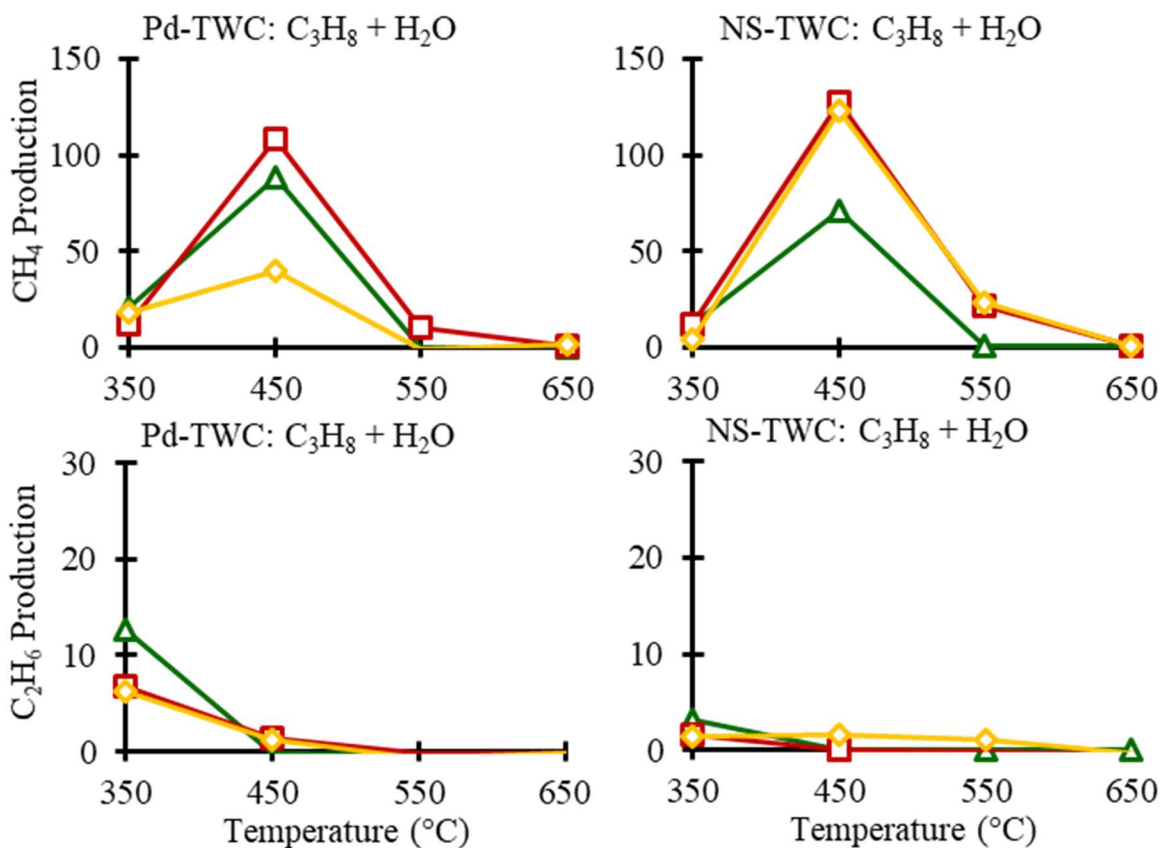
Figure 5.8: CH_4 (top) and C_2H_6 (bottom) production from C_3H_8 and H_2O for the Pd-TWC (left) and the NS-TWC (right) during SO_2 exposure (yellow), after SO_2 exposure (red), and after desulfation (green)

Figure 5.9 shows the production of CO over both the Pd-TWC and the NS-TWC when exposing the catalyst to C_3H_8 and H_2O. There is a significant difference in the production of CO before and after sulfation over the Pd-TWC. This deactivation is likely the primary cause of the difference in H_2 production over the Pd-TWC. Because of this, the change in NH_3 production on the Pd-TWC is likely due primarily to the changes in the water gas shift reaction, rather than the changes in steam reforming activity, which

does not show significant deactivation in the case of intermittent sulfation. The NS-TWC, on the other hand, does not show strongly increased CO production, indicating that the overall deactivation seen on the NS-TWC is due primarily to a deactivation in the steam reforming reaction. Under continuous sulfation conditions, there is very little change on the NS-TWC, while the Pd-TWC shows decreased CO production. This is analogous to the production of CH_4, where the decrease is due to a decrease in the conversion of C_3H_8, rather than an increase in catalyst activity.
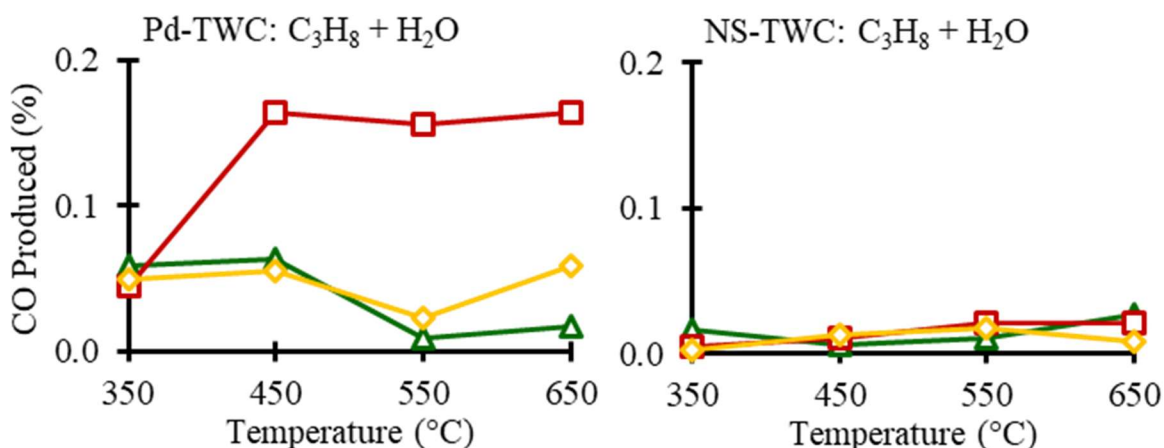
Figure 5.9: CO production from C_3H_8 and H_2O for the Pd-TWC (left) and the NS-TWC (right) during SO_2 exposure (yellow), after SO_2 exposure (red), and after desulfation (green)

Looking at the intermittently sulfated and desulfated results from these isolated reactions allows us to explain the results obtained from the simulated exhaust experiments in Chapter 4. One interesting point is that the reduction of NO into NH_3 by H_2 is unaffected by the sulfation procedure used here, but the production of NH_3 in the simulated exhaust is decreased significantly by the same procedure. This indicates that the decrease in NH_3 production in the simulated exhaust experiments is not due to the direct reaction of NO and H_2 on the surface. Rather, it is due to the decrease in the

activity of both the water gas shift and steam reforming reactions, with the Pd-TWC showing stronger deactivation for the water gas shift reaction, and the NS-TWC showing stronger deactivation for the steam reforming reaction. Additionally, from the reaction of CO, NO and H_2O, it seems that the production of molecular H_2 is not the only viable means of NH_3 production. These results suggest that, particularly at lower temperatures, a large amount of the catalyst activity can likely be attributed to the hydrolysis of isocyanates.

5.4 Conclusions

By looking at isolated reaction conditions, the reaction pathways present in automotive exhaust have been investigated. Using intermittent sulfation, isolated reactions allow for the investigation and deconvolution of the simulated exhaust results shown in the previous chapter. One of the most important results is that the production of NH_3 from NO, H_2, and H_2O was not significantly affected under these operating conditions. However, the production of NH_3 when using CO or C_3H_8 as a reductant was significantly deactivated. It was also seen that the mechanism of deactivation could vary based on the catalyst. On the Pd-TWC, the primary pathways that are deactivated are the water gas shift reaction, and the production of NH_3 from NO, CO, and H_2O. On the NS-TWC, both of those reactions are deactivated, but there is also a strong deactivation in the steam reforming reaction, particularly at high temperatures.

Continuous sulfation experiments proved that there is a very strong difference between catalyst activity under continuous sulfur exposure compared to intermittent exposure, which was used in the simulated exhaust experiments. This was particularly

apparent on the Pd-TWC, where the deactivation of NH_3 production from both H_2 and CO was significant. In contrast, the activity of the NS-TWC showed little difference in the activity of these reactions between intermittent and continuous SO_2 exposure. The reason for the difference between Pd-TWC and the NS-TWC is likely twofold. First, the Pd-TWC has Pd as the only noble metal on the surface. The NS-TWC has significant Pt loading, which has much higher resistance to sulfur poisoning than Pd. Second, the NS-TWC has significant loadings of OSC and NSC, which uptake significant amounts of SO_2. Thus, the catalyst will hold significantly more SO_2 from intermittent exposure and there will be less of a distinction between intermittent and continuous sulfur exposure. If the goal is to capture the true behavior of catalyst components, future studies should be conducted under continuous SO_2 exposure, rather than intermittent SO_2 exposure.

CHAPTER 6

THE EFFECTS OF RICH PHASE LAMBDA ON THE SULFATED
THREE-WAY CATALYST PERFORMANCE IN SIMULATED PASSIVE
SELECTIVE CATALYTIC REDUCTION EXHAUST

6.1 Introduction

As seen in the previous chapters, sulfur has a strongly negative effect on the operation of a passive SCR system, deactivating several key reaction pathways that aid in emissions reductions. However, previous simulated exhaust experiments were conducted under a single rich phase λ of 0.97. It is important to investigate the effects of varying the rich phase environment to determine if the negative effects of sulfation can be partially or completely mitigated through simple operation strategies. It has been shown in literature that rich conditions are significantly more effective for the desulfation of TWCs and NSR catalysts than lean conditions [57,110]. The extended rich operation of 2-3 minutes is one of the primary aspects that sets passive SCR apart from other emissions control technologies. Beyond that, the performance of the TWC in the rich phase is one of the key operational concerns in Passive SCR. During lean operation, the primary concern is the oxidation of CO and HCs, which modern catalysts are generally capable of at sufficiently high temperatures, even with extensive sulfation and catalyst aging as seen in previous chapters. In contrast, under rich operation, the catalyst must produce the requisite NH_3, and the activity for water gas shift and steam reforming reactions must be maintained to control CO and HC emissions. The problem arises when, under rich

conditions, there is a significant deactivation of each of these essential reactions from sulfation. The significant deactivation of the rich phase operation is likely due to the formation of sulfides on the PGM surface. Previous work by Amberntsson *et al.* has shown that sulfur preferentially forms sulfates on the metal oxide support and storage components during lean operation but can form sulfide groups with the noble metals under rich conditions [101]. While work comparing sulfation under lean conditions or rich conditions has been conducted, there has not been sufficient work conducted to determine how the sulfation changes under different rich phase λ values. Furthermore, to our knowledge, there has not been a study that looked at that variation under simulated exhaust conditions modeling a passive SCR system. This is an aspect of the passive SCR system that must be investigated if the system is to see commercial implementation.

In this chapter, the effects of rich phase λ on the deactivation of commercial TWC samples due to sulfation is investigated. The previous simulated exhaust studies discussed in Chapter 4 only looked at the catalyst under intermittent sulfation conditions, where the catalyst was not evaluated with SO_2 in the reactive stream. Rather, the catalyst was exposed to sulfur between evaluations. As evidenced in the isolated reactions shown in Chapter 5, there is a significant difference between the effects of intermittent sulfur exposure and continuous sulfur exposure. Because of this, the investigation here is conducted under continuous sulfur exposure conditions. Additionally, the catalyst evaluations in this chapter are conducted under two different temperatures, 350°C and 550°C, which are chosen as the low and high operation temperatures and roughly simulating close-coupled and under-floor operation. 350°C is chosen as the low temperature to correlate with results from the previous simulated exhaust evaluations.

550°C is chosen as the high temperature to prevent desulfation from interfering with the evaluation. Results from Chapter 4 show that the effects of sulfation on NH_3 production are strongest at 550°C. This is because, above 550°C, the sulfur compounds formed on the TWCs begin to decompose and the catalysts begin to regain their clean activity. By evaluating the catalysts at 350°C and 550°C, it will be possible to not only determine the effects of rich λ, but also how those effects change during low or high temperature operation.

6.2 Experimental

6.2.1 Catalyst Formulations and Reactor Apparatus

The catalysts studied in this chapter are the same commercial catalysts used in the previous chapters. These formulations are described in Chapter 2.2.1 and the specifications are shown in Table 6.1. The exhaust experiments presented in this chapter are conducted in the cycling reactor described in Chapter 2.2.3.

Table 6.1: Commercial catalyst formulations

Description	Pt (g/L)	Pd (g/L)	Rh (g/L)	OSC	NSC
Pd-TWC	0	7.33	0	Low	Low
NS-TWC	2.47	4.17	0.05	High	High

6.2.2 Evaluating Effects of Rich Phase λ

The catalysts are evaluated under fixed load conditions using the reactive conditions simulating the various rich phase λ shown in Table 6.2. The variation of the rich phase λ is controlled by the variation in the concentration of CO, H_2, and O_2. The

switching between lean and rich is handled through feedback controlled lean-rich cycling as outlined in Chapter 2.2.3. Much like in Chapter 4, this allows us to evaluate the system in a manner that can be expanded to the operation of the system in a real lean-burn gasoline engine exhaust

Table 6.2: Operating conditions for fixed load operation with variable rich phase λ

0.92	0.93	0.94	0.95	0.96	0.97	0.98	2.0	λ
0.82	0.87	0.92	0.97	1.02	1.07	1.12	10.0	O_2 (%)
2.6	2.4	2.2	2.0	1.8	1.6	1.4	0.2	CO (%)
1.3	1.2	1.1	1.0	0.9	0.8	0.7	0	H_2 (%)
			0.06				0.036	NO (%)
			0.1				0.1	C_3H_8 (%)
			11				6.6	H_2O (%)
			11				6.6	CO_2 (%)
			27,000				45,000	SV (hr^{-1})

The procedure used to evaluate the effects of rich phase λ on catalyst deactivation from sulfur is shown in Figure 6.1. This procedure begins with the pretreatment of the catalyst at a simulated λ of 0.92 and a temperature of 650°C to reduce the catalyst. After pretreatment, the desulfated/clean catalyst is evaluated under cycling conditions at 550°C using a fixed lean phase λ of 2.0 and a variable rich phase λ from 0.92-0.98. After this is completed, the catalyst is cooled to 350°C and the catalyst is again evaluated while the rich phase λ is varied from 0.92-0.98. Next, the catalyst is exposed to 2ppm SO_2 under cycling conditions with a rich phase λ of 0.92 until the effects of sulfation are steady.

Then, with continuous SO$_2$ exposure, the catalyst is evaluated under the same λ values used for the desulfated/clean evaluation. Finally, the catalyst is desulfated by cycling between lean and rich operation for 3 hours at 650°C.
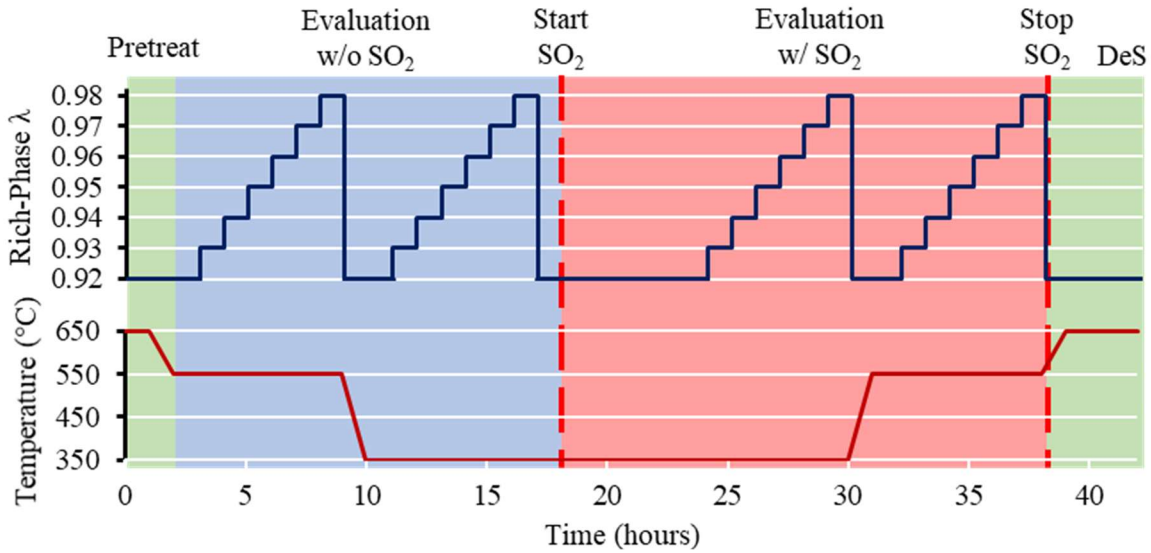
Figure 6.1: Experimental procedure for the evaluation of the effects of rich phase λ on the operation of a TWC in a passive SCR system

6.3 Results and Discussion

The effect of rich phase λ on NH$_3$ production over both Malibu-1 and ORNL-1 at both 350°C and 550°C is shown in Figure 6.2. Lowering the rich phase λ does mitigate the negative effects of sulfation on NH$_3$ production. In most cases, the NH$_3$ yield for the desulfated catalyst with a rich phase λ of 0.97, which was used in Chapter 4, is roughly equivalent to the catalyst under sulfur exposure at a rich phase λ of 0.95. On the NS-TWC, if the rich phase λ is sufficiently low, the catalyst can produce more NH$_3$ than there is NO$_X$ in the rich phase. This is because, under these conditions, a large amount of stored NO$_X$ on the catalyst can be converted into NH$_3$ because the catalyst is very rapidly reduced. However, under the evaluation at 550°C, the catalyst is no longer active for

NO$_X$ storage, and this benefit is no longer seen. This further highlights the conclusion in Chapter 4 that a NS-TWC should be maintained at a lower temperature if the full benefit of its NSC is to be gained.

Figure 6.2: The production of NH$_3$ based on rich phase λ for Malibu-1 (top) and ORNL-1 (bottom) at 350°C (left) and 550°C (right) under fixed load conditions.

The rich phase NO$_X$ conversion in relation to rich phase λ is shown in Figure 6.3. Exposure to continuous SO$_2$ leads to decreased NO$_X$ conversion as seen from previous work. This effect is particularly strong at 550°C, where both catalysts show a strong deactivation. Decreasing the rich phase λ value can help mitigate these effects, much like the effects on NH$_3$ production. This is likely due to the higher concentration of reductants present in the exhaust, which leads to more rapid reduction of NO$_X$. However, in this

case, even with lower rich phase λ, the deactivation is still apparent, particularly during the 550°C evaluation.
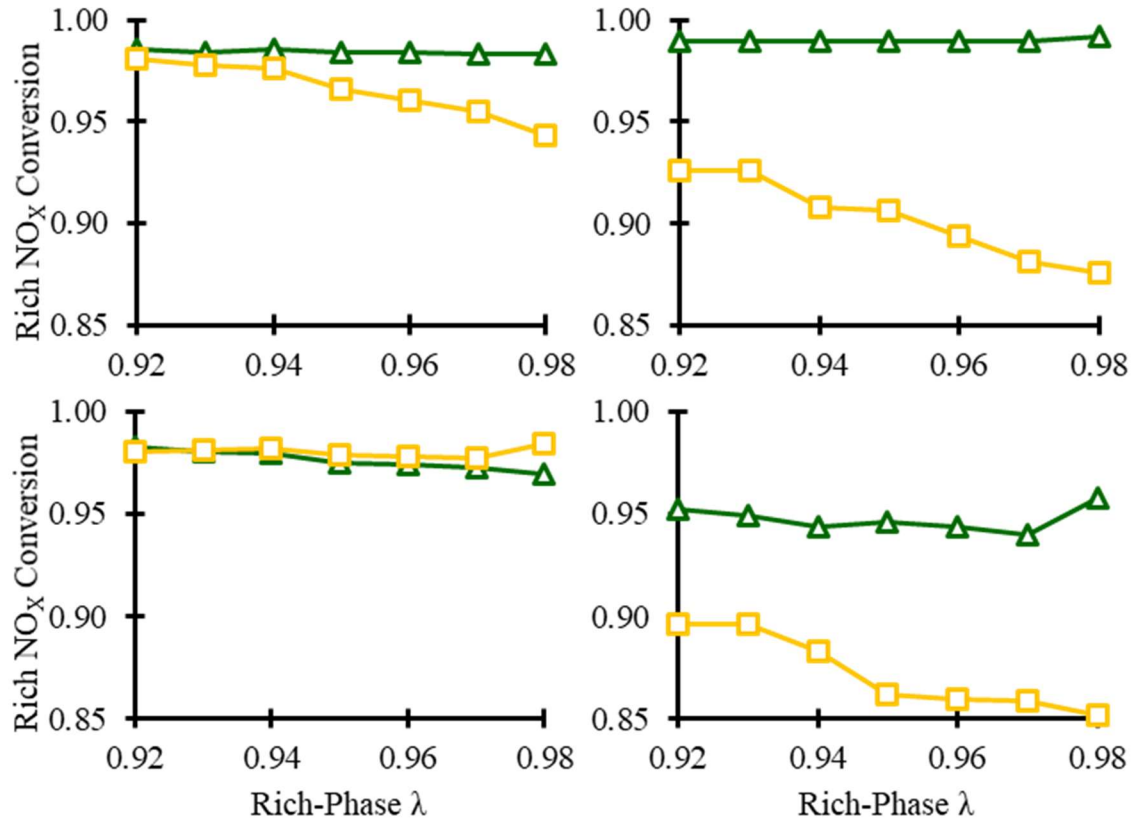
Figure 6.3: The conversion of NO$_x$ based on rich phase λ for the Pd-TWC (top) and ORNL-1 (bottom) at 350°C (left) and 550°C (right) under fixed load conditions.

The CO in the catalyst effluent in the rich phase in relation to rich phase λ for both the Pd-TWC and NS-TWC at 350°C and 550°C is shown in Figure 6.4. The trends are clear and intuitive here. Under richer λ values, there is additional CO in the exhaust and thus, more in the effluent. Furthermore, in agreement with results in previous chapters, exposure to SO$_2$ results in increased CO in the catalyst effluent for both catalysts. The deactivation of the CO conversion is particularly high under 550°C evaluation. This means that, while better NH$_3$ production and NO$_X$ conversion can be

obtained for lower rich phase λ values, there is a trade off in the form of increased CO emissions. These effects will need to be weighed against each other to determine the optimum rich phase λ for the real system.
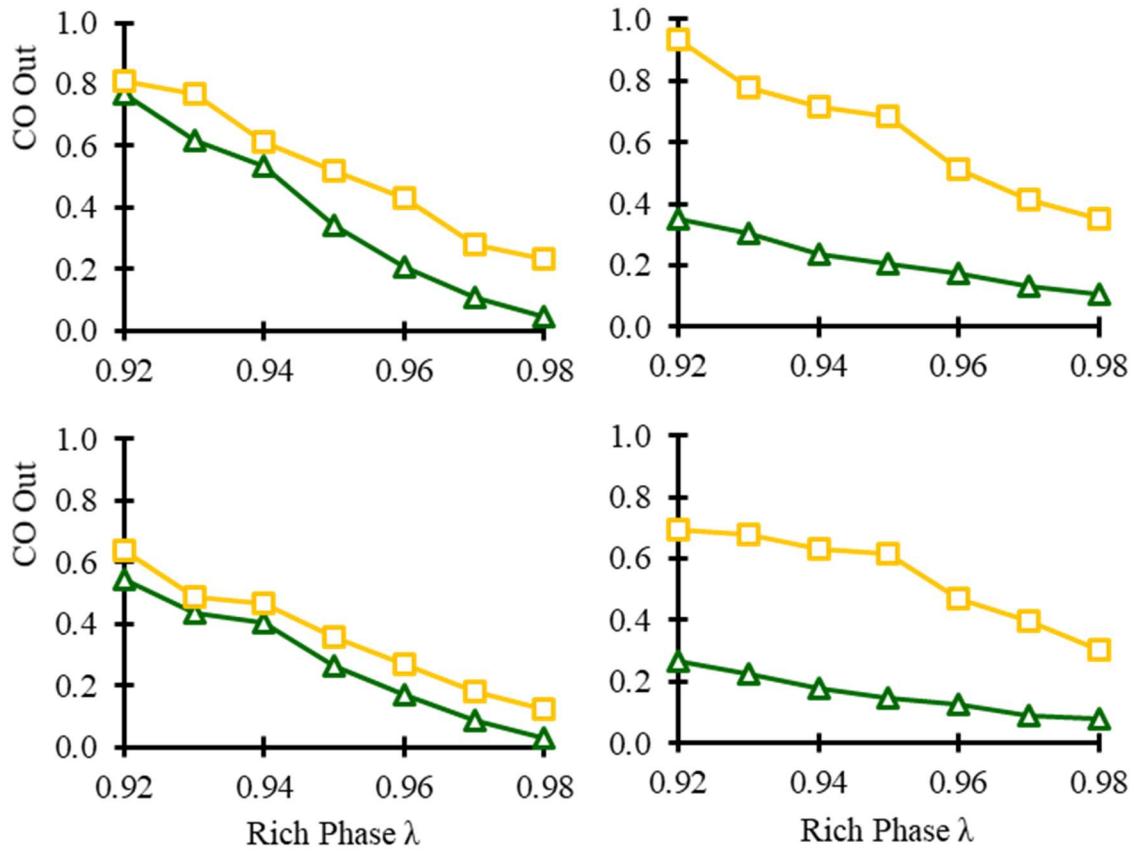
Figure 6.4: The effluent CO in the rich phase based on rich phase λ for Malibu-1 (top) and ORNL-1 (bottom) at 350°C (left) and 550°C (right) under fixed load conditions.

The changes in rich phase C_3H_8 in the catalyst effluent are shown in figure 6.5. There is a clear deactivation across both catalysts and operating temperatures. However, the C_3H_8 in the effluent does not show a significant dependence on the rich phase λ, except in the evaluation of NS-TWC at 350°C. Under most conditions, lowering the rich phase λ value shortens the rich phase because of the increased NH_3 production. However,

the breakthrough of C_3H_8 is also increased during the rich phase. These two effects balance each other under most operating conditions. However, in the case of the NS-TWC at 350°C, the breakthrough of C_3H_8 is very strongly increased at lower rich phase λ values, resulting in a net increase in C_3H_8 out, despite the shorter rich phase.
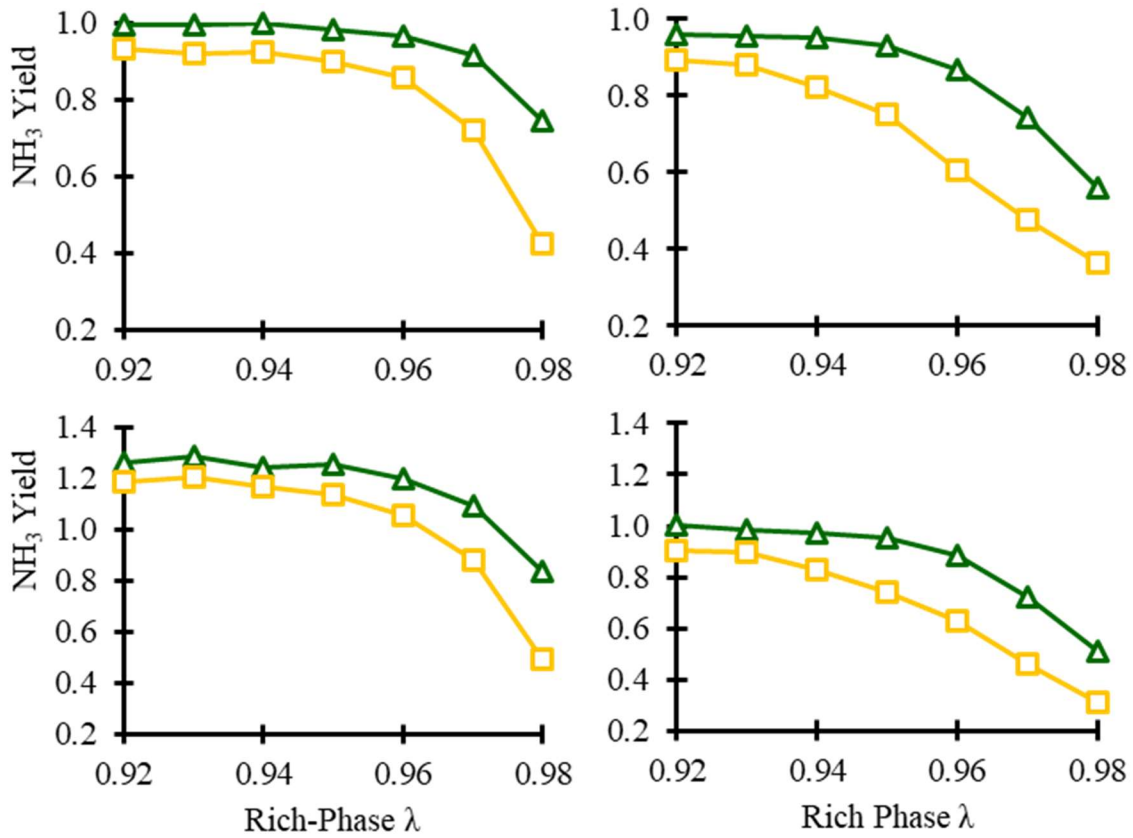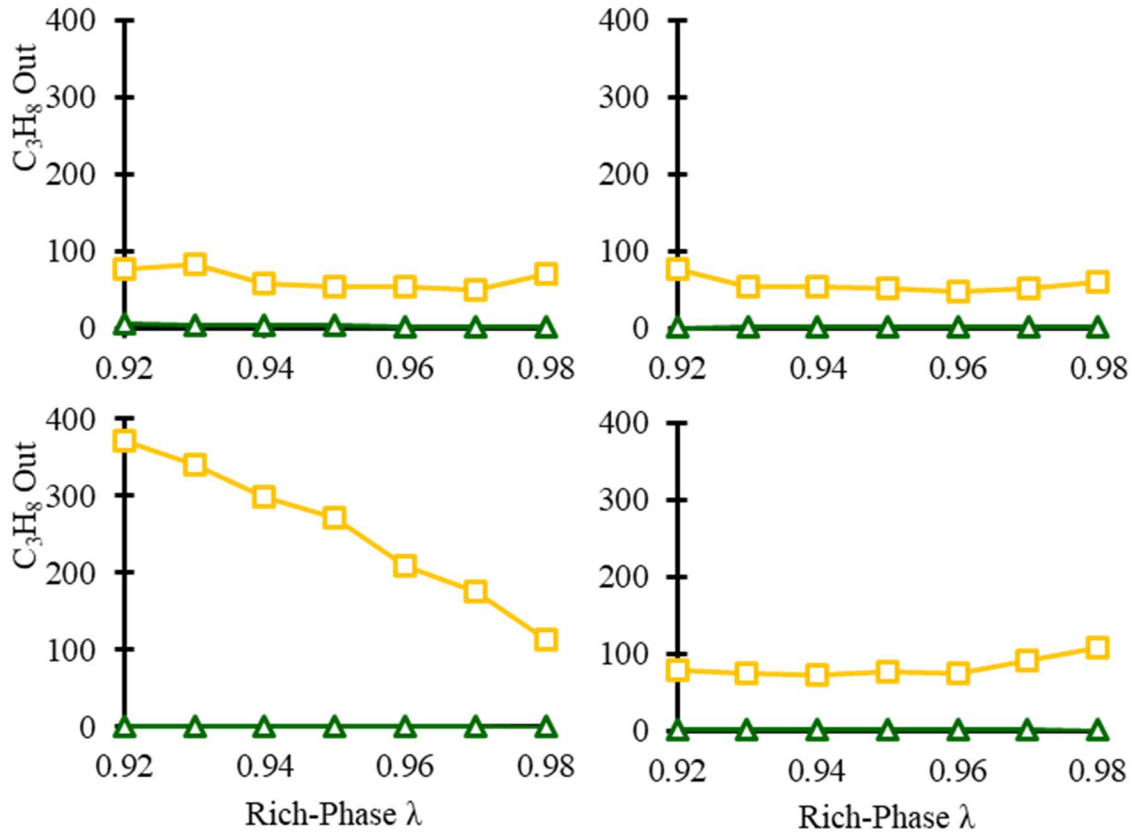
Figure 6.5: The effluent C_3H_8 in the rich phase based on rich phase λ for Malibu-1 (top) and ORNL-1 (bottom) at 350°C (left) and 550°C (right) under fixed load conditions.

6.4 Conclusions

This work has illustrated both the benefits and drawbacks of lower rich phase λ values for the mitigation of sulfation effects on NH_3 production and NO_X conversion in a passive SCR system. During sulfur exposure, the catalyst generally has a strong

deactivation in activity for the production of NH_3. However, by operating at lower λ values, the catalyst is provided with additional reductants, which allows for more rapid production of NH_3. By increasing the NH_3 production, the rich phase can be shortened. This can lead to an increase in overall fuel efficiency because the engine is running lean for a longer portion of the total operational time. However, these benefits are complicated by the costs of lower rich phase λ values. At these lower λ values, engine-out CO and HC emissions as well as fuel consumption are increased during rich operation. Over the catalyst, the outlet CO was strongly increased by richer λ values, while the HC emissions were not changed significantly, except for the NS-TWC at 350°C. This means that the benefits of lowering the rich phase λ (better fuel economy, shorter rich phase, improved NO_X conversion) must be weighed against the drawbacks (increased CO and HC breakthrough during rich operation) when determining the optimum rich phase λ for the operation of a passive SCR system.

.

CHAPTER 7

THE EFFECTS OF CERIA LOADING ON THREE-WAY CATALYSTS
FOR PASSIVE SELECTIVE CATALYTIC REDUCTION

7.1 Introduction

The work discussed in previous chapters has been conducted on fully formulated commercial TWC samples. These experiments are important because they illustrate the realistic performance and help tune the operating conditions for passive SCR. However, because of their complex nature, it can be difficult to fundamentally understand the chemical processes at play on these commercial catalysts. Many of the differences in the catalytic activity between the Pd-TWC and NS-TWC could be attributed to numerous differences in the catalytic formulations. First, there is the differences in PGM loading, with the Pd-TWC having only Pd, while the NS-TWC has a mixture of Pt, Pd, and Rh. Second, the presence of significant amounts of both OSC and NSC on the NS-TWC can drastically change its evaluation, particularly under cycling conditions. Some of these differences have been investigated in previous literature. Oh and Triplett, in their work showing the multiple roles of CO in NH_3 generation, showed that catalysts containing Ce and Rh are highly active for NH_3 decomposition [60]. Adams *et al.* investigated the differences in catalyst activity when introducing barium or cerium, showing that cerium addition is useful when CO is used as a reductant in NH_3 production [70]. Another study by Adams *et al.* investigated the effectiveness of Pd catalysts vs. Pt catalysts for the operation of passive SCR, showing that Pd was a more effective PGM and attributing its

improved activity to its increased activity for the water gas shift reaction at a lower temperature [65].

One TWC component that can have a large impact on the operation of a passive SCR system is ceria. Ceria is often used in commercial TWCs for several beneficial attributes [47,49,111]. Of particular relevance to passive SCR is ceria's oxygen storage and its promotion of the water gas shift reaction. Oxygen storage is generally a beneficial attribute of TWCs on stoichiometrically operated gasoline engines because it allows for the oxidation of CO and HCs during brief oscillations into rich operation. However, in a passive SCR system, high levels of oxygen storage inhibit the reduction of the catalyst, preventing the production of NH_3 for a significant portion of the rich phase as discussed in Chapter 3. However, ceria also promotes water gas shift, which is highly beneficial in a passive SCR system because it aids in the production of NH_3 and eliminates CO emissions. Because of these two effects, there should be some optimum ceria loading that allows for sufficient promotion of the water gas shift reaction, while minimizing the inhibitory effect on the reduction of the catalyst. Still, no research to date has isolated these individual effects of ceria on TWC performance in passive SCR.

Here, several model $Pd/CeO_X/Al_2O_3$ catalyst have been synthesized to investigate the effects of ceria loading on TWC performance in passive SCR. Pd is chosen as the PGM due to its high performance in previous evaluations [66]. The catalysts have been characterized using XRD and they have been evaluated for their activity for several reactions relevant to the performance of TWCs in passive SCR systems. The reactions are designed to evaluate the production of NH_3 using H_2 or CO as a reductant as well as the production of H_2 from the water gas shift reaction under cycling conditions. This gives us

a more fundamental understanding of the chemical processes at play in the previous commercially formulated catalyst evaluations and allows us to directly track the multiple effects ceria has on the performance of TWCs in passive SCR systems.

7.2 Experimental

7.2.1 Catalyst Preparation

Several model $Pd/Ce/Al_2O_3$ catalysts were synthesized to investigate the multiple effects of Ce loading on the activity of reactions in a passive SCR system. The formulations are shown in Table 7.1. The $Pd/Ce/Al_2O_3$ samples were synthesized with 1% Pd and 0 - 10% Ce. The model catalysts were synthesized via sequential wet impregnation of Ce followed by Pd onto the γ-Al_2O_3 support. After each impregnation, the catalysts are calcined in air for 3 hours at 650°C.

Table 7.1: Model $Pd/CeO_X/Al_2O_3$ formulations

Catalyst	1Pd	1Pd 0.5Ce	1Pd 1Ce	1Pd 2Ce	1Pd 5Ce	1Pd 10Ce
Pd Loading	1.0%	1.0%	1.0%	1.0%	1.0%	1.0%
Ce Loading	None	0.5%	1.0%	2.0%	5.0%	10.0%

7.2.2 Catalyst Characterization

XRD was used to characterize the catalysts synthesized via wet impregnation and identify what crystalline phases were present in each sample. The instrument used is a Rigaku Mini Flex II diffractometer using Cu Kα radiation. The powdered catalyst samples were scanned at 2θ values from 10 – 80 in order to capture all observable peaks in the samples.

7.2.3 Catalyst Evaluation

The powder catalysts are evaluated in a bench scale reactor. The introduction of gases into the reactor is controlled through several mass flow controllers. Water is introduced into the apparatus through a temperature-controlled bubbler. The catalysts were loaded into a quartz U-tube reactor. The temperature of the catalyst was controlled through a furnace surrounding the quartz tube. During the reaction, the catalyst effluent is analyzed with an MKS MultiGas 2030 gas phase FTIR.

The catalysts are first reduced at 550°C in 1% H_2 and 5% H_2O before being evaluated using the cycling reactive conditions outlined in Table 7.2. These reactions are used to evaluate the catalyst for the water gas shift reaction ($CO + H_2O$), the production of NH_3 when CO is used as the reductant ($CO + NO + H_2O$) and the production of NH_3 when H_2 is used as a reductant ($H_2 + NO + H_2O$). In each case, 100 mg of the catalyst is evaluated using 333 sccm gas balanced by Ar. During each reaction, the catalyst is exposed to five minutes of rich operation, where no O_2 is present, and five minutes of lean operation, where there is 10% O_2 in the reactive mixture. The effluent gas is diluted to 1000 sccm with Ar to improve time resolution measurements on the FTIR.

Table 7.2: Reaction conditions

Phase	$CO + H_2O$		$CO + NO + H_2O$		$H_2 + NO + H_2O$	
	Rich	Lean	Rich	Lean	Rich	Lean
O_2 (%)	0	10	0	10	0	10
H_2 (%)	0	0	0	0	1	1
CO (%)	1	1	1	1	0	0
NO (%)	0	0	0.05	0.05	0.05	0.05
H_2O (%)	5	5	5	5	5	5

7.3 Results and Discussion

The XRD spectra for the $Pd/CeO_X/Al_2O_3$ catalysts are shown after impregnation and calcination in Figure 7.1. The catalyst shows peaks corresponding to PdO, CeO_2, and γ-Al_2O_3. From these diffraction patterns, both PdO and CeO_2 are highly crystalline. At low Ce loadings (0.5-1%), the characteristic peaks of CeO_2 are too broad and their magnitude is too low to determine crystallite size. As the Ce loading is increased, the CeO_2 diffraction pattern becomes dominant, and the CeO_2 particles become larger up to a maximum of 11.2 nm. However, despite the changing relative magnitude of the Pd diffraction pattern, the crystallite size of Pd does not change significantly as more ceria is added and maintains a crystallite size of 20-25nm.
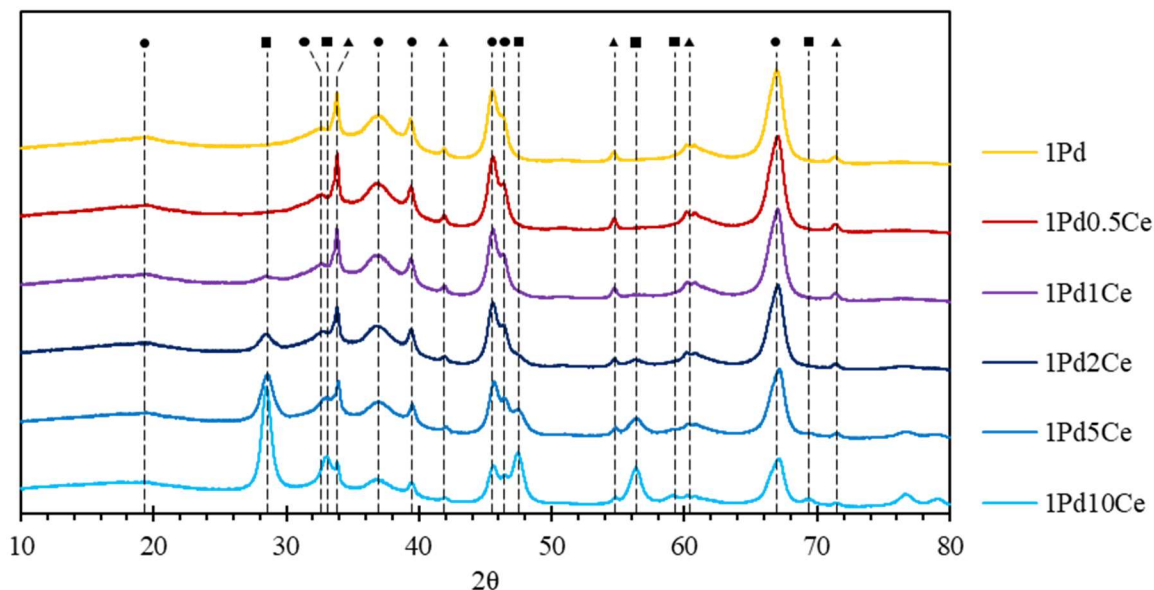
Figure 7.1: XRD for $Pd/CeO_2/Al_2O_3$ catalysts. Peaks for γ-Al_2O_3 (●), CeO_2 (■), and PdO (▲) are identified and labeled in the diffraction patterns.

The production of NH_3 during NO, H_2, and H_2O exposure over each Ce loading is shown in Figure 7.2. This data indicates that, under these reaction conditions, neither the

temperature nor the ceria loading has a strong effect on NH_3 production. This is consistent with previous results from commercial catalyst testing in Chapter 5, where the performance of the Pd-TWC and the NS-TWC were relatively similar during exposure to NO, H_2, and H_2O, and they did not vary significantly as the temperature was increased from 350°C to 650°C. Just as in that case, the ceria does not play a large role in this reaction because the reduction of NO by H_2 to form NH_3 occurs entirely on the noble metal surface. Because each of these catalysts have roughly equivalent Pd surface area, they show equivalent activity.
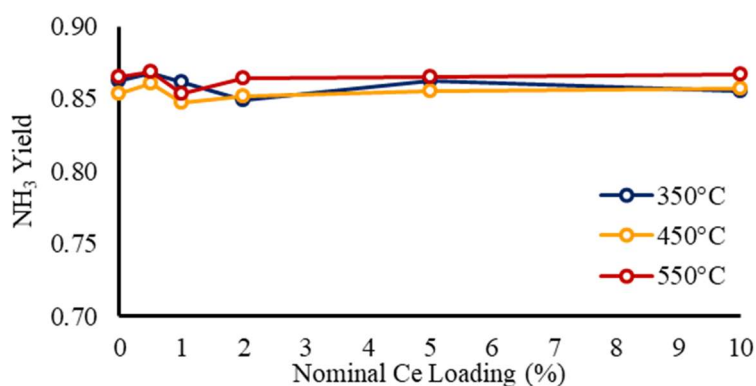
Figure 7.2: Production of NH_3 from $NO + H_2 + H_2O$

Figure 7.3 shows the production of H_2 from the water gas shift reaction. This H_2 production is measured based on the disappearance of H_2O, tracked by gas phase FTIR. Here, there is a significant dependence on the ceria loading on catalyst effectiveness, which is consistent with previous literature [35,112]. At 350°C, the 1Pd catalyst has no discernible activity for the water gas shift reaction. As more ceria is added to the formulation, there is a significant increase in H_2 production all the way to 10% ceria. However, at elevated temperatures of 450-550°C, increasing the ceria loading beyond 1-

2% has a negative effect on the cycle-averaged production of H_2. This is because, at these temperatures, ceria is highly active for oxygen storage. This leads to an inhibition in the reduction of the catalyst, which is a necessary step for NH_3 production to begin. Because of this, the presence of excess oxygen storage beyond 1-2% ceria has a negative effect on the overall generation of H_2 from the water gas shift reaction on a TWC.
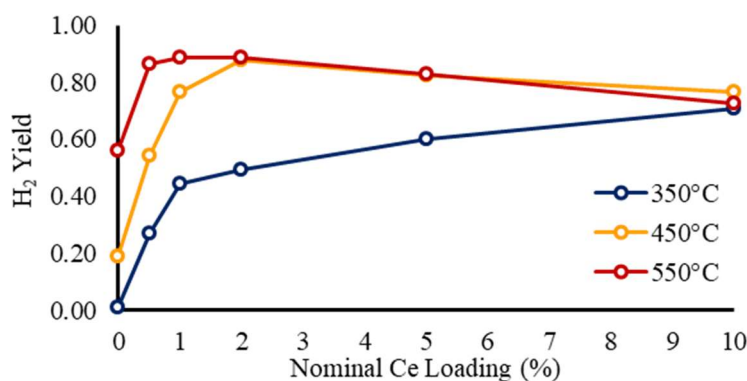
Figure 7.3: Production of H_2 from $CO + H_2O$

Figure 7.4 shows the production of NH_3 during exposure to CO, NO, and H_2O. The trends in this reaction mirror those of H_2 production quite closely. However, even at 350°C on the 1Pd catalyst, there is still a fractional NH_3 yield of 0.72. This is a very high yield considering that the catalyst is unable to produce molecular H_2 at this temperature. Looking at these two reactions together makes it clear that the formation of molecular H_2 is not a necessary step in the production of NH_3 over Pd catalysts, which was suggested in Chapter 5. This means that, under some conditions, NH_3 production must occur through the isocyanate hydrolysis pathway discussed in previous literature. However, as the ceria content of the catalyst is increased, and it becomes more active for the production of H_2, the NH_3 yield also increases dramatically. This illustrates that, while it

is not strictly necessary, the presence of molecular H_2 has a strong positive impact on the reduction of NO into NH_3. This is further illustrated by looking at higher temperature activities, where the 1Pd catalyst begins to show activity for the water gas shift reaction, and the NH_3 yield is increased accordingly. In this reaction the same detrimental effect of excess oxygen storage is seen at 450°C and 550°C, where ceria content in excess of 2% prevents the reduction of the catalyst and outweighs the beneficial effects.
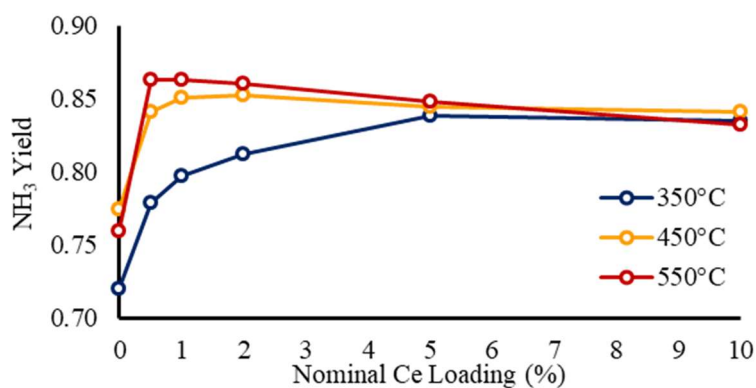
Figure 7.4: Production of NH_3 from $CO + NO + H_2O$

7.4 Conclusions

Understanding the fundamental role, or roles, of every component and promoter in commercially formulated catalysts is an ongoing challenge, and one that often shows a strong disconnect in the literature. In this chapter, it was shown that, while low loadings of Ce promote the formation of H_2 through increased activity for the water gas shift reaction, higher loadings tend to inhibit the reduction of the catalyst, creating a lower overall NH_3 production under cycling conditions. Furthermore, the ceria-free 1Pd catalyst showed very high activity for the production of NH_3 at 350°C despite showing no activity for the water gas shift reaction at the same temperature. This indicates that it is indeed

possible to produce NH_3 without the formation of molecular H_2 as suggested in Chapter 5, where several isolated reactions were investigated on the commercial catalyst formulations. Further indicating the activity of the isocyanate hydrolysis pathway shown in previous literature. Adding 0.5 weight % Ce allowed for the catalyst to be active for the water gas shift reaction at this temperature and greatly improved the NH_3 yield. This shows that, while not necessary, the presence of molecular H_2 is still greatly beneficial to the production of NH_3. However, when more than 2 wt. % ceria was added to the catalyst formulation, the overall cycling activity began to suffer at elevated temperatures. This is because the oxygen storage provided by ceria inhibits the reduction of the catalyst, which prevents the formation of NH_3 for a longer period of rich operation.

.

CHAPTER 8

CONCLUSIONS AND FUTURE WORK

Catalytic emissions control for automobile exhausts presents a challenge due to the complex reactive nature of combustion products. Even during the operation of a stoichiometric engine, small transient oscillations will always occur. Furthermore, the temperature of catalysts can vary dramatically, meaning that we need catalysts that are active under a wide degree of operating conditions. Much of our fundamental understanding of TWCs is difficult to use in applied research. This is because most fundamental research is focused on only a small subset of the reactants present in automobile exhaust and the catalysts used in these studies are often insufficiently stable for the operation in a real system. Because of these limitations, most automotive catalysts are discovered through trial and error, rather than built from a fundamental understanding of catalyst activity. These challenges are amplified when researching an advanced emission reduction strategy such as passive SCR. In particular, the long rich phase operation of required for passive SCR presents a unique challenge for TWCs that must This dissertation is intended to help bridge the gap between our fundamental understanding of the reactions that take place on a TWC and the more applied work that is used for evaluating commercial catalysts and advanced emission reduction strategies.

Beginning from commercial catalysts (Pd-TWC and NS-TWC) and full simulated exhaust mixtures, the effects of hydrothermal aging at 920°C for 100 hours was evaluated. Hydrothermally aged catalyst samples were compared to samples degreened at

700°C for 16 hours. It was found that hydrothermal aging led to increased light-off of CO, as well as degradation of oxygen and NO_X storage components. The increased light-off temperature is primarily attributed to increases in noble metal particle sizes. This lessens the metal support interactions and decreases the number of interface sites between the noble metal and oxide support. These interface sites have been proven to be essential for both water gas shift and low temperature CO oxidation activity.

Oxygen storage degradation occurs primarily through phase segregation of the ceria from the alumina support as well as the agglomeration of ceria after segregation. This means that, for the aged catalyst, there is more total ceria on the surface because of the phase segregation of the ceria from the alumina, but most of that ceria is contained on the interior of large particles due to the agglomeration. While this drastically decreased the low temperature OSC on the catalysts, which is consistent with literature, the high temperature OSC was increased. The decrease at low temperature is explained by the decreased surface ceria sites due to the agglomeration of those large ceria particles on the surface. As the temperature increases and oxygen mobility through the ceria becomes active, the interior of those large ceria particles becomes active for oxygen storage.

The mechanism for NO_X storage degradation is primarily through the formation of highly stable barium aluminate and barium cerate. The NSC of the catalysts was drastically decreased across all temperatures tested. The barium mixed metal oxides are formed at temperatures between 800-900°C, so the catalyst degreened at 700°C did not have significant deactivation. Generally, NSR catalysts that use barium to store NO_X, only see elevated temperatures briefly during desulfation treatments, but in a close coupled TWC position, the degradation of the NSC is significant. Because of this, if a

TWC with NSC were to be used for passive SCR, it would likely need to be positioned further away from the engine to avoid such rapid degradation.

The next factor that was explored was the effects of realistic concentrations of sulfur on the activity of the hydrothermally aged commercial TWCs. In this study, hydrothermally aged samples of both the Pd-TWC and the NS-TWC were exposed to 12.5 hours of 2ppm SO_2 under cycling conditions to determine what effect sulfur would have on the operation of a passive SCR system. The catalysts were evaluated before sulfation, after sulfation, and after desulfation at 650°C. Both catalysts showed increases in N_2O production, CO and HC slip, as well as a decrease in H_2 and NH_3 production. The deactivation of both catalysts was seen primarily in the rich phase. This is attributed to sulfur's tendency to form sulfates on the metal oxides during lean operation, while forming sulfides on the noble metal surface during rich operation. Furthermore, the NS-TWC showed stronger overall deactivation than the Pd-TWC, showing much higher HC slip and N_2O production as well as strong deactivation in the conversion of NO_X, particularly later in the rich phase. This is likely due to the high OSC and NSC loading of the NS-TWC. Both of these components store sulfur in the form of highly stable sulfates, which leads to a stronger deactivation under these conditions.

The effects of sulfation were further explored through the isolation of individual reactions on the commercial catalysts. These tests were conducted to try to understand the reaction pathways that were being deactivated through the sulfation in simulated exhaust. In addition to the sulfated and desulfated conditions, these catalysts were also evaluated under continuous SO_2 exposure. The results showed that the simulated exhaust results were not due to a deactivation in the production of NH_3 from the direct reduction of NO

with H_2, but rather, the changes were primarily due to the deactivation of H_2 production from the water gas shift and steam reforming reactions, as well as a deactivation in the reduction of NO by CO and C_3H_8. Furthermore, the mechanism of deactivation of H_2 production on the two catalysts was different. On the Pd-TWC, the primary mechanism of deactivation was from the water gas shift reaction. This is due to the lower loading of OSC on the Pd-TWC, leading to fewer interface sites that are available for the reaction. Deactivation of these relatively sparse sites results in rapid deactivation of the water gas shift reaction using the intermittent sulfation procedure. However, in the case of the NS-TWC, under intermittent sulfation, the catalyst maintained high activity for water gas shift and its deactivation occurred primarily through deactivation of the steam reformation reaction. These deactivations explain the changes seen in the simulated exhaust evaluations.

Under continuous sulfur evaluation, the Pd-TWC showed heavy deactivation in all evaluated reactions. However, the NS-TWC did not show the heavy deactivation of steam reforming under continuous sulfation that was observed on the Pd-TWC. In fact, the NS-TWC generally performed better than the Pd-TWC under continuous SO_2 exposure, showing no deactivation of the production of NH_3 from NO and H_2 under these conditions. This is likely attributed to the high loading of Pt present on the NS-TWC, which has been shown to be far more sulfur resistant than Pd.

The final study performed with commercial TWC formulations was an investigation of the potential mitigation of sulfur effects through the variation in rich phase λ during cycling. The catalysts in this case were evaluated under continuous sulfation in order to fully capture the effects seen in the isolated reaction studies. It was

found that, by operating at lower rich phase λ values, the deactivation of NH$_3$ production could indeed be almost entirely mitigated, leading to shorter rich phase operation. Furthermore, under lower rich phase λ values, the NO$_X$ conversion was also increased significantly. However, by operating at a lower rich phase λ, the emissions of CO and HCs were increased. Thus, there is a tradeoff in the effectiveness of the passive SCR system that must be considered when choosing operating conditions.

Finally, the multiple roles of ceria were investigated on the TWC in a passive SCR system. While ceria can be beneficial for catalyst activity for the water gas shift reaction, large amounts can inhibit the reduction of the catalyst and decrease the NH$_3$ production in a passive SCR system. Furthermore, it was found that, on the ceria-free Pd-only catalyst, a high production of NH$_3$ was observed at 350°C when the catalyst has no activity for water gas shift. This shows that molecular H$_2$ is not necessary for the production of NH$_3$, indicating that the hydrolysis of isocyanate species must play a role at this temperature. As ceria was added, activity for WGS at 350°C increased rapidly, and NH$_3$ production increased as well. Therefore, while the formation of molecular H$_2$ is not necessary for the production of NH$_3$, it is greatly beneficial, and the mechanism by which NH$_3$ production occurs may depend heavily on the operation temperature.

The studies presented in this dissertation help paint a clearer picture of the TWC in a passive SCR system and help us understand the deactivation mechanisms for the TWC in a more complete way. The simulated exhaust work illustrates how the TWC is affected by physical and chemical deactivation in realistic automotive exhausts. Through work isolating individual reactions and studies on model catalysts it has been shown how both sulfation and the presence of ceria affect the individual reactions that can take place

on a catalyst. By combining these levels of catalyst examination, we can hope to form a bridge between the fundamental catalyst studies and the applied work being conducted throughout the field.

In the future, our understanding of the deactivation mechanisms and formulation effects on the TWC in passive SCR systems can be further improved by expanding the studies presented in this dissertation. One key point is that this work has focused primarily on the continuous operation of a passive SCR system using operational temperatures of 350°C – 650°C. This is realistic for simulating the system during operation, but cold start emissions are a major concern in real exhaust systems. This was partially addressed in chapter 3, where the effects of hydrothermal aging on the qualitative changes in light-off of CO oxidation were monitored during aging. Still, the effects of hydrothermal aging and sulfur exposure on cold-start activity using simulated exhaust conditions were not conducted. In the future, more attention should be paid to the catalyst behavior during light-off in passive SCR systems.

Our understanding of the effects of hydrothermal aging on TWC activity could be improved by investigating activity differences in isolated reactions between the hydrothermally aged catalyst samples and the degreened catalyst samples. While the current work has shown the general effects of hydrothermal aging on the simulated exhaust activity, conducting work similar to the isolated reactions presented in Chapter 4 would allow for the deconvolution of these effects, potentially illuminating the individual effects leading to the changes observed in hydrothermal catalyst activity.

Regarding sulfation, additional work should be conducted to understand the effects of continuous sulfation under a wider range of temperatures. This was partially

addressed in Chapter 6 where the effects of rich phase λ on the sulfation behavior of the TWCs was examined. However, these measurements were only conducted at 350°C and 550°C. These experiments should be expanded to include intermediate temperatures to gain a better understanding of catalyst sulfation.

The isolated reaction studies shown in Chapter 5 are helpful for understanding the effects of sulfation on key rich phase reactions, such as water gas shift and steam reforming. However, in these examinations, there was no oxygen present in the rich phase. This was necessary to directly compare the activity of the reactions in the absence of oxygen, but it also prevents the determination of changes in the oxidation of the different reductants present in the rich phase has not been sufficiently examined. In the future, these isolated reaction studies should be expanded to examine the changes in reductant oxidation during rich operation. This can be accomplished by including oxygen at a low concentration and comparing it to the results presented here. This will allow for an even greater understanding of catalyst deactivation in the presence of sulfur.

Finally, more rigorous examinations of catalyst formulation effects will be an essential part of guiding the design of TWCs for passive SCR systems. In this work, a commercially formulated Pd-TWC and NS-TWC were compared. These catalysts have many formulation differences that make it difficult to attribute changes in catalyst activity to specific changes in catalyst formulation. This issue was partially addressed in chapter 7, where the effects of Ce loading were examined. However, there are many other formulation effects that have yet to be explored. Specifically, the contribution of each PGM to the overall catalyst activity is an important consideration. While Pt and Pd are both very active for oxidation reactions, previous research has indicated that Pd shows

better activity for the production of NH_3 in a passive SCR system. However, as this work has illustrated, the catalyst with high levels of Pd showed significantly stronger deactivation during continuous sulfation compared to the catalyst with Pt. In the case of Rh, while it has been shown to be very active for NO decomposition, it has also been sown to be active for NH_3 decomposition, which could potentially inhibit the production of NH_3 in a passive SCR system.

REFERENCES

[1]   S.C. Davis, S.E. Williams, R.G. Boundy, Transportation Energy Data Book Edition 36, 2017.

[2]   J.E. Parks, V. Prikhodko, W. Partridge, J.-S. Choi, K. Norman, S. Huff, P. Chambon, Lean Gasoline Engine Reductant Chemistry During Lean NOx Trap Regeneration, SAE Int. J. Fuels Lubr. 3 (2010) 2010-01-2267. doi:10.4271/2010-01-2267.

[3]   The U.S. Environmental Protection Agency (EPA), Direct Final Rulemaking for EPA Tier 3 Emission and Fuel Standards, 80 (2015).

[4]   P.L.T. Gabrielsson, Urea-SCR in Automotive Applications, Top. Catal. 28 (2004) 177–184. doi:10.1023/B:TOCA.0000024348.34477.4c.

[5]   F. Rodrigues, L. Juste, C. Potvin, J.F. Tempère, G. Blanchard, G. Djéga-Mariadassou, NOxstorage on barium-containing three-way catalyst in the presence of CO2, Catal. Letters. 72 (2001) 59–64. doi:10.1023/A:1009001630673.

[6]   S. Matsumoto, DeNOx catalyst for automotive lean-burn engine, Catal. Today. 29 (1996) 43–45. doi:10.1016/0920-5861(95)00259-6.

[7]   G. Liu, P.-X. Gao, A review of NOx storage/reduction catalysts: mechanism, materials and degradation studies, Catal. Sci. Technol. 1 (2011) 552. doi:10.1039/c1cy00007a.

[8]   S. Shwan, W. Partridge, J.S. Choi, L. Olsson, Kinetic modeling of NOx storage and reduction using spatially resolved MS measurements, Appl. Catal. B Environ. 147 (2014) 1028–1041. doi:10.1016/j.apcatb.2013.10.023.

[9]   Š. Bártová, P. Kočí, D. Mráček, M. Marek, J.A. Pihl, J.S. Choi, T.J. Toops, W.P. Partridge, New insights on N2O formation pathways during lean/rich cycling of a commercial lean NOx trap catalyst, Catal. Today. 231 (2014) 145–154. doi:10.1016/j.cattod.2013.11.050.

[10]   M. Koebel, M. Elsener, M. Kleemann, Urea-SCR: a promising technique to reduce NOxemissions from automotive diesel engines, Catal. Today. 59 (2000) 335–345. doi:10.1016/S0920-5861(00)00299-6.

[11]   M. Koebel, G. Madia, M. Elsener, Selective catalytic reduction of NO and NO2at low temperatures, Catal. Today. 73 (2002) 239–247. doi:10.1016/S0920-5861(02)00006-8.

[12]   T. V. Johnson, Review of Diesel Emissions and Control, SAE Int. J. Fuels Lubr. 3 (2010) 2010-01–0301. doi:10.4271/2010-01-0301.

[13]   M.D. Amiridis, I.E. Wachs, G. Deo, J.M. Jehng, D.S. Kim, Reactivity of V2O5catalysts for the selective catalytic reduction of NO by NH3: Influence of vanadia loading, H2O, and SO2, J. Catal. (1996). doi:10.1006/jcat.1996.0182.

[14]   I.E. Wachs, G. Deo, B.M. Weckhuysen, A. Andreini, M.A. Vuurman, M. De Boer, M.D. Amiridis, Selective catalytic reduction of NO with NH3over supported vanadia catalysts, J. Catal. (1996). doi:10.1006/jcat.1996.0179.

[15] S. Brandenberger, O. Kröcher, A. Tissler, R. Althoff, The state of the art in selective catalytic reduction of NOxby ammonia using metal-exchanged zeolite catalysts, 2008. doi:10.1080/01614940802480122.

[16] R.Q. Long, R.T. Yang, Superior Fe-ZSM-5 catalyst for selective catalytic reduction of nitric oxide by ammonia, J. Am. Chem. Soc. 121 (1999) 5595–5596. doi:10.1021/ja9842262.

[17] J.P. Dunn, P.R. Koppula, H.G. Stenger, I.E. Wachs, Oxidation of sulfur dioxide to sulfur trioxide over supported vanadia catalysts, Appl. Catal. B Environ. (1998). doi:10.1016/S0926-3373(98)00060-5.

[18] L. Ma, Y. Cheng, G. Cavataio, R.W. McCabe, L. Fu, J. Li, Characterization of commercial Cu-SSZ-13 and Cu-SAPO-34 catalysts with hydrothermal treatment for NH3-SCR of NOxin diesel exhaust, Chem. Eng. J. 225 (2013) 323–330. doi:10.1016/j.cej.2013.03.078.

[19] D.W. Fickel, E. D'Addio, J.A. Lauterbach, R.F. Lobo, The ammonia selective catalytic reduction activity of copper-exchanged small-pore zeolites, Appl. Catal. B Environ. 102 (2011) 441–448. doi:10.1016/j.apcatb.2010.12.022.

[20] T.V.W. Janssens, H. Falsig, L.F. Lundegaard, P.N.R. Vennestrøm, S.B. Rasmussen, P.G. Moses, F. Giordanino, E. Borfecchia, K.A. Lomachenko, C. Lamberti, S. Bordiga, A. Godiksen, S. Mossin, P. Beato, A consistent reaction scheme for the selective catalytic reduction of nitrogen oxides with ammonia, ACS Catal. 5 (2015) 2832–2845. doi:10.1021/cs501673g.

[21] D.Y. Wang, S. Yao, M. Shost, J.-H. Yoo, D. Cabush, D. Racine, R. Cloudt, F. Willems, Ammonia Sensor for Closed-Loop SCR Control, SAE Int. J. Passeng. Cars – Electron. Electr. Syst. 1 (2009) 323–333. doi:10.4271/2008-01-0919.

[22] W. Li, K.L. Perry, K. Narayanaswamy, C.H. Kim, P. Najt, Passive Ammonia SCR System for Lean-burn SIDI Engines, SAE Int. J. Fuels Lubr. (2010). doi:10.4271/2010-01-0366.

[23] V.Y. Prikhodko, J.E. Parks, J.A. Pihl, T.J. Toops, Ammonia Generation over TWC for Passive SCR NOX Control for Lean Gasoline Engines, SAE Int. J. Engines. 7 (2014) 2014-01-1505. doi:10.4271/2014-01-1505.

[24] D.R. Rainer, M. Koranne, S.M. Vesecky, D.W. Goodman, CO+O-2 and CO+NO reactions over Pd/Al2O3 catalysts, J. Phys. Chem. B. 101 (1997) 10769–10774.

[25] P.J. Berlowitz, C.H.F. Peden, D.W. Goodman, Kinetics of carbon monoxide oxidation on single-crystal palladium, platinum, and iridium, J. Phys. Chem. 92 (1988) 5213–5221. doi:10.1021/j100329a030.

[26] A. Martinez-Arias, M. Fernandez-Garcia, A. Iglesias-Juez, A.B. Hungria, J.A. Anderson, J.C. Conesa, J. Soria, New Pd/CexZr1-xO2/Al2O3three-way catalysts prepared by microemulsion Part 2. In situ analysis of CO oxidation and NO reduction under stoichiometric CO+NO+O2, Appl. Catal. B Environ. 31 (2001) 51–60. doi:10.1016/S0926-3373(00)00264-2.

[27] K. Nakao, S.I. Ito, K. Tomishige, K. Kunimori, Reaction mechanism and structure of activated complex of CO2 formation in CO oxidation on Pd(1 1 0) and Pd(1 1 1) surfaces, Catal. Today. 111 (2006) 316–321. doi:10.1016/j.cattod.2005.10.043.

[28] Y.F.Y. Yao, The oxidation of CO and hydrocarbons over noble metal catalysts, J. Catal. 87 (1984) 152–162. doi:10.1016/0021-9517(84)90178-7.

[29] Z.Q. Zou, M. Meng, N. Tsubaki, J.J. He, G. Wang, X.G. Li, X.Y. Zhou, Influence

of Co or Ce addition on the NOx storage and sulfur-resistance performance of the lean-burn NOx trap catalyst Pt/K/TiO2-ZrO2, J. Hazard. Mater. 170 (2009) 118–126. doi:10.1016/j.jhazmat.2009.04.125.

[30] R.J. Baxter, P. Hu, Insight into why the Langmuir-Hinshelwood mechanism is generally preferred, J. Chem. Phys. 116 (2002) 4379–4381. doi:10.1063/1.1458938.

[31] B.L.M. Hendriksen, S.C. Bobaru, J.W.M. Frenken, Oscillatory CO oxidation on Pd(1 0 0) studied with in situ scanning tunneling microscopy, Surf. Sci. 552 (2004) 229–242. doi:10.1016/j.susc.2004.01.025.

[32] H. Conrad, G. Ertl, J. Küppers, Interactions between oxygen and carbon monoxide on a Pd(111) surface, Surf. Sci. 76 (1978) 323–342. doi:10.1016/0039-6028(78)90101-2.

[33] M. Li, X. Wu, Y. Cao, S. Liu, D. Weng, R. Ran, NO reduction by CO over Rh/Al2O3and Rh/ALPO4catalysts: Metal-support interaction and thermal aging, J. Colloid Interface Sci. 408 (2013) 157–163. doi:10.1016/j.jcis.2013.07.023.

[34] K. Polychronopoulou, C. M. Kalamaras, A. M. Efstathiou, Ceria-Based Materials for Hydrogen Production Via Hydrocarbon Steam Reforming and Water-Gas Shift Reactions, Recent Patents Mater. Sci. 4 (2011) 122–145. doi:10.2174/1874465611104020122.

[35] S. Aranifard, S.C. Ammal, A. Heyden, On the importance of metal-oxide interface sites for the water-gas shift reaction over Pt/CeO2catalysts, J. Catal. 309 (2014) 314–324. doi:10.1016/j.jcat.2013.10.012.

[36] C. Ratnasamy, J.P. Wagner, Water Gas Shift Catalysis, Catal. Rev. 51 (2009) 325–440. doi:10.1080/01614940903048661.

[37] T. Bunluesin, R.J. Gorte, G.W. Graham, Studies of the water-gas-shift reaction on ceria-supported Pt, Pd, and Rh: Implications for oxygen-storage properties, Appl. Catal. B Environ. 15 (1998) 107–114. doi:10.1016/S0926-3373(97)00040-4.

[38] F.C. Meunier, D. Tibiletti, A. Goguet, S. Shekhtman, C. Hardacre, R. Burch, On the complexity of the water-gas shift reaction mechanism over a Pt/CeO2 catalyst: Effect of the temperature on the reactivity of formate surface species studied by operando DRIFT during isotopic transient at chemical steady-state, Catal. Today. 126 (2007) 143–147. doi:10.1016/j.cattod.2006.10.003.

[39] R. Burch, D.J. Crittle, M.J. Hayes, C–H bond activation in hydrocarbon oxidation on heterogeneous catalysts, Catal. Today. 47 (1999) 229–234. doi:10.1016/S0920-5861(98)00303-4.

[40] D. Chatterjee, O. Deutschmann, J. Warnatz, Detailed surface reaction mechanism in a three-way catalyst, Faraday Discuss. 119 (2002) 371–384. doi:10.1039/b101968f.

[41] F. Garin, Mechanism of NOx decomposition, Appl. Catal. A Gen. 222 (2001) 183–219. doi:10.1002/pro.2005.

[42] J.M. Dasch, Nitrous Oxide Emissions from Vehicles, ISSN J. Air Waste Manag. Assoc. 42 (2012) 1047–3289. doi:10.1080/10473289.1992.10466971.

[43] I. Mejía-Centeno, G.A. Fuentes, Nitrous oxide formation during light-off over a commercial pd-containing three-way catalytic converter: The effect of low-sulfur gasoline, Chem. Eng. Commun. 196 (2009) 1140–1151. doi:10.1080/00986440902831664.

[44] C. Bozo, F. Gaillard, N. Guilhaume, Characterisation of ceria-zirconia solid solutions after hydrothermal ageing, Appl. Catal. A Gen. 220 (2001) 69–77. doi:10.1016/S0926-860X(01)00710-4.

[45] M. Shelef, G.W. Graham, Why Rhodium in Automotive Three-Way Catalysts?, Catal. Rev. 36 (1994) 433–457. doi:10.1080/01614949408009468.

[46] G. Kim, Ceria-Promoted Three-Way Catalysts for Auto Exhaust Emission Control, Ind. Eng. Chem. Prod. Res. Dev. 21 (1982) 267–274. doi:10.1021/i300006a014.

[47] B.B. Harrison, A.F. Diwell, C. Hallett, Promoting Platinum Metals by Ceria - metal-support interactions in autocatalysts, Platin. Met. Rev. (1988) 73–83.

[48] E. Mamontov, T. Egami, R. Brezny, M. Koranne, S. Tyagi, Lattice Defects and Oxygen Storage Capacity of Nanocrystalline Ceria and Ceria-Zirconia, J. Phys. Chem. B. 104 (2000) 11110–11116. doi:10.1021/jp0023011.

[49] H.C. Yao, Y.F.Y. Yao, Ceria in automotive exhaust catalysts. I. Oxygen storage, J. Catal. 86 (1984) 254–265. doi:10.1016/0021-9517(84)90371-3.

[50] L.F. Liotta, G. Deganello, D. Sannino, M.C. Gaudino, P. Ciambelli, S. Gialanella, Influence of barium and cerium oxides on alumina supported Pd catalysts for hydrocarbon combustion, Appl. Catal. A Gen. 229 (2002) 217–227. doi:10.1016/S0926-860X(02)00029-7.

[51] J. Wang, J. Wen, M. Shen, Effect of Interaction between Ce $_{0.7}$ Zr $_{0.3}$ O $_2$ and Al $_2$ O $_3$ on Structural Characteristics, Thermal Stability, and Oxygen Storage Capacity, J. Phys. Chem. C. 112 (2008) 5113–5122. doi:10.1021/jp711331g.

[52] S.Y. Christou, H. Bradshaw, C. Butler, J. Darab, A.M. Efstathiou, Effect of thermal aging on the transient kinetics of oxygen storage and release of commercial CexZr1-xO2-based solids, Top. Catal. 52 (2009) 2013–2018. doi:10.1007/s11244-009-9402-2.

[53] N.W. Cant, M.J. Patterson, The storage of nitrogen oxides on alumina-supported barium oxide, Catal. Today. 73 (2002) 271–278. doi:10.1016/S0920-5861(02)00010-X.

[54] L. Castoldi, I. Nova, L. Lietti, P. Forzatti, Study of the effect of Ba loading for catalytic activity of Pt-Ba/Al2O3model catalysts, Catal. Today. 96 (2004) 43–52. doi:10.1016/j.cattod.2004.05.006.

[55] P.T. Fanson, M.R. Horton, W.N. Delgass, J. Lauterbach, FTIR analysis of storage behavior and sulfur tolerance in barium-based NOχstorage and reduction (NSR) catalysts, Appl. Catal. B Environ. 46 (2003) 393–413. doi:10.1016/S0926-3373(03)00275-3.

[56] R.J. Gorte, T. Luo, J.M. Vohs, An examination of sulfur poisoning on Pd/Ceria catalysts, J. Catal. 210 (2002) 397–404. doi:10.1006/jcat.2002.3689.

[57] F. Rohr, S.D. Peter, E. Lox, M. Kögel, A. Sassi, L. Juste, C. Rigaudeau, G. Belot, P. Gélin, M. Primet, On the mechanism of sulphur poisoning and regeneration of a commercial gasoline NOx-storage catalyst, Appl. Catal. B Environ. 56 (2005) 201–212. doi:10.1016/j.apcatb.2004.09.011.

[58] P.R. Dasari, R. Muncrief, M.P. Harold, Elucidating NH 3 formation during NO x reduction by CO on Pt-BaO/Al 2O 3 in excess water, Catal. Today. 184 (2012) 43–53. doi:10.1016/j.cattod.2011.12.009.

[59] K. Rahkamaa-Tolonen, Investigation of NO Reduction by H2 on Pd Monolith with Transient and Isotopic Exchange Techniques II. H2/D2 Exchange in the Reduction

of NO, J. Catal. 210 (2002) 30–38. doi:10.1006/jcat.2002.3669.

[60]   S.H. Oh, T. Triplett, Reaction pathways and mechanism for ammonia formation and removal over palladium-based three-way catalysts: Multiple roles of CO, Catal. Today. 231 (2014) 22–32. doi:10.1016/j.cattod.2013.11.048.

[61]   M.L. Unland, Isocyanate Intermediates in Ammonia Formation over Noble Metal Catalysts for Automobile Exhaust Reactions, Science (80-.). 179 (1973) 567–569. doi:10.1126/science.179.4073.567.

[62]   M.L. Unland, lsocyanate Intermediates in the Reaction of NO Over Noble Metal Catalysts, J. Catal. 31 (1973) 459–465.

[63]   M.L. Unland, Reactions of Surface Isocyanate Groups with Selected Compounds, J. Phys. Chem. 79 (1975) 610–615. doi:10.1021/j100573a013.

[64]   N. Macleod, R.M. Lambert, In situ ammonia generation as a strategy for catalytic NOx reduction under oxygen rich conditions, Chem. Commun. (Camb). (2003) 1300–1301. doi:10.1039/b302959j.

[65]   E.C. Adams, M. Skoglundh, M. Folic, E.C. Bendixen, P. Gabrielsson, P.A. Carlsson, Ammonia formation over supported platinum and palladium catalysts, Appl. Catal. B Environ. 165 (2015) 10–19. doi:10.1016/j.apcatb.2014.09.064.

[66]   J. Parks, T.J. Toops, J.A. Pihl, Emissions Control for Lean Gasoline Engines, (2015). https://www.energy.gov/sites/prod/files/2015/06/f23/ace033_parks_2015_o.pdf (accessed March 14, 2018).

[67]   V.Y. Prikhodko, J.E. Parks, J.A. Pihl, T.J. Toops, Ammonia Generation and Utilization in a Passive SCR (TWC+SCR) System on Lean Gasoline Engine, SAE Int. J. Engines. 9 (2016) 2016-01–0934. doi:10.4271/2016-01-0934.

[68]   C.D. DiGiulio, J.A. Pihl, J.S. Choi, J.E. Parks, M.J. Lance, T.J. Toops, M.D. Amiridis, NH3 formation over a lean NOX trap (LNT) system: Effects of lean/rich cycle timing and temperature, Appl. Catal. B Environ. 147 (2014) 698–710. doi:10.1016/j.apcatb.2013.09.012.

[69]   E.C. Adams, M. Skoglundh, T. Elmøe, P.A. Carlsson, Water–gas-shift assisted ammonia formation over Pd/Ce/alumina, Catal. Today. 307 (2018) 169–174. doi:10.1016/j.cattod.2017.05.035.

[70]   E.C. Adams, M. Skoglundh, P. Gabrielsson, M. Laurell, P.A. Carlsson, Ammonia formation over Pd/Al2O3modified with cerium and barium, Catal. Today. 267 (2016) 210–216. doi:10.1016/j.cattod.2016.01.012.

[71]   C.M. Parish, MT3FT-15OR0204122: Report on the acquisition and installation of FEI Talos F200X S/TEM., ORNL/LTR-2015/461. Oak Ridge Natl. Lab. (ORNL), Oak Ridge, TN (United States). (2015) 1–7.

[72]   C.D. Digiulio, J.A. Pihl, J.E.P. Ii, M.D. Amiridis, T.J. Toops, Passive-ammonia selective catalytic reduction (SCR): Understanding NH3formation over close-coupled three way catalysts (TWC), Catal. Today. 231 (2014) 33–45. doi:10.1016/j.cattod.2014.01.027.

[73]   J. Wang, H. Chen, Z. Hu, M. Yao, Y. Li, A review on the Pd-based three-way catalyst, Catal. Rev. - Sci. Eng. 57 (2015) 79–144. doi:10.1080/01614940.2014.977059.

[74]   M.A. Fortunato, D. Aubert, C. Capdeillayre, C. Daniel, A. Hadjar, A. Princivalle, C. Guizard, P. Vernoux, Dispersion measurement of platinum supported on Yttria-

Stabilised Zirconia by pulse H2chemisorption, Appl. Catal. A Gen. 403 (2011) 18–24. doi:10.1016/j.apcata.2011.06.005.

[75] T. Kobayashi, T. Yamada, K. Kayano, Effect of basic metal additives on NOxreduction property of Pd-based three-way catalyst, Appl. Catal. B Environ. 30 (2001) 287–292. doi:10.1016/S0926-3373(00)00240-X.

[76] T. Maunula, K. Kallinen, A. Savimäki, T. Wolff, Durability Evaluations and Rapid Ageing Methods in Commercial Emission Catalyst Development for Diesel, Natural Gas and Gasoline Applications, Top. Catal. 59 (2016) 1049–1053. doi:10.1007/s11244-016-0588-9.

[77] Q. Xu, K.C. Kharas, B.J. Croley, A.K. Datye, The Sintering of Supported Pd Automotive Catalysts, ChemCatChem. 3 (2011) 1004–1014. doi:10.1002/cctc.201000392.

[78] A. Iglesias-Juez, A. Martínez-Arias, M. Fernández-García, Metal-promoter interface in Pd/(Ce,Zr)Ox/Al2O3 catalysts: Effect of thermal aging, J. Catal. 221 (2004) 148–161. doi:10.1016/j.jcat.2003.07.010.

[79] M. Casapu, J.D. Grunwaldt, M. Maciejewski, M. Wittrock, U. Göbel, A. Baiker, Formation and stability of barium aluminate and cerate in NOx storage-reduction catalysts, Appl. Catal. B Environ. 63 (2006) 232–242. doi:10.1016/j.apcatb.2005.10.003.

[80] M. Eberhardt, R. Riedel, U. Gobel, J. Theis, E.S. Lox, Fundamental investigations of thermal aging phenomena of model NOx storage systems, Top. Catal. 30–31 (2004) 135–142.

[81] Y. Zhang, M. Flytzani-Stephanopoulos, Hydrothermal stability of cerium modified Cu-ZSM-5 catalyst for nitric oxide decomposition, J. Catal. (1996). doi:10.1006/jcat.1996.0369.

[82] Q. Ye, L. Wang, R.T. Yang, Activity, propene poisoning resistance and hydrothermal stability of copper exchanged chabazite-like zeolite catalysts for SCR of NO with ammonia in comparison to Cu/ZSM-5, Appl. Catal. A Gen. 427–428 (2012) 24–34. doi:10.1016/j.apcata.2012.03.026.

[83] V.Y. Prikhodko, J.E. Parks, J.A. Pihl, T.J. Toops, Passive SCR for lean gasoline NOX control: Engine-based strategies to minimize fuel penalty associated with catalytic NH3 generation, Catal. Today. 267 (2016) 202–209. doi:10.1016/j.cattod.2016.01.026.

[84] M. Clairotte, T.W. Adam, A.A. Zardini, U. Manfredi, G. Martini, A. Krasenbrink, A. Vicet, E. Tournié, C. Astorga, Effects of low temperature on the cold start gaseous emissions from light duty vehicles fuelled by ethanol-blended gasoline, Appl. Energy. 102 (2013) 44–54. doi:10.1016/j.apenergy.2012.08.010.

[85] M.Y. Kim, E.A. Kyriakidou, J.S. Choi, T.J. Toops, A.J. Binder, C. Thomas, J.E. Parks, V. Schwartz, J. Chen, D.K. Hensley, Enhancing low-temperature activity and durability of Pd-based diesel oxidation catalysts using ZrO2supports, Appl. Catal. B Environ. 187 (2016) 181–194. doi:10.1016/j.apcatb.2016.01.023.

[86] C. Wang, A.J. Binder, T.J. Toops, J. Lauterbach, E. Sasmaz, Evaluation of Mn and Sn-Modified Pd-Ce-Based Catalysts for Low-Temperature Diesel Exhaust Oxidation, Emiss. Control Sci. Technol. 3 (2017) 37–46. doi:10.1007/s40825-016-0056-9.

[87] A.I. Boronin, E.M. Slavinskaya, I.G. Danilova, R. V. Gulyaev, Y.I. Amosov, P.A.

Kuznetsov, I.A. Polukhina, S. V. Koscheev, V.I. Zaikovskii, A.S. Noskov, Investigation of palladium interaction with cerium oxide and its state in catalysts for low-temperature CO oxidation, Catal. Today. 144 (2009) 201–211. doi:10.1016/j.cattod.2009.01.035.

[88] I. Heo, J.W. Choung, P.S. Kim, I.S. Nam, Y. Il Song, C.B. In, G.K. Yeo, The alteration of the performance of field-aged Pd-based TWCs towards CO and C3H6 oxidation, Appl. Catal. B Environ. 92 (2009) 114–125. doi:10.1016/j.apcatb.2009.07.016.

[89] F. Rohr, U. Göbel, P. Kattwinkel, T. Kreuzer, W. Müller, S. Philipp, P. Gélin, New insight into the interaction of sulfur with diesel NOxstorage catalysts, Appl. Catal. B Environ. 70 (2007) 189–197. doi:10.1016/j.apcatb.2005.12.033.

[90] S.J. Schmieg, D.N. Belton, Effect of hydrothermal aging on oxygen storage/release and activity in a commercial automotive catalyst, Appl. Catal. B, Environ. 6 (1995) 127–144. doi:10.1016/0926-3373(95)00011-9.

[91] J.A. Lupescu, J.W. Schwank, K.A. Dahlberg, C.Y. Seo, G.B. Fisher, S.L. Peczonczyk, K. Rhodes, M.J. Jagner, L.P. Haack, Pd model catalysts: Effect of aging environment and lean redispersion, Appl. Catal. B Environ. 183 (2016) 343–360. doi:10.1016/j.apcatb.2015.10.018.

[92] H.S. Gandhi, W.B. Williamson, E.M. Logothetis, J. Tabock, C. Peters, M.D. Hurley, M. Shelef, Affinity of lead for noble metals on different supports, Surf. Interface Anal. 6 (1984) 149–161. doi:10.1002/sia.740060402.

[93] A. Kalantar Neyestanaki, F. Klingstedt, T. Salmi, D.Y. Murzin, Deactivation of postcombustion catalysts, a review, Fuel. 83 (2004) 395–408. doi:10.1016/j.fuel.2003.09.002.

[94] M.J. Rokosz, A.E. Chen, C.K. Lowe-Ma, A. V. Kucherov, D. Benson, M.C. Paputa Peck, R.W. McCabe, Characterization of phosphorus-poisoned automotive exhaust catalysts, Appl. Catal. B Environ. 33 (2001) 205–215. doi:10.1016/S0926-3373(01)00165-5.

[95] L.D. An, Y.Q. Deng, Mechanism of sulfur poisoning of supported Pd(Pt)/Al2O3 catalysts for H2-O2 reaction, Appl. Catal. 66 (1990) 219–234.

[96] H.S. Gandhi, M. Shelef, Effects of sulphur on noble metal automotive catalysts, Appl. Catal. 77 (1991) 175–186. doi:10.1016/0166-9834(91)80063-3.

[97] C. Sedlmair, K. Seshan, A. Jentys, J.A. Lercher, Studies on the deactivation of NOxstorage-reduction catalysts by sulfur dioxide, Catal. Today. 75 (2002) 413–419. doi:10.1016/S0920-5861(02)00091-3.

[98] J. Kašpar, P. Fornasiero, N. Hickey, Automotive catalytic converters: Current status and some perspectives, Catal. Today. 77 (2003) 419–449. doi:10.1016/S0920-5861(02)00384-X.

[99] M. Waqif, P. Bazin, O. Saur, J.C. Lavalley, G. Blanchard, O. Touret, Study of ceria sulfation, Appl. Catal. B Environ. 11 (1997) 193–205. doi:10.1016/S0926-3373(96)00040-9.

[100] J.A. Poston, R. V. Siriwardane, E.P. Fisher, A.L. Miltz, Thermal decomposition of the rare earth sulfates of cerium(III), cerium(IV), lanthanum(III) and samarium(III), Appl. Surf. Sci. 214 (2003) 83–102. doi:10.1016/S0169-4332(03)00358-1.

[101] A. Amberntsson, M. Skoglundh, S. Ljungström, E. Fridell, Sulfur deactivation of

NOxstorage catalysts: Influence of exposure conditions and noble metal, J. Catal. 217 (2003) 253–263. doi:10.1016/S0021-9517(03)00027-7.

[102] T. Luo, R.J. Gorte, A mechanistic study of sulfur poisoning of the water – gas-shift reaction over Pd / ceria, Catal. Letters. 85 (2003) 139–146. doi:10.1023/A:1022125209602.

[103] J.C. Summers, K. Baron, The effects of SO2on the performance of noble metal catalysts in automobile exhaust, J. Catal. (1979). doi:10.1016/0021-9517(79)90004-6.

[104] J.T. Kummer, Laboratory experiments evaluating the effects of S and Cu on a PtAl2O3 auto exhaust oxidation catalysts, J. Catal. (1975). doi:10.1016/0021-9517(75)90074-3.

[105] B.W. Williamson, H.K. Stepien, H.S. Gandhi, Poisoning of Platinum-Rhodium Automotive Three-Way Catalysts : Behavior of Single-Component Catalysts and Effects of Sulfur and Phosphorus, Environ. Sci. Technol. 14 (1980) 319–324. doi:10.1021/es60163a008.

[106] J.S. Choi, W.P. Partridge, J.A. Pihl, M.Y. Kim, P. Kočí, C.S. Daw, Spatiotemporal distribution of NOx storage and impact on NH3 and N2O selectivities during lean/rich cycling of a Ba-based lean NOx trap catalyst, Catal. Today. 184 (2012) 20–26. doi:10.1016/j.cattod.2011.11.007.

[107] I. Mejía-Centeno, A. Martínez-Hernández, G.A. Fuentes, Effect of low-sulfur fuels upon NH3and N2O emission during operation of commercial three-way catalytic converters, Top. Catal. 42–43 (2007) 381–385. doi:10.1007/s11244-007-0210-2.

[108] D.D. Beck, J.W. Sommers, C.L. DiMaggio, Impact of sulfur on model palladium-only catalysts under simulated three-way operation, Appl. Catal. B, Environ. (1994). doi:10.1016/0926-3373(93)E0035-A.

[109] M. Shelef, R.W. McCabe, Twenty-five years after introduction of automotive catalysts: what next?, Catal. Today. 62 (2000) 35–50. doi:10.1016/S0920-5861(00)00407-7.

[110] W.S. Epling, L.E. Campbell, A. Yezerets, N.W. Currier, J.E. Parks, Overview of the fundamental reactions and degradation mechanisms of NOx storage/reduction catalysts, Catal. Rev. - Sci. Eng. 46 (2004) 163–245. doi:10.1081/CR-200031932.

[111] A. Törncrona, M. Skoglundh, P. Thormählen, E. Fridell, E. Jobson, Low temperature catalytic activity of cobalt oxide and ceria promoted Pt and Pd: - influence of pretreatment and gas composition, Appl. Catal. B Environ. 14 (1997) 131–146. doi:10.1016/S0926-3373(97)00018-0.

[112] V. Easterling, Y. Ji, M. Crocker, J. Ura, J.R. Theis, R.W. McCabe, Effect of ceria on the desulfation characteristics of model lean NOx trap catalysts, Catal. Today. 151 (2010) 338–346. doi:10.1016/j.cattod.2009.12.007.